Medicinal chemistry
ISSN: 2161-0444

Miksa, Med Chem (Los Angeles) 2016, 6:10
DOI: 10.4172/2161-0444.1000406

Review Article Open Access

Fluorescent Dyes Used in Polymer Carriers as Imaging Agents in Anticancer Therapy

Beata Miksa*

Centre of Molecular and Macromolecular Studies, Polish Academy of Science, Lodz Sienkiewicza, Poland

Abstract

This review highlights the role of fluorescent dyes as active "molecular photoswiches" focusing on the application in bioimaging and anticancer therapies in the field of therapeutic delivery. The author describes the development of prodrugs targeted to specific cell types and polymeric nanocarriers (capsules, micelles and silica nanoparticles) used as fluorescent probes which offer advantages in the integration of "smart" features of fluorescent dyes into synthetic materials. The incorporation of biologically responsive components that cleave upon changes in pH or light irradiation is fundamental to the successful design of such carriers with capabilities to load and release therapeutics specifically at a target site.

Keywords: Fluorescent; Polymer; Nanocarriers; Theranosticscapsules; Silica dots; NIR dyes

Introduction

Optical fluorescence technology has been widely applied in recent biological analysis and bioimaging, owing to its high sensitivity, high resolution, and the availability of simple and rapid noninvasive analytical systems. Along with advances in fluorescence detection which is the basic method for direct visualization of dynamic protein interactions and material transport in living cells, live-cell imaging has become an essential tool for the study of changes in cell morphology. Moreover, fluorescence imaging methods are currently being developed to image specific molecular targets *in vivo*, thus fluorescent labeling is a central tool for studying localization, trafficking, and expression levels of biomolecules in live cells. So dyes can be attached to targeting molecules to make fluorescent probes due to a specific interaction between carriers and cell or tissue components. These probes have been recently used in active targeting to image receptors, antigens, antibodies, DNA and enzymes [1]. Despite the fact that dyes as imaging agents offer advantages in screening by enabling visual detection of the probe-target interaction, an ideal labeling reagent would remain nonfluorescent until bound to its target. The conjugates of fluorescent chromophores with anticancer therapeutics can be used also as prodrugs and nanoprobes for application them towards diagnosis and therapy in live cells. The different dyes including derivatives of fluorescence scaffolds (e.g., rosamine, BODIPY, chalcone, and xanthone) that cover a very wide range of near-infrared (NIR) and visible fluorescence spectra (400-800 nm) can provide microscopic details of biological molecules *in vivo* and *in vitro* [2]. Moreover, NIR light can penetrate skin and tissue to a few millimeters, enabling fluorescence detection in dermatological or *in vivo* diagnostic devices [3,4]. Therefore, multiphotochromic molecular systems should be used to build highly functional materials due to their potential multi-addressability and/or multi-response properties [5]. This review focuses on the progress made in developing fluorescent polymer capsules and the dye-doped silica nanoparticles (SiNPs) with tunable properties such as size, surface chemistry composition, morphology and functionality in respect of imaging and cellular detection, which is crucial in targeted drug delivery for biomedical and diagnostic applications [6,7]. Additionally, this review is designed to give an overview of passive targeting with fluorescent prodrugs that either works as active targeting systems. Furthermore, polymer nanocapsules [8,9] due to the polymer molecular weight or size have come to refer to the accumulation of drug by using physicochemical or pharmacological factors [1]. The integration of "smart" features i.e., chemically responsive components (which cleave upon changes in pH or redox potential) into synthetic materials is fundamental to the successful design of such carriers with capabilities to load and release therapeutics specifically at a target site. Thus, therapeutic molecules can be sequestered and/or released in a controlled manner from polymeric carries that labeled with pH- or light sensitive dyes which may regulate a process of diffusion. Polymer dye-doped capsules with compartmentalized, water-filled cavities and the synthetic amphiphilic shell have tremendous potential applications in nanomedicine because enable to create biomimetic nano- or multi-compartment reactors and this system could function also as a biomolecular analysis tool. The general methods to produce polymer capsules are described in literature [10,11].

Fluorescent small molecules as cell-type-specific imaging probes accomplished active targeting functions

Fluorescent dyes applied in biological labeling have many advantages, such as fast detection speed, good repetitiveness, low dosage, and non-radiation [12]. Molecules of dyes can label compounds by a covalent bonding using an active group (-SH, -COOH, -NH_2) or might be inserted into the double-helix structure of DNA by affinity, as in the case of thiazole orange, oxazole yellow and their dimers [13,14]. Antibodies (their size is about 12 nm) endowed with fluorescent dyes (e.g., Alexa Fluor 488 λEm=525 nm and Texas Red λEm=609 nm) [15-17] were used in the development of a wide range of effective targeted therapies [18-22] but they create clustering artifacts due to limited antibody penetration, which have an impact on insufficient labeling density. Thus, ligands that have been exploited for chemotherapeutic agent targeting systems can include monoclonal antibodies [23-28] but also low molecular weight receptor-binding conjugates such as dye-labeled peptides (arginine-glycine-aspartic acid-Cyt5,5) [29], peptide

***Corresponding author:** Beata Miksa, Centre of Molecular and Macromolecular Studies, Polish Academy of Science, Lodz Sienkiewicza 112, 90-363, Poland, Tel: +48426815832; E-mail: miksa@cbmm.lodz.pl

Received September 22, 2016; **Accepted** October 12, 2016; **Published** October 17, 2016

Citation: Miksa B (2016) Fluorescent Dyes Used in Polymer Carriers as Imaging Agents in Anticancer Therapy. Med Chem (Los Angeles) 6: 611-639. doi:10.4172/2161-0444.1000406

hormones [30,31], receptor antagonist and agonists [32], aptamers [33-35], transferrin [36-37], oligosaccharides [38], glycoconiugates [39], polyunsaturated fatty acids [40], oligopeptides [41,42], vitamin B12 [43], folic acid [44-54] and hyaluronic acid [55,56]. These ligands can be regarded as a tumor-specific receptor to construct a "guided molecular missile" with different therapeutic warheads. In an effort to contribute to the development of optical imaging modalities, a variety of fluorescent dyes e.g., fluorescein, Texas Red, the rhodamines, the cyanines (indocyanine green, thiazole orange) [57-59], polymethine cyanine dyes (the Cy3, Cy5, Cy5.5, Cy7 series) and the Alexa Fluors have been conjugated to folic acid [60-64]. Nowadays, the development of fluorescent dyes with longer excitation wavelengths (λEx>500 nm) transparent to human tissues [65,66] shows great promise, because imaging of malignant cells by optical means is not hazardous for living organisms [67]. Moreover, with improved optical sensors that can excite fluorophores deep in a tumor mass under low light intensities but with the higher fluorescence quantum yields detection [68] the problems associated with tissue autofluorescence and tissue absorption/scattering of light [69] might be neglected. Another advantage of ligand-targeted therapies is the ability to design a cognate imaging agent with the same targeting ligand [70,71]. Furthermore, ligand (2-[3-(1,3-dicarboxypropyl)ureido]pentanedioic acid) (DUPA) can selectively bind to a cell surface glycoprotein and it is known as prostate-specific membrane antigen [72,73]. The efficiency of drug release from respective DUPA-conjugates with chemotherapeutics was assessed by treating the conjugate with either glutathione (GSH, tripeptide) or dithiothreitol (DTT) to reduce the disulfide bonds. In addition, whenever membrane impermeable drugs must be delivered, ligand-targeted therapies are generally preferred, since a good targeting ligand will often carry its attached cargo into the target cell by receptor-mediated endocytosis.

Photosensitizers as selective therapeutic and imaging agents

The spectral work outside the range of autofluorescence of cell and tissue (350-700 nm) is the main advantage of using fluorophores with longer excitation and emission wavelengths for labeling of the biomolecules [74]. Near-infrared fluorescence (NIR**,** region 700-900 nm) is expected to have a major impact on biomedical imaging of specific targeting. In the NIR range the absorbance spectra for all biomolecules reach their minima and it allows to avoid interference by endogenous chromophores within the body. NIR fluorescence technology can minimize background interference, improve tissue depth penetration and tumor contrast. Shi et al. [75] reported the newly developed NIR dyes or NIR dye-encapsulated nanoparticles by conjugation with tumor specific ligands and their potential applications in cancer targeting and imaging. The potential of NIR dyes was assessed in photodynamic therapy (PDT) for a skin cancer model *in vivo*. PDT is a minimally invasive procedure based on the light-induced excitation of a photosensitizer (light-activatable chemical) to the singlet state due to the absorption of photons. Irradiation of photosensitizers can generate highly reactive singlet oxygen species or superoxide radical anion ($^1O_2$ and/or O_2^-) that causes destruction in malignant tissue [76-78]. Light-responsive compounds offer the promise of targeted therapy, which has several benefits including: prolonged action at the target site, overall reduced systemic dosage, reduced adverse effects, and localized delivery of multiple agents [43]. An efficient PDT photosensitizer requires the following features: a high quantum yield for singlet oxygen generation ($\phi\Delta$), efficient uptake into the diseased tissue (be preferentially retained by the target tissue), and localization in regions of the cell which are vulnerable to singlet oxygen damage [79-81]. In addition, other important requirements such as low dark toxicity (only be cytotoxic in the presence of light) and good pharmacokinetics (be rapidly excreted from the body to provide low systemic toxicity) are needed. Some examples of common organic dyes used as photosensitizers and imaging agents are illustrated in Table 1.

Current NIR probes with much improved photostability, high fluorescence intensity and long fluorescent life include three categories: *i*) organic chromophores (with squaraine, phtalocyanines, indocyanine green, porphyrin derivatives, BODIPY - borondipyrromethane anologues) [82], *ii*) inorganic silica nanoparticles (SiNPs) with NIR dyes (trimethine Cy3, pentamethine Cy5, Cy5.5, or heptamethine Cy7) [83] and *iii*) polymer dye-labeled capsules [Chapter 6]. Farther, fluorescence efficiency is greatly increased upon binding of cyanine dyes with nucleic acids or proteins as a result of the rigidization of the fluorophores [84-87]. Thus, Strekowski et al. [88] have developed bis(heptamethine cyanine) dyes containing two cyanine subunits, which exhibit a strong increase in the fluorescence (1000-fold) upon binding with protein. Gragg [89] reported a zwitterionic heptamethine indocyanine dye (Cy7), which has superior advantages for *in vivo* applications, such as no serum protein binding, rapid renal clearance, ultra-low non-specific tissue uptake, and high signal-to-background ratio after conjugation with tumor targeting ligands. Finally, Cy5.5 (λAb.max=675 nm, λEm.max=694 nm) is a promising contrast agent for the optical imaging studies *in vivo* providing a demarcation line between healthy and tumor cells [29]. However, cyanine dyes are far from perfect and have several limitations such as moderate to poor photostability, undesired reactivity with nucleophiles, and propensity to self-quench [41,90]. Therefore, different NIR dyes as squaraines [91] (i.e., bis(3,5-diiodo-2,4,6-trihydroxyphenyl)squaraine) that emit in the "optical window of tissue" at wavelengths above 800 nm in aqueous solution was assessed in PDT therapy. Squaraine derivatives consist of an oxocyclobutenolate core with aromatic or heterocyclic components at both ends of the molecules [92]. The bis-squaraine dye in which two squaraine units are bridged by a phenyl, biphenyl, thiophene or pyrene spacer exhibit fluorescence enhancements with red emissions in trizma buffer and present noncovalent labeling of human serum albumin (HSA) or bovine serum albumin (BSA) [93]. Water-soluble NIR fluorescent labeling probes named KSQ-3 and KSQ-4 substituted with four sulfo groups ($-SO_3-$) based on the squaraine backbone exhibited significant fluorescence emission at λ=817 nm. In the presence of BSA which was covalently labeled with KSQ-4 the conjugate showed a strong absorption peak at λ=787 nm and fluorescence emission at λ=812 nm [94,95]. These compounds have satisfying optical characteristics and functionality for bioanalyses thus they enable the

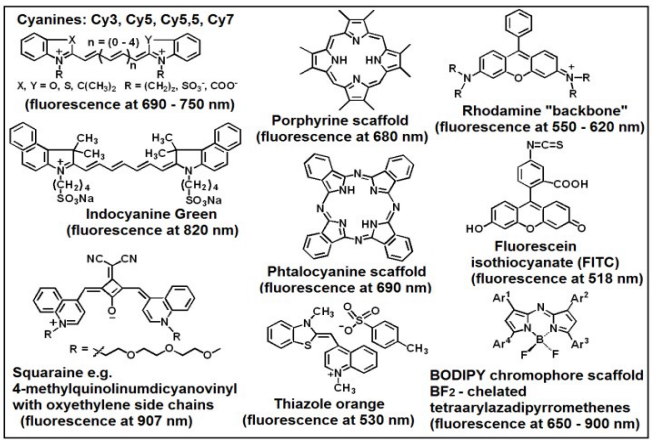

Table 1: The example of dyes used as photosensitizers or imaging agents.

development of noninvasive and simple diagnosis techniques. Moreover, squaraine rotaxanes were developed as fluorescence imaging probes and chemosensors [96]. They can be converted into bright and highly stable deep-red fluorescent probes useful in biomedical imaging analyses. The depth of penetration doubles from 4 mm observed between λ=(500 - 600 nm) to 8 mm at λ=850 nm, where light penetration is most effective [81]. Furthermore, deep-red light can potentially penetrate several centimeters (2.5 cm) through skin and tissue [97]. The photosensitizers with high fluorescence detection are phtalocyanines, used to generate fluorescence contrast for the selective identification of diseased tissue. Phtalocyanines, are two-dimensional 18π-electron aromatic porphyrin derivatives, consisting of four isoindole rings bridged by four imino nitrogen atoms at the *meso*-position. Their unique properties as a result of the π electrons strongly delocalized around their perimeter make phatlocyanines and porphyrin analogues (hematoporphyrins) well-known for molecular materials used in biomedicine [98]. Despite the fact that a long π-π electronic conjugation provides phtalocyanine high photostability and strong absorption bands, most of them exhibit absorption and emission maxima below λ=700 nm. Studies have demonstrated that the addition of benzene groups or multiple electron-donating substituents moves the absorption bands from the visible to the NIR spectral region. A series of conjugated porphyrin dimmers with intense absorptions ranging from 650 to 800 nm and fluorescence emission from 700 to 800 nm have been used in imaging studies [99]. In porphyrins, the Soret band in the 400 nm range is typically excited for diagnosis, taking advantage of the large Stokes shift between excitation and emission bands. Besides imaging applications as biosensors, phatocyanines and porphyrin derivatives have also been known as photosensitizers for photodynamic therapy of cancers and "photodynamic diagnosis", since this kind of dye can be taken up in malignant and dysplastic tissue and generate singlet oxygen (highly toxic for tumor cells) when the tumor area is exposed to light [79]. Therefore, with excellent stability and suitable photophysical properties, versatility of newly developed phtalocyanines and porphyrin derivatives such as bacteriochlorins, gives them great potential to be extensively applied in clinics and evaluated for their application for both biological imaging and cancer photodynamic therapy [81]. The development of organic chromophores based on the BF2 chelated-tetraarylazadipyrromethene scaffold and they related structural analogues with spectral emission in the NIR and visible regions (650-900 nm) offers optical benefits by utilizing them *in vitro* and *in vivo* as imaging agents [100] with controllable photophysico-chemical properties. These highly emissive dyes, which are derivatives of 4,4'-difluoro-4-bora-3a,4a-diaza-*s*-indacene (hereafter abbreviated to BODIPY; boron-dipyrromethane) have been widely utilized in various polymers [101-103] because they tend to be strongly UV-absorbing small molecules and emit relatively sharp fluorescence peaks with high quantum yields. This system provides the framework for more elaborate receptors to detect other analytes [104,105]. The comprehensive review summarizing the basic chemistry and spectroscopic properties common BODIPY-derivatives probes intended to intracellular imaging was prepared by Burgess et al. [101]. BODIPY dyes depending on the electronic structure of conjugated aromatic groups can indicate fluorescence in a broad range of wavelengths from green to red. A BODIPY derivative labeling of recombinant protein molecules FABP7-expressing 293HEK cells (i.e., a protein encoded by a gene) are well-known as intracellular markers of radial glial cells [106,107]. Chang et al. [108,109] discovered BODIPY which selectively stain Langerhans islets composed of glucagon-secreting α-cells (in the presence of glucagon the fluorescent compound was named Glucagon Yellow) and insulin-secreting β-cells in pancreas tissue sections. They also developed chemical imaging probes that specifically stain live microglia of brain cells [110]. The coordination capsules prepared from derivatives of phenylanthracen molecules linked by Pt(II) can co-encapsulate BODIPY with coumarin 153 or Nile red. These structures indicated that the emission color of the fluorescent guest within a cavity of such capsules was readily modulated upon pairwise encapsulation with planar aromatic molecules [111]. The encapsulated complex enclosed by the shell having Pt (II)-phenylanthracen demonstrated the guest-guest interaction within synthetic molecular host-capsules. So, the emission color of BODIPY-guest is sensitive to the identity of the co-encapsulated guest (Figure 1). Thus, pair-selective encapsulation of two substrates modulates the intensity of fluorescence and fine-tuning of the emission properties of dyes. The observed unusual color changes most probably stemmed from the exclusively formation of excimer-like complexes in the confined nanospace of the capsule. The non-covalent approach for the straightforward preparation of aqueous fluorescent nanocomposites capable of modulating the emission color upon encapsulation could lead to the development of new photofunctional sensing and labeling materials.

Fluorescent dyes as "molecular photoswiches" and molecular chromophores for imaging

The interesting progress has been made in disulfide-based cleavage systems in thiol detection connected with biological applications [112]. The disulfide cleavage reactions have a great impact on chemical sensing of drug delivery involved in the polymer and pharmaceutical chemistry. The concentration of contrasting glutathione (GSH) inside cells and in plasma play an important role in the cellular antioxidant defense system and detoxification of reactive oxygen species [113,114]. The regulation of cellular redox status i.e., the equilibrium established between reduced free thiols (GSH) and oxidized disulfides (GSSG) is associated with a healthy condition and some kind of imbalance due to their abnormal levels are often related to diseases [115,116]. Moreover, intracellular GSH concentrations is 4-fold higher in tumor cells than in the corresponding normal cells and 1000-fold higher than in blood plasma [117-120]. More precisely, GSH can keep the cysteine thiol group in proteins in the reduced state and protect the cells from oxidative stress by trapping free radicals that damage DNA and RNA. Imbalance of GSH/GSSG ratio in cells associated with oxidative stress can be estimated by various fluorescent probes. The breakdown of the disulfide bond upon attack by specific thiols can cause rapid response and changes in the fluorescent signals of the probes. The GSH/GSSG cellular ratios can be estimated by using targeting fluorescent probes that allow for fluorescence imaging of reduced thiols both *in vitro* and *in vivo* in liver cells. To develop a new fluorescent tool for analysis of GSH content in cells and tissue Zhai et al. [121] obtained a convenient

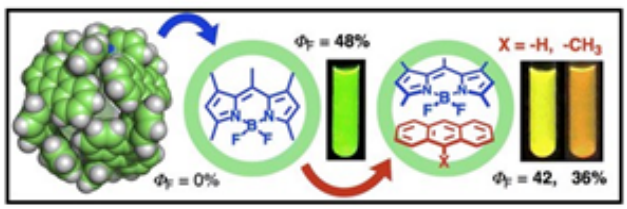

Figure 1: The highly emissive (with good quantum yield, ϕ_F) hostguest complex prepared upon encapsulation of various fluorescent dyes (e.g., BODIPY with non-substituted antracene (λ_{max}=554 nm, yellow) and 9-methylantracene (λ_{max}=577 nm, orange) by a Pt(II) ions linked coordination capsule with bent bispyridine ligands substituted phenylantracene in water.

compound named Glutathione Green (λEx/λEm=565/585 nm) which shows a significant hypsochromic shift (λEx/λEm=512/522 nm) in response to GSH but not to the oxidized form of glutathione (GSSG). This compound has a BODIPY scaffold with a furan ring as a small functional group, which is likely to be a binding site for GSH (Figure 2).

Kim et al. [122] described a tool embedded with a single galactose subunit (which guides the probe to hepatocytes) and a disulfide-linked 4-amino-1,8-naphthalimide moiety. The probe provides an easy-to-monitor fluorescent change when exposed to endogenous thiols as the result of disulfide cleavage. The signal of an emission probe at λ=473 nm (yellow) decreases gradually with increasing concentrations of GSH while the emission at λ=540 nm (green) increases linearly towards GSH (Figure 3). Thus, upon exposure to free thiols the tool can be useful in diagnostics and in the screening of new potential drug agents. The same group of researchers described a probe bearing triphenylphosphine-naphthalimide with a disulfide moiety in order to measure the activity of the mitochondrial thioredoxin (Trx) level in cells. Such information may also indicate illnesses related to cancer [123].

The triphenylphosphonium headgroup guides the probe to the mitochondria and also improves its water solubility. The fluorescence emission was induced by the cleavage of a disulfide bond of the probe, resulting from a reaction with Trx and subsequent intramolecular cyclization by the released thiolate, thus a green fluorescence product was obtained. A fluorescence off-on change of the maxima at λ=376 nm and λ=472 nm shifts a new emission band centered at λ=482 nm (yellow) and λ=540 nm (green) respectively (Figure 4). In this case linear correlation between the concomitantly increasing fluorescence intensity at λ=540 nm and increasing concentration of Trx was retained. So, the naphthalimide unit provides a suitable fluorescent scaffold owing to its excellent spectroscopic characteristics and structural flexibility for introducing various modifications [124].

The fluorescent thiol probes have been obtained in reactions of conjugates endowed with thiols together with maleimides (α,β-unsaturated ketones) [125]. The sensitive fluorogenic probe which works preferentially with the cysteine (Cys) was obtained by condensation of coumarinaldehyde and diethyl malonate [126]. The coumarin-based chemodosimeter selectively recognizes thiols through the 1,4-addition reaction (Michael type) to the α,β-unsaturated carbonyl group in the conjugate of the coumarin analogues and formed thioeters. As a result fluorescent spectra were enhanced 107-fold (with a green emission of the maximum at λ=502 nm) (Figure 5). The probe did not react with GSH, homocysteine (Hcy) and amino acid due to an intermolecular charge transfer blocking event.

Lin et al. [127] reported the new NIR fluorescent probe chloro-hydroxyl-merocyanine-thiol or (CHMC-thiol) containing 2,4-dinitrobenzenesulfonate moiety as a fluorescence quencher. The nucleophilic substitution by thiols of the chloro moiety in the chloro-substituted cyanine conjugate can induce a ratiometric mode in fluorescence of the probe CHMC-thiol. In this way, the unique probe CHMC-thiol containing both the high-sensitivity site (the 2,4-dinitrobenzenesulfonate moiety) and the low-sensitivity site (the chloro moiety) can provide a turn-on fluorescence response upon interactions with thiols. So the probe may serve as a powerful molecular tool useful for the estimation of the thiols concentration in biological and clinical studies in living cells (Figure 6). The different chemodosimeter which can effectively discriminate Cys from Hcy and GSH in living cells with notable fluorescence enhancement was reported by Peng et al. [128]. They synthesized the colorless and weakly fluorescent Rhodamine-6G-conjugate including a spirolactam-ring

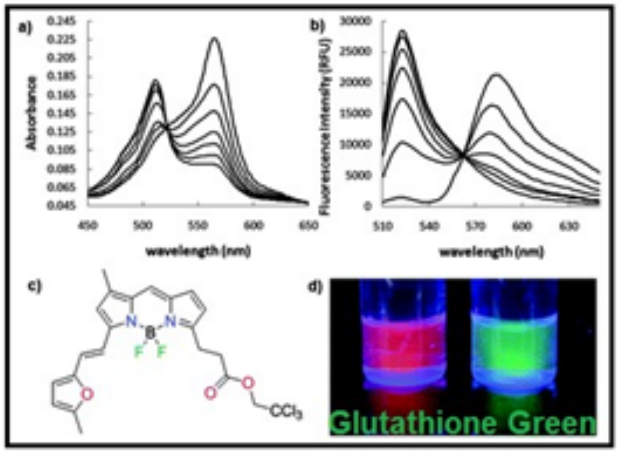

Figure 2: Glutathione Green: spectra (a) absorbance and (b) fluorescence, (c) structure, (d) a picture with GSH (right) and without (left) under UV irradiation at λ=365 nm.

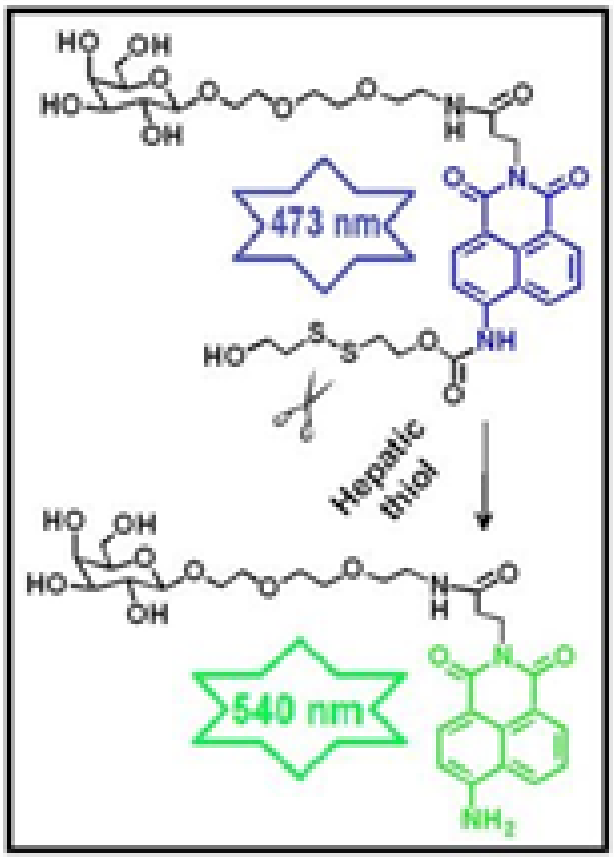

Figure 3: Schematic representation of hepatocyte-targeted imaging and cleavage of disulfide bond to induce fluorescence changes.

with an unsaturated aldehyde. This probe provides a facile way to visualize the changes of Cys concentration depending on the cyclization of N-terminal Cys residues (endowed with -SH and -NH2 groups) which reacts with the aldehyde group to form thiazolidine ring.

The Rhodamine-6G-COOH was released from the probe embedded

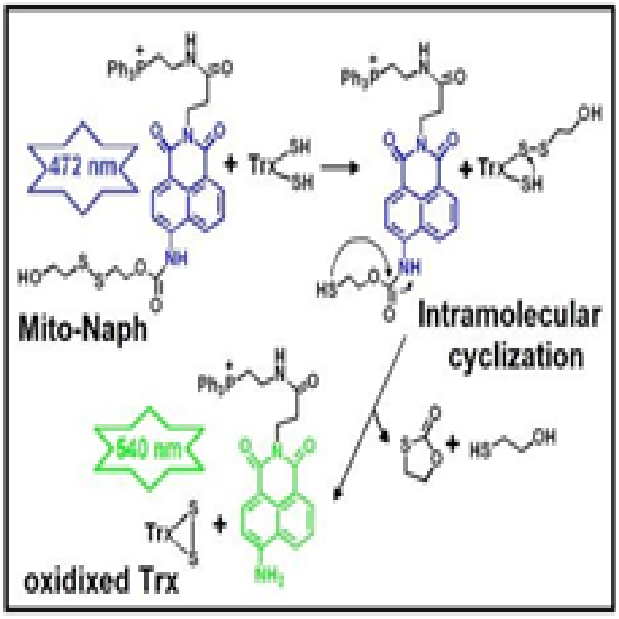

Figure 4: Proposed mechanism of the reaction of Mitochondria Naphthalimide with Thioredoxin.

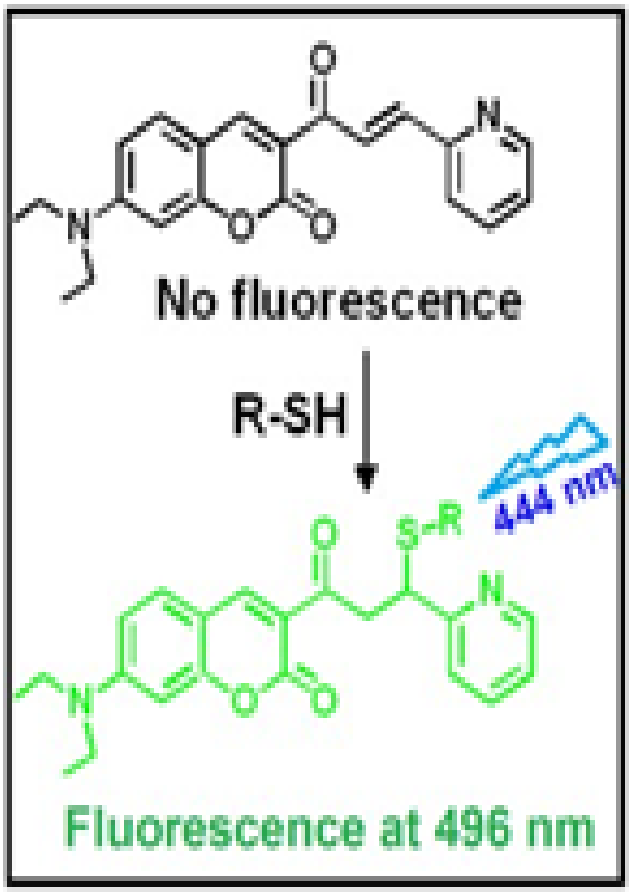

Figure 5: The design concept of fluorescent turn-on probe for thiol adduct.

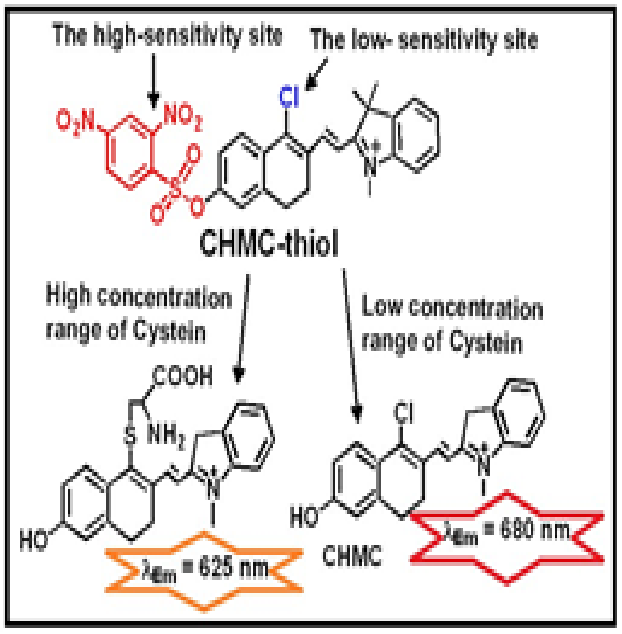

Figure 6: The structure of NIR fluorescent probe chloro-hydroxylmerocyanine-thiol (CHMC-thiol) containing 2,4dinitrobenzenesulfonate moiety. It can induce a ratiometric mode in fluorescence which depends on the concentration of thiols.

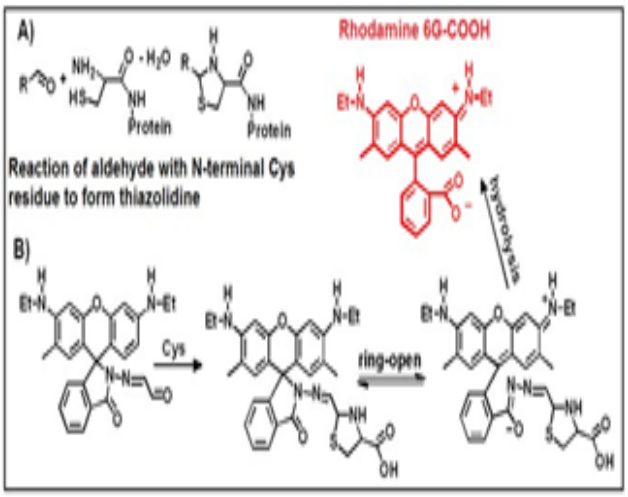

Figure 7: Proposed mechanism of discrimination of Cys by using rhodamine 6G-conjugate with unsaturated aldehyde group. In the presence of Cys the color developed from colorless to pink by rhodamine 6G-COOH.

with a thiazolidine derivative due to the hydrolysis and the ring-opening reaction. The interaction of the probe with Cys accompanied by a color change from colorless to pink and strong fluorescence intensity which increased linearly (peaking at λEm=552 nm) with the Cys concentration (Figure 7).

Wender et al. [129] reported that conjugation of luciferin through a disulfide-carbonate linker with an octaarginine, cyclosporine A or oligoguanidine transporter, produces conjugates that are water soluble and readily enter cells and tissue [130]. The linker-luciferin system allowed to assess the uptake of various transporters in cells and also

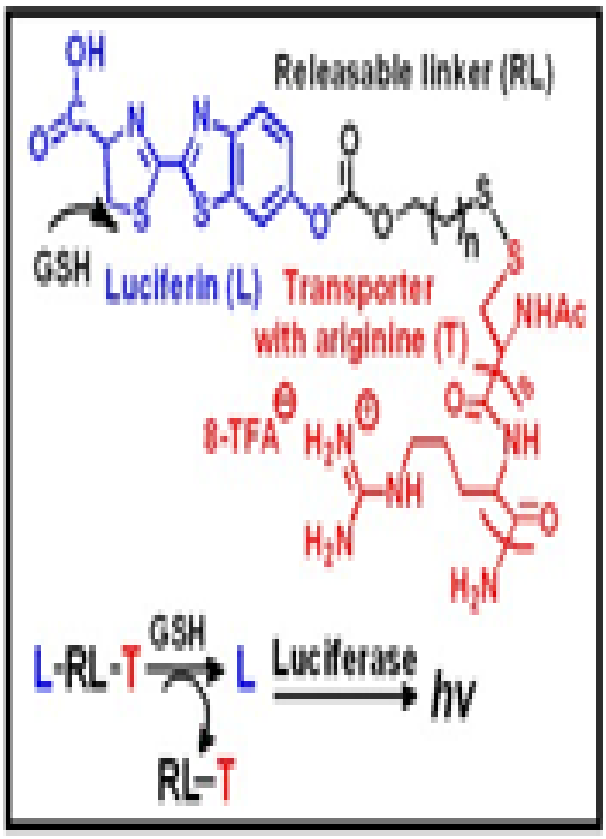

Figure 8: The scheme of conjugates of ariginine-reach transpoters with luciferin, which can be released by luciferase.

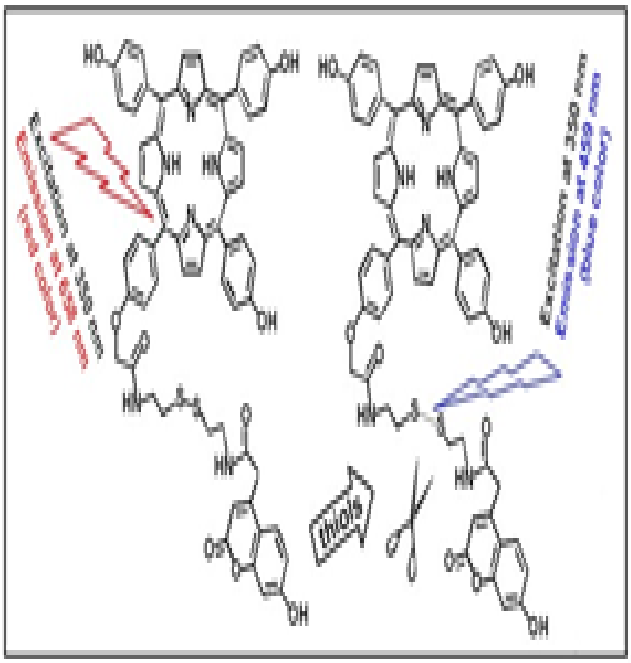

Figure 9: The scheme of a ratiometric fluorescent probe for thiols based on a tetrakis(4-hydroxyphenyl)porphyrin-coumarin scaffold.

released cargo only after cell entry. The decomposition of the conjugate (luciferin-linker-transporter) mediated by GSH caused the disulfide cleavage and developed a strong luminescence of released luciferin (Figure 8).

Thus, the development of probes with disulfide-based luciferin conjugates with a variable distance of releasable linkers between carbonyl groups and the proximal disulfide linkage of octaarginine would allow to release in a controllable way a drug attached to transporters. Moreover, these conjugates incubated with the PC3 prostate cancer cell line were transfected with a luciferase gene (PC3M-luc-C6) [131,132] and the emission of light was caused by luciferase activity which utilizing luciferin from the disulfide cleavage of the conjugates. Yu et al. [133-135] prepared a different fluorescent probe using a porphyrin-coumarin scaffold for detection thiols based on Förster fluorescence resonance energy transfer (FRET) which is a "spectroscopic ruler" between a donor and an acceptor species due to photoinduced electron transfer. FRET requires two fluorescent dyes: one (the fluorescent donor) emits high-energy photons and the other (the fluorescent acceptor) emits low-energy photons. Thus, within the Förster distance, fluorescent color switches from the donor to the acceptor, or from high- to low-energy photons. The excitation energy of a coumarin fluorophore (an energy donor) can be transferred through a radiationless transfer of energy to a neighboring porphyrin fluorophore (an energy acceptor) within 100 Å, if there is good overlap between the donor emission and acceptor absorption spectra [129]. In this case the orientation of the donor-acceptor dipole moment is not perpendicular and the donor molecule can transfer energy *via* a dipole-dipole interaction to the acceptor. Then the acceptor can emit a photon at a longer wavelength than the fluorescence of the donor [5]. The FRET off-on sensing system provides advantages over conventional fluorescence detection methods based on single fluorophores, because it has greater sensitivity and less background interference. Upon excitation of the probe (which composed of a porphyrin attached to a coumarin scaffold through a disulfide linker) at λ=350 nm, the characteristic emission of porphyrin at λ=658 nm appeared with little fluorescence. In the presence of thiols significant fluorescence enhancement was observed at λ=459 nm due to the coumarin emission and a concomitant decrease in emission at λ=658 nm was evident (Figure 9).

Thus, the FRET was turned off by disulfide cleavage reaction induced by the thiol. This probe was suitable for ratiometric fluorescence imaging of thiols in living HeLa cells [133]. The photoactive fluorophores (caged dyes) are useful tools as fluorescent marks in dynamic, biological systems [136]. They serve like powerful imaging probes to follow the trajectory, speed, and timing of molecular and cellular movements and to provide information regarding spatio-temporal resolution in living tissue [137-139]. The nonfluorescent caged fluorophore can be homogeneously distributed within the system of interest and a mark is generated by UV photolysis, which can be controlled spatially and temporally with good precision. These caged dyes are weakly fluorescent when key functional groups of fluorophores are masked by photoremovable protecting groups like 2-nitrobenzyl derivatives. The 1-(2-nitrophenyl)ethyl or (NPE) is by far the most common photolabile group (Figure 10) [140].

Photoactivation with ultraviolet (UV) light removes the protecting group (uncage) and abruptly switches on the fluorescence of parent dyes. The key requirement for caged fluorophores is that parent fluorophores should be photostable to resist photobleaching. This class of cage coumarins was developed by Li et al. [141]. They improved properties of coumarin analogues like good water solubility,

biocompatibility, photostability of parent fluorophores, and high photolytic efficiency by both one photon and multiphoton excitation. Since the used coumarins emit only blue light these NPE-coumarin cages were conjugated with other fluorescent dyes which had a longer wavelength of the emitted light. This method expanded the fluorescent imaging window for multicolor simultaneously imaging in live cells. This group of researchers designed a cage coumarin-calcein green fluorophore used as a FRET probe. The NPE-cage coumarin 3-carboxyamide and a calcein 6-carboxyamide (as the energy acceptor) connected by a cyclohexyl linker led to an extensive spectral overlap between coumarin emission and fluorescein excitation (Figure 11). The efficient energy transfer from coumarin to calcein caused the increase of emission fluorescence intensity at λ=520 nm more than 14- fold using λ=410 nm excitation (of the coumarin maximum absorbance) [141].

The rational design of highly fluorescent fluorophore compounds with optical switches for high-contrast optical lock-in detection used in imaging microscopy in living cells was reported by Marriott et al. [142,143]. They designed a highly fluorescent probe consisted of tetramethylrhodamine (TMR) and spironaphthoxazine (NISO) or (TMR-NISO) which was an optical switch to improve the image contrast. The TMR-NISO molecule integrated a reversible excited-state and a transition is carried out between a colorless spiro (SP)-state and a colored merocyanine (MC)-state in response to irradiation with near ultraviolet (λ=365 nm) or with visible (λ>530 nm) light respectively (Figure 12). In the MC-state, the TMR (donor) emission is almost completely extinguished by FRET to the MC probe (acceptor), whereas in the colorless SP-state, the quantum yield for TMR fluorescence is maximal [142]. Irradiation of TMR-NISO with a defined sequence of λ=365 nm and λ=546 nm manipulates the levels of SP and MC with concomitant modulation of FRET efficiency and the TMR fluorescence signal. This cell permeable probe presents greatly improved quantum yields for both fluorescence emission and optical switching in the same molecule.

Kikuchi et al. [144] developed a no-wash fluorogenic protein labeling system by exploiting FRET-based probes of fluorescein-cephalosporin-azopyridinium (i.e., the synthetic *β*-lactam probe) and a mutant of 29-kDa TEM-1 *β*-lactamase tag (BL-tag) (Figure 13). This technique is useful for labeling cellular proteins with synthetic molecules under physiological conditions [145,146]. The labeling mechanism in live cells imaging involves two steps: an initial noncatalytic enzyme reaction with the probe and subsequent quencher elimination *via* a self-immolative reaction. Elimination rates of the leaving group (2-(4-dimethylaminophenylazo)pyridinium) which works as a quencher then converted into the neutral azopyridine form is accelerated by a decrease in the p*K*a (4.3) value of the conjugate acid. The hydrolysis of the *β*-lactam ring induces fast elimination from 3'-position and the leaving quencher allows to switch on the probe fluorescence [147,148].

The absorption spectrum of the azopyridinium shows the maximum at λ=581 nm and broadly ranges from λ=500 nm to λ=600 nm. So this compound works as an efficient quencher for fluorescein and rhodamines. This technology enables adequate discrimination of the location of proteins labeled with the same protein tag, in conjunction with different color probes, by dual-color fluorescence [149]. These systems operate in a nonspecific manner and do not allow specific analysis at the level of individual organs.

Non-fluorescent prodrugs/converted into fluorescent active drugs

Prodrugs by definition are precursors (derivatives) of drugs that are metabolized or activated in the body to release or generate the

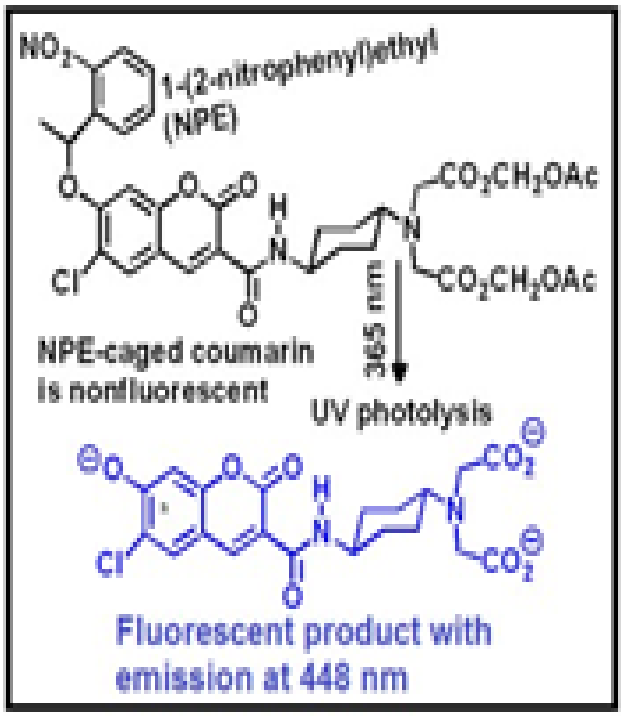

Figure 10: The example of a cell permeable caged coumarin fluorophore for *in vivo* cellular imaging applications.

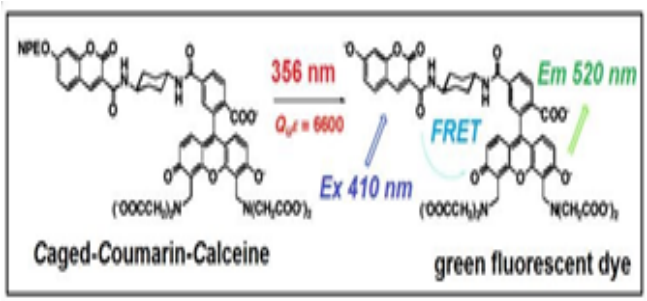

Figure 11: The photoactivable FRET probe based on a caged coumarin and a calcein analogue, which can be efficiently photolyzed by ultraviolet light.

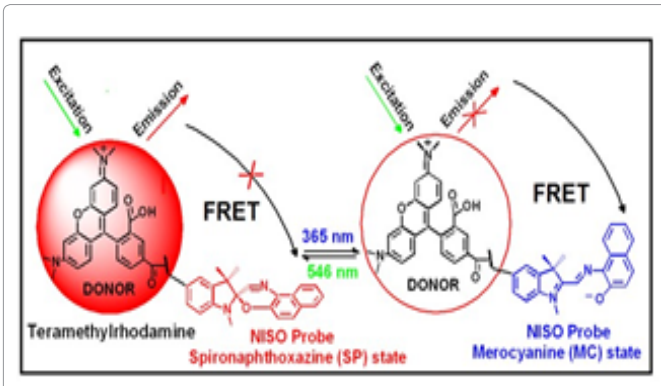

Figure 12: Optical control of TMR fluorescence intensity in TMRNISO probes. Optical switching between SP- and MC-state of NISO generates the modulation of TMR fluorescence intensity by FRET.

active pharmacological agent. Efficiency of chemotherapy crucially depends on the concentration of the effective agent in the cancer tissue (resulting in the therapeutic effect) and on the concentration in healthy tissues (resulting in side effects). The instantaneous report on the release of drugs *in vivo* is a great-benefit, especially if the reported signal could be detected in a non-invasive manner (as in the fluorescence detection technique). This type of cancer treatment with biodistribution that can be imaged in real time has been called *theranostic* (therapy combined with diagnostics). Chemotherapeutic prodrugs which provide a signal that allows determination of locations and activation of the drug upon selective cell internalization are being widely investigated for cancer treatment. The disulfide bond is used as a cleavable linker of a drug to a conjugate as an inactive prodrug, which can be converted into the corresponding active parent drug by an activation process. Ojima et al. [150] developed a prodrug conjugate with biotin (vitamin H or B-17) as the tumor-targeting molecule [151] bearing a self-immolative disulfide linker with a second-generation taxoid (SB-T-1214) as the cytotoxic agent (Figure 14). The conjugate can be internalized efficiently into tumor cells (e.g., L1210FR leukemia cells) overexpressing cell-surface biotin receptors *via* receptor-mediated endocytosis (RME). Taxoid was released *via* GSH-triggered disulfide cleavage. In order to monitor and validate the RME of drug release and drug binding to the target protein, three different probes with fluorescent or fluorogenic molecular chromophores were synthesized: biotin-fluorescein (FITC), biotin-linker-coumarin, and biotin-linker-taxoid-fluorescein. Kim et al. [124] studied direct fluorescence monitoring of a delivery and cellular uptake of a cancer-targeted cyclic peptide RGD (with sequence Arg-Gly-Asp). The multifunctional molecule containing a disulfide bond as a cleavable linker was built from a naphthalimide moiety as a fluorescent reporter, RGD as a cancer targeting unit and camptothecin (CPT) as a model active anticancer reagent. Thus, a peptide-appended naphthalimide pro-camptothecin conjugate was a theranostic prodrug (Figure 15).

Upon reaction with free thiols in aqueous media at pH 7.4 disulfide cleavage occurs. This leads to release of the free CPT drug in endoplasmic reticulum, as well as the production of a red-shifted fluorescence emission at λmax=535 nm. Low et al. [152] synthesized a folate-peptide-camptothecin conjugate prodrug with releasable disulfide carbonate linker. The poor water solubility of CPT is a drawback of its therapeutic agent. Therefore, a folate conjugate linked with the drug *via* a hydrophilic peptide spacer (Pt-γ-Glu-Asp-Arg-Arg-Asp-Asp-Cys) containing a disulfide releasable carbonate linker resolves the water solubility problems and provides efficient release of unmodified CPT *via* endosomal disulfide reduction. The cytotoxicity of folate-peptide-CPT *in vitro* was evaluated using KB cells (a human cervical cancer cell line) and revealed inhibition of cells proliferation. Shabat et al. [153] designed a prodrug composed of a specific triggering substrate (phenylacetamide) attached to a self-immolative linker with a pair of identical fluorophores (fluorescein moieties) and CPT. Cleavage of the phenylacetamide group by the enzyme penicillin-G-amidase (PGA) and subsequent elimination reactions released the free CPT moiety and fluorescein molecules (Figure 16).

Coumarin derivatives as a phototrigger have been widely used in drug delivery system mainly due to the strong fluorescence nature and their ability to the fast disintegration and the rapid release. Singh et al. [154,155] synthesized photoresponsive and pH sensitive theranostic conjugates based on benzothiazole-coumarin derivatives linked with the anticancer drug chlorambucil. In a physiological milieu (pH=7.4) fluorescence of the conjugate was only in the blue range (λ=406 nm). In such conditions the coumarin moiety occurs in the phenolic form (with –OH group). At acidic pH green fluorescence from the tautomeric keto

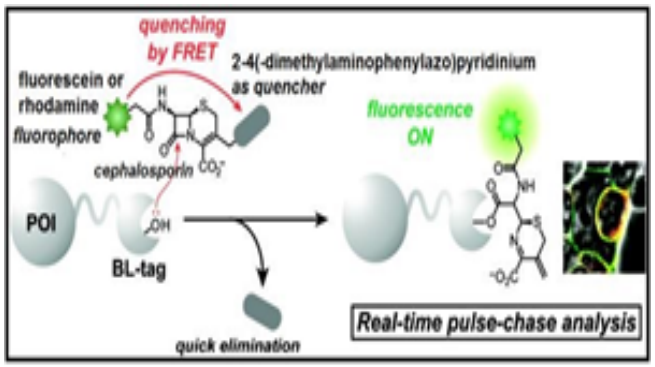

Figure 13: The scheme of a no-wash fluorogenic labeling system by exploiting fluorescence resonance energy transfer (FRET)-based fluorescein-cephalosporin-azopyridinium probes and a mutant βlactamase tag.

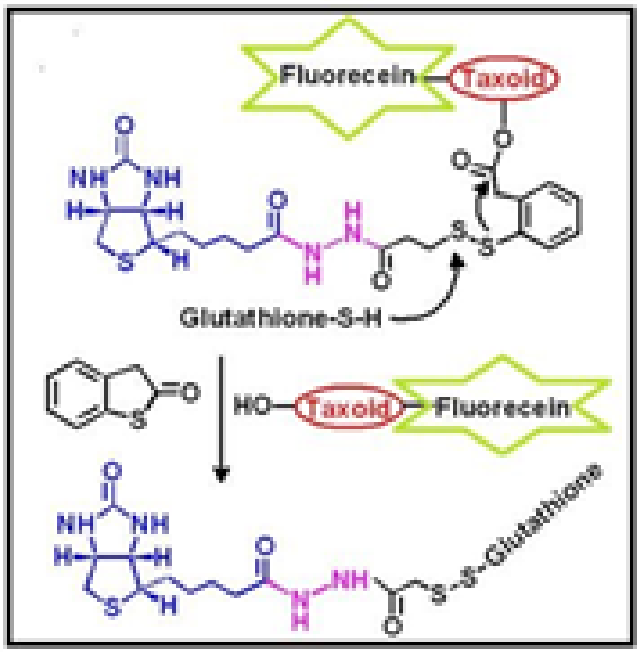

Figure 14: Second-generation self-immolative disulfide linkers with biotin as tumor-targering module and a fluorescent taxoid.

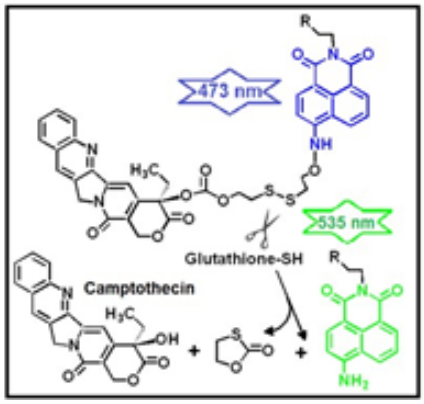

Figure 15: The scheme of the theranostic prodrug of a naphthalimide pro-camptothecin molecule with a disulfide bond as a cleavable linker. The R-describes the group of an RGD cyclic peptide.

form with a protonated benzotiazole group was turned on (λ=516 nm) resulting from the intramolecular proton transfer. Photolysis of anticancer drug chlorambucil was carried out using soft UV irradiation at λ ≥ 365 nm. *In vitro* studies showed that a coumarin-benzothiazole-chlorambucil conjugate can act both as an imaging agent due to its highly fluorescent nature and a phototrigger for controlled drug release (Figure 17).

The different coumarin conjugates e.g., coumarin-quinoline are also pH-dependent. The above mentioned compound indicates a significant red-shift of the maximum intensity in fluorescence emission from λ=544 nm to λ=644 nm before and after protonation of a quinoline ring in neutral and acidic conditions respectively. Unfortunately, the two emission peaks are poorly resolved because of relatively broad profiles which cover each other [156]. Moreover, a coumarin phototrigger was used as a photoremovable protecting group for nucleobases [157]. Furthermore, in recent years coumarino-pyrimidine conjugates have been studied for their diverse pharmacological properties (antitumor activity) [158-160]. A different delivery strategy based on the nontoxic B-subunit of Shiga toxin (termed STxB) which is produced by intestinal pathogenic bacteria was reported by Schmidt et al. [161]. The prodrug consisted of SN-38 (that belongs to the class of camptothecin derivatives) linked *via* a disulfide bond to STxB. Such structures can bind to the glycolipid Gb3 cellular toxin receptor and then internalized into tumor cells e.g., colorectal carcinoma. This strategy termed the retrograde route was used for delivery prodrugs targeting to membranes of the biosynthetic/secretory pathway, by using STxB (Figure 18).

Perez et al. [162] synthesized a folate receptor targeting theranostic molecular probe with both imaging and therapeutic properties due to covalently linked doxorubicin (DOX). The prodrug containing a disulfide linker i.e., dithiobis(succinimidyl propionate) conjugated with a folate unit and the DOX moiety retained fluorescence and cytotoxic ability. The disulfide bond linking DOX with the targeting folate unit (DOX-S-S-Fol) is cleaved within the cell by gluthatione-mediated dissociation. Thus, it allowed to turn on fluorescence (at λEx=497 nm, λEm=594 nm) and activated cellular toxicity of the probe by subsequent release of DOX-SH (Figure 19).

Latent fluorophores (pro-fluorophores) [163] are attractive candidates as labels for the imaging strategy due to coupling their activation to the drug release event in a delivery system [164-166]. In recent years, the quinone-methide elimination has proven to be a valuable tool for drug delivery, molecular probe design, signal amplification, stimulus supramolecular assembly, and self-immolative dendritic and polymeric molecular systems [167]. In this manner, intramolecular charge transfer (electron rearrangement) can lead to formation of π-conjugated quinone-methide-type dye compounds (fluorochrome) with long-wavelength emission of fluorescence. These dyes (e.g., QCy7 derivatives) [168,169] can also be applied as latent fluorophore linkers of theranostic prodrugs that provide a turn-on NIR fluorescence response upon activation (Figures 20 and 21).

The mitochondria-targeting carrier QCy7HA (with two positive charges on each molecules) is illustrated in Figure 22. The prodrug based on a QCy7HA scaffold endowed with the covalently attached doxorubicin (DOX) was studied by Lee et al. [170]. Such therapeutics are useful for treatment of drug-resistant cancers.

For clinical use, the homo and heterodimeric prodrug [171] with a latent fluorophore was designed due to monitoring of drug-release in activated therapy for inhibition of Molt-3 leukemia cells by taking the catalytic antibody $38C_2$. Moreover, Shabat et al. [171] synthesized a theranostic prodrug based on 7-hydroxycoumarin which was

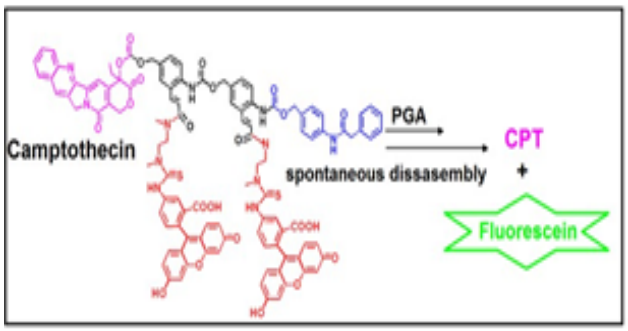

Figure 16: The self-immolative theranostic prodrug activated by the enzyme penicillin-G-amidase (PGA) can release two fluorescein derivatives as reporters and the active drug camptothecin (CPT).

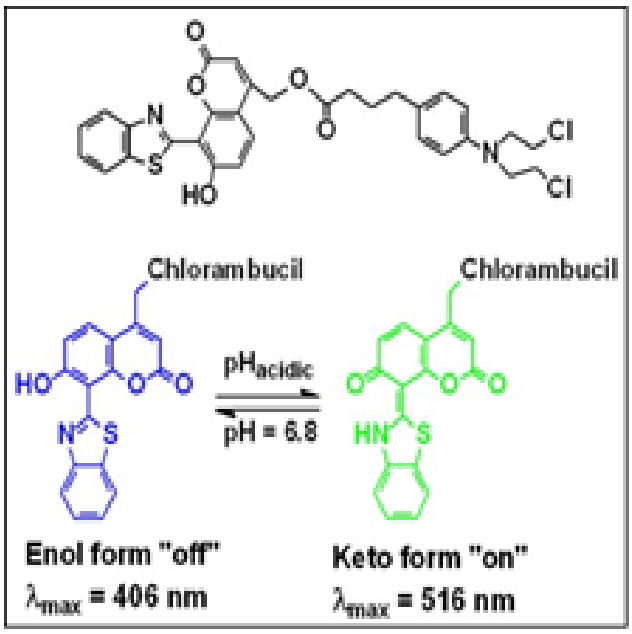

Figure 17: The enol and keto forms of Coumarin-BenzothizoylChlorambucil conjugate.

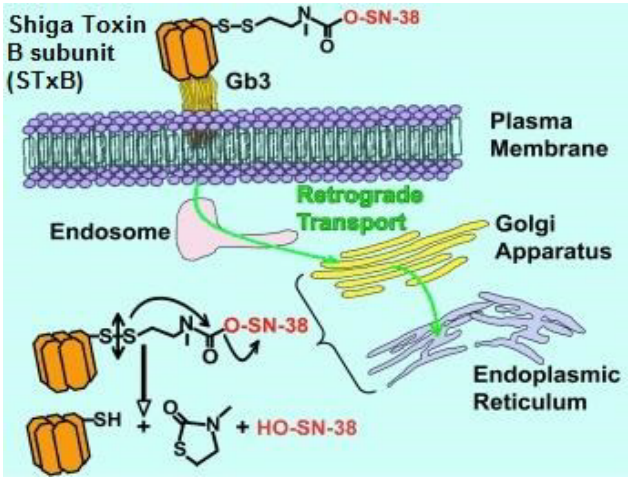

Figure 18: Principle of retrograde delivery.

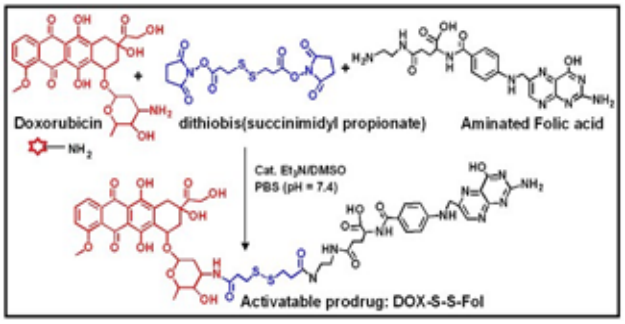

Figure 19: The targetable theranostic prodrug (DOX-S-S-Fol) leading to target specific cytotoxicity and fluorescence emission (ON) due to cleavage of the disulfide bond by GSH.

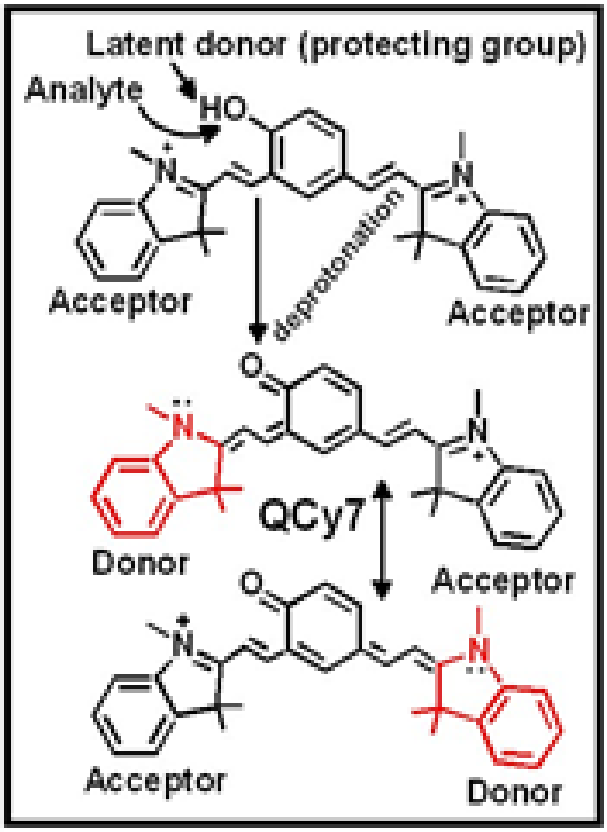

Figure 20: Activation of a QCy7 molecular probe by a specific analyte to produce a fluorescent turn-on response.

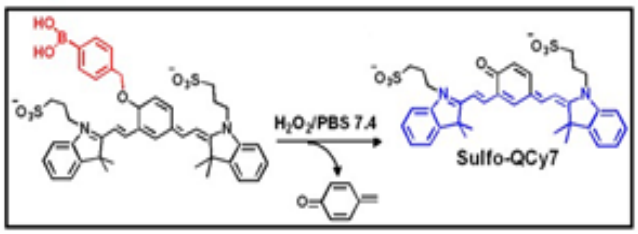

Figure 21: Oxidation of the phenylboronic acid derivative by hydrogen peroxide releases fluorophore sulfo-QCy7.

covalently bound with melphalan and the dipeptide Phe-Lys. This linker is the triggering substrate for Cathepsin B. The conjugate was disintegrated due to cleavage of the amide bond at the C-terminus of the lysine initiated by Cathepsin B. As a result the free melphalan and a fluorescent coumarin derivative were released (Figure 23). However, fluorescent emission at λEm=460 nm is in the blue region, which is not practical used in studies *in vivo*.

To summarize, new chemotherapeutic prodrugs that can report on the localization and activation of the drug upon internalization into select cells are being widely investigated for cancer treatment [172]. Thus, a new molecular design for a theranostic prodrug based on a self-immolative linker attached to a pair of FRET dyes that produces a fluorescent signal upon disassembly are still very interesting.

The design of polymer membranes with controlled pore sizes by using different fluorescent moieties

Synthetic membranes containing pores facilitate transport therefore, they are desired in biological applications [173-180]. Recent developments in methods for the preparation of smart responsive polymer membranes and the mechanism of their response to external stimuli with particular attention to the behavior of light responsive polymer membranes was reported in reviews [181,182]. The possibility of an opening or a closing of pores inside the membrane upon the light irradiation or by interaction with different pH of the surrounding solution [183] was taken to the design of polymer capsules used as carriers of therapeutics. The polymer material building the shell of capsules should be sensitive to external actions but not hazardous for the patient. Additionally, the shell should keep capsules intact without their destruction during "smart" activities such as drug release. The transport across the shell by using light to modulate the channel's activity is possibly due to the application of photoswitchable copolymers [184-187] incorporated into lipids bilayers [187] or the doping them with photosensitive amphiphiles [188-195] and using photoswichable lipids (e.g., containing malachite green) [196] or cerasomes with a porous silicate framework containing azobenzene moieties [197]. Light is a useful trigger to manipulate ion channels externally, because does not change the chemical environment of the studied system. The synthetic molecules called "molecular photoswitches" e.g., photocaged small molecules like coumarin derivatives [198] or azobenzenes [199], spiropyranes [200], and malachite green leuconitriles [196] can change their structure and properties upon light irradiation. These dyes are often characterized by having two or more isomeric forms. They are adapting to changing conditions in a reversible manner during illumination with light of a specific wavelength. The presence of dyes in phospholipid bilayers or polymer membrane can modify the shell of capsules by creating light-sensitive ion channels. In the result of a photoinduced charge separation the channel can be opened. For example, the bacterial α-helical channel protein (with 3 nm pore) was converted into a pH-sensitive valve by chemical modulators [201]. The chemical modulator (i.e., sulfhydryl reactive molecules with a photocleavable group as the cage-modulator) was attached to the protein (linked with glycine-22 mutated into cysteine (G22C)). After removal of the protecting group from small photocaged molecules by long-wavelength UV (365 nm) irradiation and photolysis, the channel becomes responsive to the pH of the environment [202]. Furthermore, UV-irradiation of azobenzene molecules promotes the *trans-cis* isomerization at the central double bond, resulting in considerable changes in geometry and polarity [203,204]. Azobenzene is known to exist in *cis* (loose spacing) and *trans* (tight spacing) configurations in dark and light conditions, respectively [205,206]. This reversible

process is controlled both thermally and by irradiation with visible light [207]. The isomerization involves a decrease in the distance between the para carbon atoms in azobenzene from about 9.0 Å in the trans-form to 5.5 Å in the *cis*-form. The modification of the capsule shell by incorporation of light-sensitive molecules such as polymer derivatives of azobenzene [208-211] or coumarin [212] caused changes in the capsule diameter and their illumination. Moreover, the absorbed light was transferred into the local heating of the capsules resulting in increasing permeability of their membranes. Additionally, metal nanoparticles (i.e., Au) inside the shell [213] and IR dyes which doped the outer layer of capsules (e.g., IR-860) [214] allowed to increase the release of the encapsulated compounds. Besides, spiropyrane molecules are very promising as switches. In spiropyrans (SP) [181] the CSP–O bond undergoes heterolytic cleavage upon UV-irradiation (360-370 nm) resulting in the formation of a polar zwitterionic conjugates system as merocyanine (MC) with a large change in polarity. The ring opening can be reversed both thermally and photochemically by irradiation with visible (>460 nm) light. It causes a dramatic increase in surface wettability and the hydrophilicity of the pore lining. This approach is a promising non-invasive method for controlled delivery of therapeutics. Farther, infrared light (750-1000 nm) has been used for releasing encapsulated a hydrophobic molecule from a micellar system containing 2-diazo-1,2- naphthoquinones (DNQ) [215,216]. These groups constitute an attractive trigger because UV light induced Wolff rearrangement of DNQ to a 3-indenecarboxylic acid group with hydrophilic properties enhancing water solubility of that compound. Moreover, infrared light can be applied in photodynamic therapy [217-220] and liposome degradation [221]. Furthermore, mechanopores along the polymer poly(methyl acrylate) backbone (e.g., cyclobutane mechanopores) can be activated in polymers containing a coumarin dimer probe by mechanochemical scisson under pulsed ultrasound conditions (sonochemical) in solid state [222]. The use of force-reactive functional units (mechanopores) has become a promising approach to the development of new stress-responsive materials. Finally, the light activation of hollow capsules with bacteriorhodopsin (bR, 26 kDa) molecules [223] incorporated into the shell was reported by Erokhin et al. [224]. Capsules were prepared by the polyelectrolyte self-assembly technique [225] using alternate layers of positively charged polyallylamine hydrochloride (PAH) with negative charge polystyrene sulfonate (PSS). The captured into the shell the bR (PAH/PSS-bR) caused destruction of a polymer membrane [226]. The LbL adsorption technique demonstrated that the biological activity of the bR embedded in PAH is preserved and not denatured after deposition, because the characteristic absorption of bR at around 552 nm is still observed distinctly. The shell permeability was induced under the illumination with low light intensity (daylight illumination) which caused the local pH change, necessary for the opening of pores and the releasing of encapsulated compounds [227,228]. The average diameter of pores about 400 nm is an important parameter that can be useful for the prediction of the release rate [229]. The bR is polyanion (purple membrane fragments of *Halobacterium salinarium* or *Halobacterium halobium*) [230] with a single-chain polypeptide folded into seven α-helices which contain a single covalently bound chromophore present in every helix [231-233]. Thus, the bR is well-known transmembrane protein working as a proton pump creating a light-driven pH gradient between intracellular and extracellular parts of purple bacteria [234-238]. The bright ion channels embedded in a lipid bilayer (approximately 5 nm thick) control the selective passage of ions and their movements from one side of the cell to the other [239].

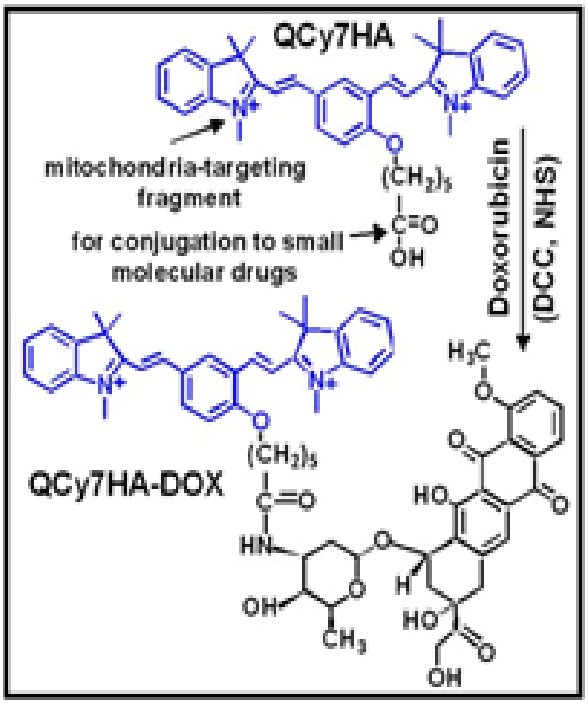

Figure 22: The scheme of synthesis of the mitochondrial-targeting conjugate QCy7HA-DOX (by using NHS: N-hydroxyl succinimide; DCC: *N,N'*-dicyclohexylcarbodiimide).

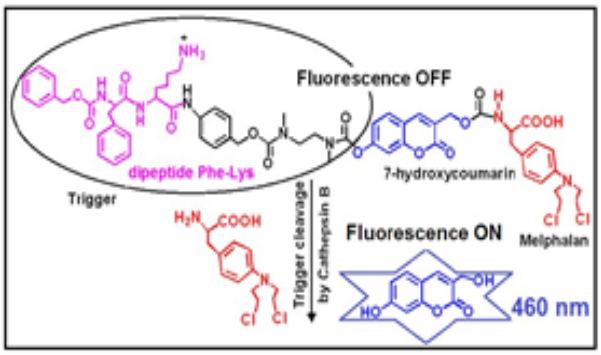

Figure 23: Melphalan theranostic prodrug activated by cathepsin B.

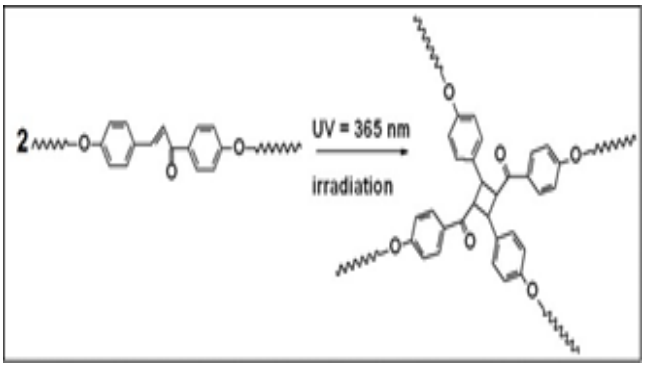

Figure 24: Crosslinking reaction of chalcone groups by UV irradiation.

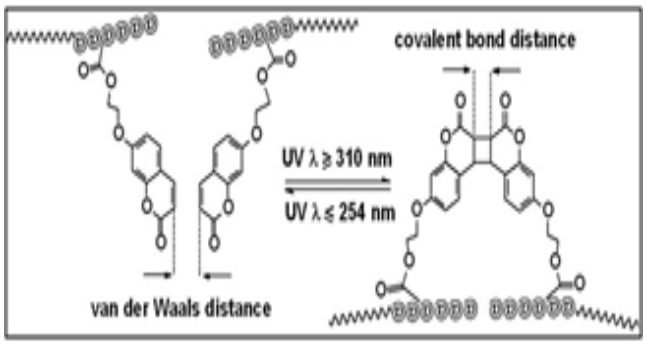

Figure 25: Molecular distance before and after photodimerization and the reverse-dimerization of coumarin derivatives.

The role of caged fluorophores in a polymer carrier design

Chalcone (1,3-diphenyl-2-propen-1-one) moieties upon illumination with ultraviolet (UV=365 nm) light induced photodimerization of two chromophores due to the [$2\pi + 2\pi$] electron transfer cycloaddition reaction [240] can modify polymers resulting in their cross-linking (Figure 24). These versatile molecules can generate photoactivatable fluorescent probes which strategies rely on the photo-"uncaging" of "caged" fluorophores [241]. Fluorescent chalcones give useful potential applications in photoresponsive polymer technology as well as in medicinal prospects in the synthesis of antitumor therapeutics (i.e., nitrogen mustard-linked chalcones) [242].

The most well-known cage molecules belonging to coumarin derivatives are applied in polymeric materials obtained by using dynamic covalent chemistry [243]. The photoreactive coumarin derivative units underwent dimerization (λ=300-350 nm) and the reverse-dimerization (λ=254 nm) by photoirradiation, thus are usually used as a reversible cross-linking point in polymers (Figure 25).

The reversible photodimerization of coumarin moieties undergoes [$2\pi + 2\pi$] cycloaddition during the formation of a cyclobutane ring causes a decline of olefinic moieties (-C=C-) in chromophores and a diminution of the fluorescence emission. Static quenching typically resulted from the formation of non-fluorescent cyclobutane rings between two fluorophores increasing with increasing illumination time. The cleavage of the resulting cyclobutane ring by the irradiation of the corresponding wavelength of light (λ=254 nm) causes de-cross-linking of polymers. Photodimerization of coumarin derivatives units proceeded faster in lower *T*g (glass transition temperature) polymers [244]. The *T*g describes the mobility of a main copolymer chain and it is an essential factor to affect the rate of photodimerization [245-247]. The intramolecular photodimerization is preferred in high *T*g polymers because of the low mobility of a main chain, thus the higher conversion to dimers i.e.,, larger number of cross-linking points [247,248]. Instead, in low *T*g polymers (used e.g., 2-ethyhexyl methacrylate or n-butyl acrylate monomers) the intermolecular photodimerization competed with the intramolecular photodimerization and a performed network is loosely cross-linked. Photodimerization of coumarin derivative units in low *T*g polymers tended to proceed faster than in high *T*g. The release of small molecules *via* the network of cross-linked materials coincides with a change in the mobility of polymer chains which is important to limit passive drug release [249]. The tuning of a polymer's *T*g *via* copolymerization with hydrophobic monomers and varying network cross-linking density has been successfully used to create clinically applicable products such as self-tying sutures and implantable stents. This approach can be investigated for the triggered release of drugs either. Thus, polymer capsules should limit passive diffusion, and release a drug in a repeatable manner with light exposure. So the coumarin-containing amphiphilic diblock copolymer has been explored for functional photocontrollable polymer micelles [250] and nanoparticles [251]. Such micelles could be reversibly cross-linked and de-cross-linked using light at two different wavelengths for the reversible photoisomerization and photocleavage of coumarin derivatives. Kim proposed [252] to modify of the surface of liposomes with the copolymer poly(hydroxyethyl acrylate-*co*-coumaryl acrylate-*co*-2-ethylhexylacrylate). Agarwal et al. [253] synthesized micelle-drug conjugates of {PEO-*b*-poly(*n*-butyl methacrylate-*co*-4-methyl-[7-(methacryloyl)-oxyethyloxy]coumarin)} by covalent bonding of anticancer drug 5-fluorouracil to the coumarin units under UV irradiation. Furthermore, Miksa et al. [198] prepared nanocapsules for 5-fluorouracil delivery decorated with a poly(2-ethylhexyl methacrylate-*co*-7-(4-trifluoromethyl)coumarin acrylamide) cross-linked wall which fulfilled the versatile strategy of release drug combining a long shelf-life with the ability for rapid release using external factors such as light (Figure 26). In this case a monomer of 2-ethyhexyl methacrylate was used as a "linactant" - line active molecule that reduce the line tension thereby modulating the lipid bilayer membrane texture [254-257]. Zhao et al. [257] reported the near-infrared light sensitive polypeptide block copolymer PEO114-*b*-P(LGA0.62-*co*-COU0.38)34 with coumarin moieties which self-assembled into micelles for drug delivery of an antibacterial Rifampicin and an anticancer Paclitaxel. They studied the biocompatible block copolymer composed of poly(ethylene oxide) (PEO) and poly(L-glutamic acid) (PLGA) containing a number of 6-bromo-7-hydroxycoumarin-4-ylmethyl groups. The micelles could be disrupted by λ=794 nm NIR light excitation *via* two-photon absorption [258,259]. Disruption followed from the NIR light-induced removal of coumarin groups from the polypeptide block that shifted the hydrophilic-hydrophobic balance toward the destabilization of the micelles in aqueous solution [260].

Thereafter, spiropyran (SP) is the exciting dye useful for polymeric carriers because it enables a single molecule dual-color fluorescence on-off photoswitching. One molecule alternately emits two distinct fluorescent colors and photoexcitation can switch one fluorescence color to the other [261-263]. The UV illumination induces the spiropyran (SP) to merocyjanine (MC) conversion and switches on fluorescence (Figure 27).

The SP ring-closed form exposure to UV-irradiation (360- 370 nm) undergoes heterolytic cleavage and converts to MC ring-opened mero form resulting in the formation of a polar, zwitterionic conjugated system, which absorbs strongly at λAb.max=570 nm and emits vivid red fluorescence at λEm.max=665 nm [264]. The visible photoexcitation of the MC accelerates the back conversion and returns the photoswiching dye into the off "dark" state. Thus, photoswitchable derivatives of SP were used to fabricate feature-packed polymer nanoparticles (NPs), whose fluorescence color can be optically switched either from one color to another. Li et al. [265] obtained polymer NPs from poly(styrene-*co*-2,2'-*N*-isopropylacrylamide) (PS-NIPAM) containing SP-MC photoswitches and employed the whole polymer particle as a switching unit. NPs are colorless in the SP form and turn to dark blue under UV irradiation at λ=365 nm to emit a strong red fluorescence. These photochromic NPs are capable of undergoing reversible fluorescence photoswitching and demonstrate that on-off switching can be controlled with specific frequencies of light. In aqueous solutions, the fluorophores were protected in the hydrophobic (polystyrene) core of the particle and their fluorescence was unlikely to

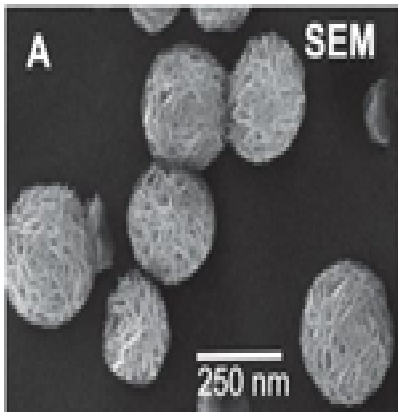

Figure 26: The scanning electron microscopy (SEM) image of nanocapsules with the copolymer wall from a poly(2-ethylhexyl methacrylate-*co*-7-(4-trifluoromethyl)coumarin acrylamide). The polymer nanocapsules were successfully generated due to dimerization of the coumarin moiety, whose content has a large impact on cross-linking and nanocapsules formation. The diameter of the capsules is 250 nm.

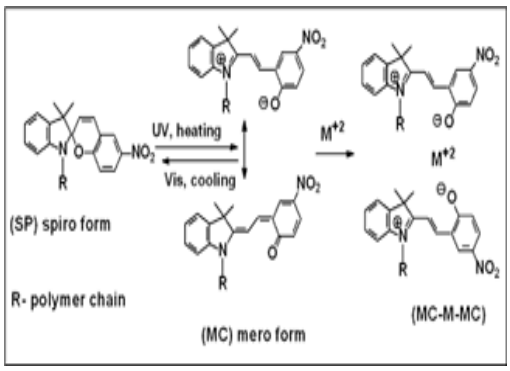

Figure 27: Isomeric structures of spiropyran (SP) and two canonical forms of merocyanine (MC). The dimeric complex of MC with metal ions is also shown.

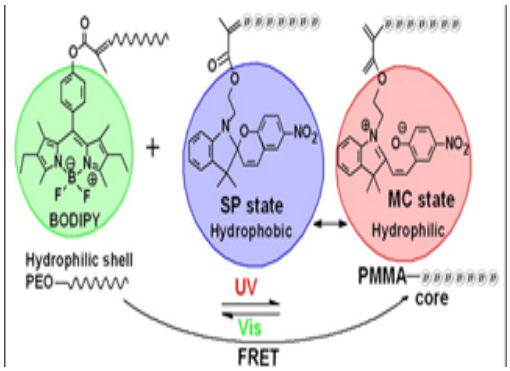

Figure 28: Schematic illustration of amphiphilic NPs *via* covalently combining polymerizably dyes BODIPY-methacrylate with photochromic derivatives spiropyrane methacrylate.

be quenched by components of the biological milieu. The hydrophilic shells of NPs consisting of NIPAM moieties and the water-soluble carboxylic groups from the initiator (4,4'-azobis-(4-cyano-valeric acid)) at the end of polymer chains allowed to incorporate them into the polar cavities of liposomes. Using liposomes as a delivery vehicle, NPs were introduced into HEK-293 cells as biological markers. Li also prepared NPs containing butyl acrylate and acrylamide monomers with a SP single chromophore [266,267]. These optically switchable dual-color NPs binding with HMGA1 proteins undergo endocytosis and they can be identified from autofluorescence of live cells, thus improve a tool for imaging. Furthermore, the SP molecules were grafted onto a diblock copolymer polystyrene-*co*-polyacrylic acid chain (PSPAA-SP) obtained from atom-transfer radical polymerization (ATRP) by using monomers of styrene and *tert*-butylacrylate [268]. Thus, copolymers of PSPAA-SP containing both the hydrophilic and hydrophobic segments self-assembled into nanomicelles in nonpolar solvent (toluene). In this synthesis a dye was embedded in the interior of high polar cores inside the micelles, which can promote the concentration of the MC form. The PSPAA-SP micelles loaded with rhodamine 6G as a model might be used for controlled release of drug substances [269]. Moreover, self-assemblies of amphiphilic poly(ethylene glycol-*block*-spiropyrane methacrylate) (PEG-*b*-PSPMA) [270-272] were a salt-induces (e.g., FeCl3 used as inorganic ions) micelles obtained in a DMF/water (v/v 10 : 1) mixture [273]. The inorganic ions were gathered inside the hydrophobic core which was surrounded by the PEG chains formed the hydrophilic coronae. Upon UV irradiation, the hydrophobic SP units in the cores were isomerized into hydrophilic MC forms. The complex formation between inorganic ions and MC isomers plays a key role in the self-assembly process. The different amphiphilic micelles synthesized from block copolymer spiropyrane-poly(2-methacryloyloxyethyl phosphorylcholine) (SP-PMPC) exhibited superior biocompatibility and were used as smart drug nanocarriers with doxorubicin [274]. The photostable amphiphilic BODIPY-photoswichable fluorescent NPs with SP derivatives were obtained as a result of copolymerization of the methyl methacrylate (MMA) in the presence of PEO as a macro-RAFT agent in the miniemulsion polymerization (Figure 28). Both chromophores were covalently incorporated into polymer backbones and NPs displayed reversible distinct dual-color (green-red) fluorescence by irradiation of UV or visible light *via* occurring switchable interparticle FRET [275]. The fluorescence switching conversion of NPs occurs also thermally in the living A549 cells (human lung carcinoma).

The photoresponsive reversible aggregation and dissolution of rod-coil polypeptide i.e., poly(L-glutamic acid-*b*-PEO) diblock copolymers containing SP as side-chain motif (PLGASP20-*b*-PEO460) was reported by Mezzenga et al. [276]. The PLGA with SP can undergo conformational changes (from α-helix to random coil and *vice versa*) with UV and visible light respectively [277-279]. So, polypeptides are attractive in the biomedical field due to their unique protein-mimetic properties thus micelles can be used in the drug delivery. Recently, the new bi-functional compounds was synthesized, in which chalcone was connected with indolinospiropyran moieties and doped in poly(methyl methacrylate) to increase the stability of photochromic materials [280].

Stimulus Responsive Shell-tuning Capsules for Drug Delivery

The delivery of encapsulated drugs to the target position in live cells requires specifically targeted capsules. Such capsules sensitive to external conditions e.g., magnetic field should contain magnetic particles [281] or they have special receptor molecules like antibodies (Ab) attached to the outer side of the shell [282]. The Ab can be adsorb by electrostatic interactions [283] or covalently liked to surfaces [284-288]. For uncharged materials like poly(ethylene glycol) (PEG) or poly(*N*-vinylpyrrolidone) (PVPON) covalent attachment of the Ab is required since electrostatic attachment is not effective for low-fouling materials because they inhibit nonspecific protein binding.

Moreover, pH-responsive capsules [289,290] linked with glutamic acid residues and containing disulfide groups within the shell or on the surface of polymeric capsules can be gathered into endosomes. The disulfide acts as a linker to attach different functional moieties to the surface of polymer capsules *via* a covalent or noncovalent interaction. Additionally, the cytotoxicity of drugs can be largely decreased by encapsulating them into polymer capsules. Such carriers improve the enhanced permeability retention effect (EPR) of the drugs [112]. The interesting example of self-assembly of molecular components into nanometer scale capsules with irreversible covalent bond formation using photoinitiated thiole-ene "click" reactions was reported by Kim et al. [291]. The synthesis was carried out with (allyloxy)12cucurbit[6] uril as a disk shape monomer embedded with multiple polymerizable groups at the periphery and oligoethylene oxide or alkyl-based dithiols (Figure 29).

Polymer micelles and capsules loaded with fluorescent therapeutic complex-cargoes

The self-assemblies (micelles or vesicles) fabricated from polymeric amphiphiles have a large capacity for guest molecules. Although they are often thermally stable but it has been a great challenge to construct regular capsules with a monomodal distribution. In general, the layer-by-layer (LbL) assembly based on the sequential adsorption of charged species onto an oppositely charged surface (using electrostatic as the main driving force) is the facile method for the fabrication of polyelectrolyte multilayer films on homogenous particle supports from sacrificial spherical substrates [8]. Moreover, the same size distribution of capsules can be obtained after removal of their template. The combination of multilayer structures of capsules providing a high level of control over film properties such as thickness, composition, and nanostructure. This system of the assembly makes the modification of the surface relatively simple for inclusion of compounds with stimuli-responsive properties and enables loading of drugs inside the capsules [287]. The polyelectrolyte capsules for intracellular purposes comprising both therapeutic as well as imaging applications need to be biodegradable. Thus, several degradable multilayers of bio-polyelectrolytes, such as polysaccharides, polypeptides or polynucleotides have been reported by Picart et al. [292]. Lynn et al. [293-301] introduced poly α,β-aminoesters for the fabrication of capsules with degradable multilayers. Harashima et al. [302] reported multifunctional envelope-type-nanocapsules including a nucleic acid core complex with polycations or lipid aggregates and also different polymeric shell structures equipped with specific functional groups binding ligand-targeted agents and cell-penetrating proteins. Polycations are commonly used for gene delivery because they self-assemble and condense DNA into nanoparticles that can be internalized readily by cells [303]. Several vehicles have been created for improving efficiency of delivery small interfering RNA (siRNA) to animal tissues [304]. For example, Davis et al. [305] reported linear cyclodextrin-based polymer (CDP) nanoparticles containing camptothecin. The CDP are embedded with a highly water soluble, neutrally charged backbone containing polyethylene glycol (PEG) with incorporated *β*-cyclodextrins cyclic sugar moieties. Such structures get the ability to form inclusion complexes with hydrophobic drugs within the center of its cup-ring. As a result macromolecular prodrugs self-assemble into nanoparticles. Moreover, Davis's group of researchers developed of effective anticancer therapies (against the EWS-FLII gene) by using a cyclodextrin-containing polycation (endowed with imidazole groups) binding with siRNA and a human transferrin protein (Tf) as a target ligand. Terminal imidazole groups assist in the intracellular trafficking and release of the nucleic acid [306]. The

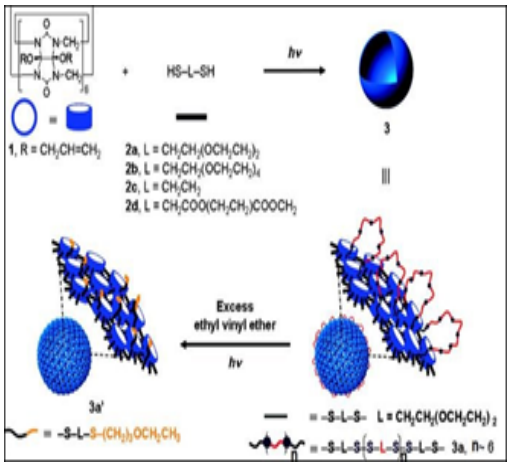

Figure 29: The scheme of the synthesis of polymer nanocapsules from $(allyloxy)_{12}$cucurbit[6]uril as a disc shape monomer and alkyl-based dithiols.

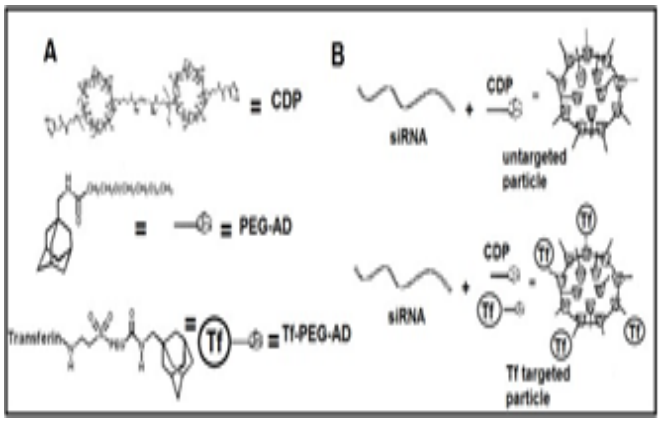

Figure 30: Schematic illustration of delivery system. A) Components: The CDP condenses siRNA and protects it from nuclease degradation. The AD-PEG conjugate stabilizes the particles in physiologic fluids via inclusion compound formation. The Tf-PEG-AD conjugate confers the targeting ligand to particles (CDP), promoting their uptake by cells. B) assembly of nontargeting and targeting polyplex particles.

formulation of particles rely on mixing the components together and allowing for further the self-assembly process. The surface of colloidal particles was covered with PEG *via* inclusion of terminal adamantine (PEG-AD) into cyclodextrins. Some of PEG chains contained targeting ligands (AD-PEG-Tf) for specific interactions with cell-surface receptors (Figure 30).

Additionally, the stabilization of the surface of particles *via* thiolated polyethylene glycol (PEGSH) with the terminal adamantine allowed to bind cyclodextrins with a more multivalent way. The administration of siRNA using a targeting ligand Tf was possible with a 5 nm gold particle (λEm=507 nm) that was capped with the thiol group of PEGSH at the end distal to the adamantine (AD-PEG-Au) [307]. So, specific hydrophobic drugs are suitable dwellers in *β*-CDs cavities (e.g., doxorubicin [308,309], camptothecin, paclitaxel, fluorouracil) [310]. The introduction of light sensitive chromophores like azo-groups, or a redox ferrocene (Fc) moiety, and pH- sensitive dansyl residues, or a benzyl moiety allowed to control CDs conjugates by temperature and obtained stimuli-responsive switching sol-gel systems [311]. The reversible association/dissociation of the polymer

sol-gel transition under an external stimulus can alter the cross-link density of CDs conjugates [312-314]. There are a few examples of nanoassemblies prepared from diblock hydrophilic copolymers i.e., the PEG-*b*-polyaspartamide carrying *β*-CDs units on the side chain which created inclusion complexes with hydrophobic molecules (pyrene, coumarin 102 and indomethacin – an anti-infammatory drug) [310]. Furthermore, the hydrophobic poly(*ε*-caprolactone) (PCL) unit was connected with the hydrophilic diblock poly(*N*-isopropylacrylamide-*co*-*N*-acryloxysuccinimide) segment by the *α*-*β*-CDs dimer used as a "bride" [315]. These components formed noncovalently integrated self-assembly micelles obtained through host-guest interactions between the *α*-*β*-CDs dimer and the guest molecules (rhodamine B and fluorescein isothiocyanate). The both dyes were functionalized respectively with the hydrophilic (PEG-FITC) and the hydrophobic (PCL-RhB) segments and switched on after removing the PEG segment in sites of a tumor because of the thermoinduced phase transition (T>37°C, pH<6.8). The addition of a short peptide (Arg-Gly-Asp) as a target ligand to these micelles improved their cell uptake efficacy [315]. Moreover, dextran (Dex) based microgels e.g., dextran-hydroxyethyl methacrylate (Dex-HEMA) could easily be loaded with macromolecules such as proteins and dyes (FITC) as well as latex nanoparticles (NPs, 20kDa) labeled with dyes [316-319]. The bio-polycation i.e., a poly-L-arginine (pARG) labeled with rodamine B isothiocyanate (RITC) or tertramethylrodamine isothiocyanate (TRITC) can form coatings on the Dex-HEMA microgel yielding a clear red fluorescence [320,321]. The microgels with a cationic surface charge due to the addition of dimethyl aminoethyl methacrylate (DMAEMA) can be subsequently coated with four bilayers of poly(styrene sulfonate)/diazoresin (PSS/DAR)4. Upon light irradiation the cationic diazo groups of DAR form a covalent bond with the anionic sulfonate groups of PSS resulting in a cross-linked multilayer structure with a semipermeable membrane [322]. When the microgel core degrades through the hydrolysis of the carbonate esters which link the polymerized methacrylate groups to the dextran backbone, the swelling pressure increases. Thus, the surrounding rigid membrane ruptures and the encapsulated material is released from the exploding microcapsule. Such self-exploding microcapsules may find advanced applications in many fields for example as a "single shot" vaccine delivery system and release antigens enclosed in microgels [323]. Additionally, cationic nanogels for therapeutics were prepared in an inverse miniemulsion photopolymerization method from dextran and [(2-(methacryloyloxy)ethyl)trimethylammonium chloride] with 2-aminoethyl methacrylate hydrochloride. These nanogels were loaded with a negatively charged conjugate of AlexaFluor 488-labeled 25/27–mer siRNA [324]. Then, neutral nanogels were consecutively PEGylated by using NHS (*N*-hydroxysuccinimide) activated methoxyPEG5000 propionic acid and such hemocompatible dextran nanogels were used in the intravenous delivery [324-326]. Furthermore, the efficient delivery of deoxyribonucleic acid plasmid DNA (pDNA) to the nucleous of cells becomes easier especially in the presence of chromatin targeting peptides, which enhance the nuclear inclusion and a probability that DNA can be passed on during subsequent cell divisions in gene therapy. The preparation of the red fluorescent pDNA labeled with an intercalating hydrophobic far-red cyanine dye Cy5 (mono-reactive NHS ester) allowed to obtain the complex of Cy5-pDNA/peptides which was encapsulated and *co*-delivery with lipid-based carriers. The pre-condensation of pDNA with peptides improves lipid-based delivery systems and transfection efficiencies [326]. At last, by using LbL method Caruso et al. [284-288] synthesized redox-active polymeric microcapsules with the cross-linked shell containing disulfide bonds for the delivery of a siRNA targeting to PC-3 prostate cancer cells. The polycation-polylysine (PLL) for a siRNA complexation was infiltrated into the pores of nanoporous silica particles prior to an assembly of layer from the negatively charged poly(methacrylic acid) with thiol-modified groups (PMASH). The core was dissolved after the cross-linking of deposited the PMASH layer. In these PMASH-PLL microcapsules, the layer of PMASH was labeled with AlexaFluor 488 (with a green fluorescence) and PLL by using TRITC (with red fluorescence). The negatively charged siRNA cargo was postloaded into performed microcapsules by a diffusion through the multilayer film and formed complex with the positively charged amino groups of PLL. The complexation of siRNA inside the cavity of microcapsules prevents it from leaking, thus the PLL/siRNA polyplex covered with the multilayer film was shielded from the direct effects of a milieu. The PLL-siRNA complexes can be released when disulfide bonds in the membrane are broken by pore-forming GSH, then the PLL can be enzymatically degraded within cells into the amino acid lysine [288]. According with the LbL method the similar redox capsules were prepared but amine-functionalized silica particles as templates were used for coating by alternately assembled the PMASH layer and poly(vinylpyrrolidone) (PVPON). In the acidic conditions at pH 4 the integrated shell with hydrogen-bonded networks was formed. The siRNA cargo was preloaded onto the template particle before a preparation of multilayer films. The disulfide bridge was produced by oxidation thiols using chloramine T and after cores removal (with HF) the film was washed into a neutral pH solution, in which the PVPON was released. In this way microcapsules were filled with an uncomplexed siRNA [288]. In addition, Jin et al. [327] reported magnetically vectored nanocapsules based on polystyrene seeds with incorporated Fe_3O_4 surrounded by porous SiO_2 shells. The polystyrene core was removed by dissolving or burning polymeric materials within the capsule and anticancer drugs (CPT or DOX) were loaded. Such obtained capsules for tumor penetration allowed a controlled on-off switchable release of an anticancer cargo. Thus, the remote RF magnetic field induces magnetic particle (Fe_3O_4) heating and makes the localized temperature inside the capsule rise. The resultant temperature gradient between inside versus outside of the capsule is likely to be the key element that stimulates accelerated diffusion and drug release.

Polymer capsules containing the fluorescent shell

One of the most interesting feature of the LbL technique is that it allows different macromolecular species for molecular self-assembly on a nanometer length scale. This method enables the arrangement of "reactants" (e.g., optically active molecules with chemically reactive functional groups) at a molecular level to create theranostic tools with *co*-operative chemical sensitive and optical fragile properties. For example, the incorporation of a dye (e.g., anionic Congo Red) [328] into layers is affected by size, number of charge and spatial orientation of dye molecules, thus enables one to use it as a probe to obtain detailed information about local features such as a polarity and molecular mobility [329,330]. Further works in this area demonstrate that the formation of capsules with a polymer shell containing different segments can enhance drugs loading and modify the release of drugs by sequestering their molecules in both the core and shell compartments. For instance, decomposable hollow capsules were obtained by adsorption of sperimidine (which is a low molecular weight organic polyamine) alternately with DNA on colloids ($MnCO_3$ particles). The multilayers DNA/spermidine formed the shell of capsules then a templated core was removed with acid [331-335]. DNA is negatively charged due to the phosphate group in its backbone, while a sperimidine in its ionized form contains three positive charges. Sperimidine forms complexes with DNA which can be suppressed by increasing the monovalent salt (NaCl) concentration [336-339]. Thus, a

decomposition of hollow bio-capsules can occur readily upon exposure to the sodium chloride solution. Such capsules may be exploited for the release of many other encapsulated compounds such as dyes or drugs. So, selecting a composition of the capsules wall by using e.g., rhodamine-labeled DNA [332] can provide tailored delivery vehicles with a specific targeting capability. Moreover, the anionic dye pyrene chromophore (i.e., pyrenetetrasulfonic acid) (4-PSA) which exhibits four negative charges forms a complex with cationic polyelectrolyte chains with a very high binding constant [340]. Thus, 4-PSA was sequentially deposited in polyelectrolyte-dye thin films consisted of alternating poly(allylamine hydrochloride) (PAH) with poly(styrene sulfonate) (PSS) multilayers films [341,337]. So, binding of 4-PSA moieties to the polyelectrolytes causes changes in their fluorescence emission. The excitation spectra of probe molecules which form excimers in polymer systems were seen as a broad structureless fluorescence band centered around λEm.=500 nm. This phenomena was explained by sequestering 4-PSA in the polyelectrolyte which caused an increase of the local concentration of probe molecules along the polymer chain that promoted an excimer formation and a quenching of dyes fluorescence emission [340]. The similar phenomena connected with excimer formation was observed in the case of coumarin 6 dye molecules incorporated within the cross-linked poly(styrene-*co*-divinylbenzene) shell of polymer capsules which can be used for imaging [187] (Figure 31).

The application of the 6-carboxyfluorescein (6-CF) dye in the presence of polyelectrolytes such as: PAH, poly(diallyldimethylammonium chloride) or (PDADMAC), poly(diallyldimethylammonium chloride-*co*-acrylamide) or (DADMA-acrylamide) copolymers can induce a fluorescence self-quenching of 6-CF due to increase probe-probe interactions [341]. Furthermore, the FITC dye can label PAH polymers and the following FITC-PAH was deposited in the polyelectrolyte poly(styrene sulfonate) PSS films [342]. The permeability of the PAH/PSS film was measured after incorporation of the FITC molecules to the polymer in which fluorescent moieties were embedded in a defined, variable depth inside the film. The dye rhodamine B (RhB) was chosen as the quencher molecule for penetrating barriers in the film. The diffusion of probes RhB through layers caused a decrease of fluorescence intensity thus gave information on its depth and transport phenomena in films. The FITC emission (at λmax.=527 nm) decayed simultaneously with an increase of rhodamine fluorescence

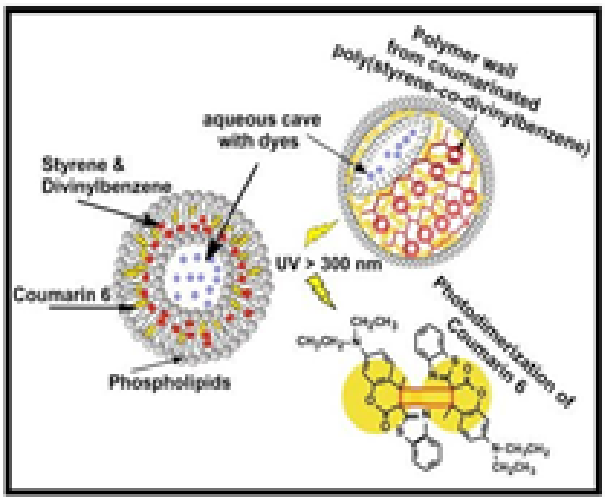

Figure 31: Nanolipopolymersomes with a nanometer-thick fluorescent film from cross-linked poly(styrene-*co*divinylbenzene) embedded with coumarin 6 moieties.

(at λmax=583 nm) and the energy transfer occurred from fluorescein to rhodamine *via* dipole-dipole interactions with an interaction radius about 60 Å (Förster energy transfer). The different mechanism of quenching was obtained with the smaller molecule 4-hydroxy-2,2,6,6-tetramethylpiperidine 1-oxide (TEMPOL) as a quencher (fluorescent intensity was integrated at λEm=515-550 nm). The spin label TEMPOL enhances the spin-orbit coupling in the FITC dye with an interaction radius of 6 Å (paramagnetic quenching). So, electrostatic attraction and a binding of ionic probes to oppositely charged polyelectrolytes is manifested by quenching of the fluorescence emission, the appearance of excimer emission, and changes in the probe fluorescence excitation and absorption spectra. Besides, a combination of LbL assemblies with "click chemistry" allowed to obtain covalently stabilized hollow capsules from biodegradable polymers with modified alkyne and azide moieties e.g., poly(L-lysine) (PLL) with properties promoting a cell adhesion and biocompatible poly(L-glutamic acid) (PGA) [285]. Capsules were postfunctionalized due to monolayers deposition from heterobifunctional poly(ethylene glycol, PEG) i.e., NHS-PEG3500-biotin and NHS-PEG2300-OMe (with *N*-hydroxy-succinimidyl ester at one end and methoxy-terminated group) that provided low-fouling properties and simultaneously enhanced specific protein binding. The combination of "click chemistry" and LbL provides flexibility to design materials with tailored properties to better target these materials for various diagnostic and therapeutic applications. Thus, PLL-Alk, PGA-Alk (with alkyne functionality) and PLL-Az, PGA-Az (with azide functionality) were fluorescently labeled with red rhodamine B isothiocyanate (RITC) or green AlexaFluor 488 *N*-hydroxy-succinimidyl ester respectively. The low level of adhesion drug molecules to blood proteins and their long circular times in the bloodstream are very important in drug delivery applications. Therefore, adsorption of proteins e.g., fluorescent labeled bovine serum albumin (BSAFITC) (the most abundant plasma protein in coow's blood) and streptavidin (SAFITC) (due to its high affinity to the biovine) on the surface of capsules was analyzed by the use of flow cytometry [285]. In addition, an antibody (Ab) was functionalized with an azide (Az) by coupling a linear bifunctional NHS-PEG2000-Az polymer with a succinimidyl ester group at one end which was active toward the lysine. Moreover, efficiency of the functionalization of polymer capsules from poly(vinylpyrrolidone) (PVPON) endowed with alkyne moieties (PVPONAlk) with azide-functionalized human monoclonal antibodies (huA33mAbAz) by using "click chemistry" was qualitatively monitored by flow cytometry [286]. The activity of the immobilized antibody was confirmed by incubating these capsules with the AlexaFluor 488-labeled A33 antigen that could bind specifically to huA33 mAb. The efficient click functionalization of capsules in the presence of a Cu(I) chelator prevented antibodies from aggregation. These functionalized capsules showed highly specific binding to cancer cells. Furthermore, silica "nanobubbles" similar to hollow nanospheres were synthesized by using the core-shell/gold-SiNPs method [343]. These structures used as nanocontainers for drugs could also be applied to a wide range of fluorescent probes. For instance, FITC molecules approximately in 25% modified the surface of colloidal gold nanoparticles by reversible dyes chemisorption. The rest of the available surface was covered with bifunctional amino-silane molecules (i.e., 3-aminopropyltrimethoxysilane, APS) used as a "primer" which introduced hydroxyl groups prior to silane deposition but the amine group of the primer molecule bound to the gold particle. Hydrolysis of the surface-bonded siloxane moieties formed silane triols which allowed condensation of silica over the particles. The gold core was removed by diffusion of cyanide ions (NaCN) through the porous silica shell. Thus, the fluorescent molecules remained inside the

water-filled silica capsules were isolated from the external environment [344]. In other words, the direct attachment of a probe molecule to the gold surface before construction of the silica shell, allows the probe to remain inside the silica shell at the internal water-silica interface, after dissolution of the gold particle.

Bio-inspired poly(dopamine) capsules with a fluorescent shell

The metal-organic film i.e., a natural polyphenol [345,346] containing tannic acid (TA) and Fe^{+3} due to non-covalent coordination complexes can fulfil the criteria required for a dual-functional shell of capsules (Figure 32) [347]. Capsules with the metal-phenolic network (MPN) shell were synthesized by the complexation between the organic ligand deposited on removable - sacrificial templates and inorganic metal ions as a cross-linker that produced robust nanoscale coordination layers [348,349]. Such films are structurally rigid but could respond to external stimuli and they can be degraded under cytocompatible physiological conditions.

The fluorescent shell of capsules from poly(dopamine) (F-PDA) [350,351] was obtained *via* the polymerization of dopamine i.e., 3-hydroxytyramine hydrochloride (Figure 33) on sacrificial templates ($CaCO_3$ or SiO_2 nanoparticles) in the presence of H_2O_2. The removal of templates (by using ethylenediaminetetraacetic acid (EDTA) or HF respectively) allowed capsules to retain their spherical shape and the well-defined size. The F-PDA shell was pH- dependent and exhibited a broad range of intrinsic fluorescence from λ=350 nm to λ=600 nm with the maximum of fluorescence intensity at pH 3.

However, PDA slowly degrades, thereby its application in therapeutic delivery is limited. Therefore, a polyanion endowed with catechol groups i.e., a poly(acrylic acid-*co*-dopamine) was used as a building layer for LbL assembly together with a polycation i.e., poly(allylamine hydrochloride) [352]. Furthermore, the stimuli-responsive (pH-induced) capsules with a doxorubicin (DOX) conjugated to a thiolated poly(methacrylic acid) (PMASH) were obtained due to the alternately deposition of conjugate and PDA. So, a maleimide derivative of DOX with hydrazine groups was attached to PMASH by a pH-cleavable hydrazone bond [353]. Then, the polymer-drug conjugate was immobilized on the PDA wall of capsules *via* the thiol-catechol robust reaction. Thus, in a milieu at pH 5.0 only the DOX was released. Moreover, the adjunctive fluorescent labeling of PDA-DOX capsules by AlexaFluor-488 C5-maleimide (AF488mal) allowed to indicate locations of capsules after cellular uptake due to their direct visualization. The labeling also helped to circumvent the problem with broadband absorption of PDA in the ultraviolet and visible light regions [353]. Therefore, modifications of PDA by reactions with thiols and amines *via* Michael addition or Schiff base formation influence on excellent biocompatibility and low cytotoxicity of that polymer and enable to use polymer capsules in an anti- cancer therapy (Figure 34) [354-357]. Besides, $CaCO_3$ particles mixing with DOX and covered with the poly(styrene sulfonate) (PSS) layer formed templates which were stabilized by different: electrostatic, hydrogen bonding and hydrophobic interactions. Then, the outer layer on their surface was formed by subsequently deposited TA-Al^{+3} molecules. The template was dissolved in a typical way and monodisperse DOX-loaded MPN capsules (DOX-Al^{+3}-TA) were created.

The formation of coordination bonds between polyphenols and Al^{+3} is pH-dependent, and the stability of the capsules Al^{+3}-TA is generally decreasing in pH 5.0, thus at physiologically relevant pH values (7.4 - 5.0). The strong fluorescence of capsules came from encapsulated DOX (red) and also from the Al^{+3}-TA shell labeling with FITC-bovine serum albumin (green). Moreover, other drugs (Irinotecan,

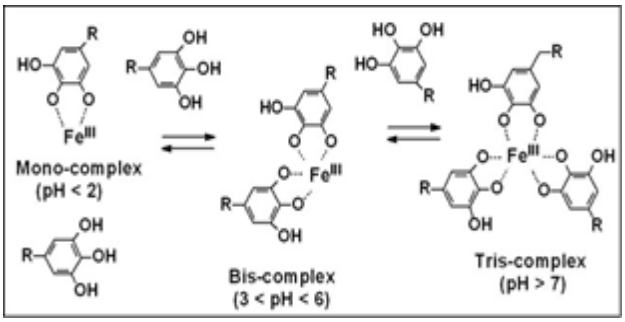

Figure 32: pH-responsive Fe^{III}-TA complexation state in which R represents the remainder of the TA molecule.

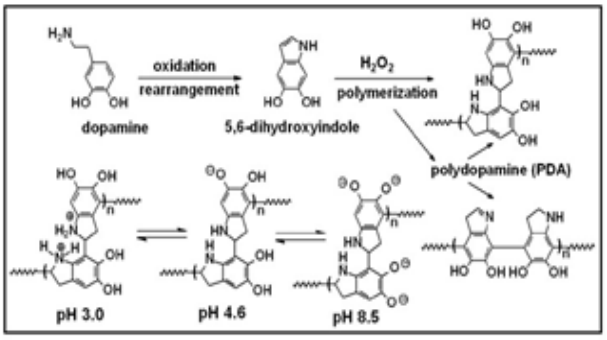

Figure 33: The suggested structure of polydopamine and the response to pH.

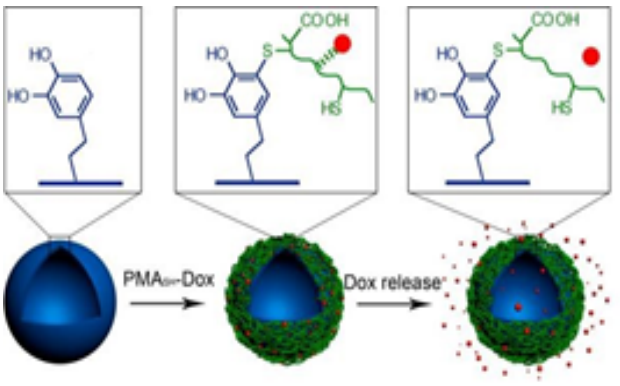

Figure 34: Immobilization and pH-responsive release of DOX from PDA capsules. The red dots represent DOX.

Topotecan, Verapamil) can also be loaded within MPN capsules by using this method. The ability to incorporate multiple metals into MPN capsules demonstrates their diverse applications including drug delivery, positron emission tomography (PET), magnetic resonance imaging (MRI), biomedical imaging and catalysis [358]. Furthermore, a synthetic PEG-polyphenol derivative was prepared as a result of the PEG-NHS reaction with dopamine hydrochloride and then used it as a building layer [359]. Such obtained the conjugated polymer was labeled with AlexaFluor 488-cadaverine (AF488cad) to visualize the polymer shell after deposition on $CaCO_3$ particles which were loaded dextran-FITC or a AF488-biovine serum albumin. After removal of $CaCO_3$ templates by using ethylenediaminetetraacetic acid (EDTA) obtained capsules were covered with the PEG shell endowed with multiple

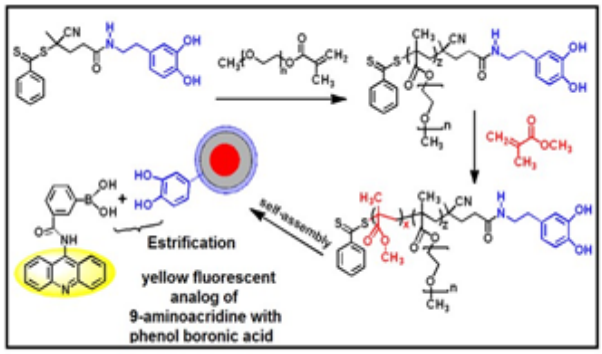

Figure 35: Micelles containing catechol groups on the surface conjugated to 9-amino acridine *via* boronic acid ester.

catechol groups. They allowed the formation of MPN films due to the multivalent coordination Fe^{+3} bonding. The color of the mixed PEG-polyphenol-Fe^{+3} complexes changed progressively from colorless, green, blue, purple to red when the pH was gradually increasing from 3 to 11. The color change was attributed to the transition of coordination complexes from mono- to bis- to tris-catechol complexes. The pH-dependent stoichiometry of the PEG-polyphenol-Fe^{+3} complex allowed the formation of stable coordination networks at physiological pH 7.4 and enabled their disassembly under mild acidic conditions. The pH-dependent encapsulation and release of small molecules (e.g., methyl orange, alizarin red, rhodamine 6G) were observed as a model [360,361]. At last, a reversible addition fragmentation chain transfer (RAFT) polymerization based on dopamine as a catechol-terminated RAFT agent and used subsequent oligo(ethylene glycol methyl ether methacrylate) (OEGMEMA) after chain extension with methyl methacrylate monomer (MMA) allowed to form the block copolymer POEGMEMA32-*b*-PMMA71 which self-assembled into micelles (Figure 35) [362].

Micelles with dopamine functionalities (containing catechol groups) on the surface can readily react with an analog of 9-amino acridine dye functionalized with a phenol boronic ester. The reaction between phenylboronic acid and 1,2-dihydroxyl functionalities (catechols) *via* a reversible boronate ester formation is described in literature [363]. Such labeling and traceability of capsules allowed direct monitoring of the yellow fluorescent complex in the cell. Thus, boronic acid ester conjugate polymer with dopamine was used as a tool for bioconjugation and visualization of cell apoptosis [364]. Moreover, these micelles loaded with highly efficient anti-cancer drugs (Oxoplatin and Abendazole) are recommended in therapy.

Silica Nanoparticles for Bioimaging in Therapy

Dye-doped SiNPs as labeling reagents have been used for imaging and detecting biological agents due to the attachment of sensitive biorecognition molecules (e.g., antibodies) to the silica surface through bioconjugation chemistries [365-369]. One of the greatest advantage of dye-doped SiNPs is a large number of fluorescent dye molecules encapsulated into nanoparticles, thus they provide high-quality luminescent signals and can serve as a probe with excellent photostability. The synthesis of organic-dye-doped SiNPs as dots with an uniform shape and size can be carried out by a) the Ströber method [370] and b) the reverse-micelle method which is known as the water-in-oil (W/O) microemulsion system with a negatively charged surfactant (e.g., polyoxyethylene (10) isooctylphenyl ether (Triton X-100), dioctyl sulfosuccinate sodium salt (AOT), polyoxyethylene (5) nonylphenylether (NP-5)) [367]. In both methods, the dye-doped SiNPs are photostable and exhibit amplification of an emission signal of chromophores. Ströber's method [371] depends on the hydrolysis process of a silica alkoxide precursor [$Si(OR)_4$] (i.e., tetraethyl orthosilicate, TEOS) in ethanol with addition of ammonium hydroxide in a water solution. The silicic acid is produced during hydrolysis and, when its concentration is above its solubility in ethanol, it nucleates homogeneously and forms silica nanoparticles. So, Van Blaaderen et al. [372] according with this method synthesized organic-dye-doped SiNPs. They incorporated hydrophobic rhodamine 6G molecules inside the SiNPs by using two compounds as precursors with a different lipophilicity i.e., more hydrophobic phenyltriethoxysilane (PTES) [$PhSi(OCH_3)$] which keeps the organic dye in the silica matrix and [$Si(OR)_4$] (TEOS) which can turn into a hydrophilic comopound, thus it allows obtained SiNPs to be dispersed in an aqueous solution [373]. All SiNPs have approximately the same size and composition but selected dyes (e.g., fluorescein, pyrene) [374,375] might exhibit different photophysical properties [376]. The silica matrix provides embedded dyes an effective barrier to protect them against the surrounding environment and both photobleaching and photodegradation phenomena can be minimized [377]. Van Blaaderen et al. [372] used also direct coupling of FITC dye molecules to the silane reagent (3-aminopropyl)triethoxysilane (APTS) by a covalent bonding to incorporate chromophore into the silica matrix. Moreover, different tracer nanoparticles embedded with photochromic dyes (e.g., *ortho*-nitrostilbene, rhodamine B, coumarin 343, pyrene) that molecules were covalently bound with reactive groups of (chlorobenzyl) trimethoxysilane as a core precursor can be synthesized and they form SiNPs with a core-shell architecture [378]. Therefore, the fluorescence intensity of the labeled SiNPs depends on dye concentrations, since reabsorption effects due to an overlap of absorption band influence on the fluorescence emission spectrum ("self-quenching"). However, the mobility of dye molecules i.e., their rotation inside the SiNPs is hindered by the silica matrix (caging effects) [376]. Moreover, covalent immobilization of dyes may cause an increase of the fluorescence quantum yield due to suppression of the radiationeless-decay pathways. Thus, the fluorescence intensity per dye molecule increases as the thickness of the protective shell rises, because of lower mobility of the dye labels incorporated inside the spheres. As a result, the photoemission intensity of dyes increases due to the loss of their molecular degrees of freedom [379]. In addition, the local environment (polarity effects) also influence on the intensity of fluorescence spectra. The synthesis of fluorophore-doped core-shell SiNPs can protect the fluorophore from environmental factors because dyes were shielded inside a certain shell matrix, thus the fluorophore still demonstrated the fluorescent characteristics. On the contrary, poly(organosiloxanes) spheres with the porous shell and a dye molecule inside a pore did not change the fluorescent emission characteristic of the free dye, because the local polarity of the pore environment is not differ very much from the polarity of the pure solvent. Thus, SiNPs containing a few labels protected by a relatively thick poly(organosiloxane) shell and therefore well embedded within the network of the core, show the highest fluorescence yield per single label [376]. In contrast, SiNPs with thinner shells containing dyes closer to the particle surface are more mobile, thus can exhibit a decrease of the fluorescence yield. This method to prepare the well-defined SiNPs is much simpler than the preparation of micelles from dye-labeled block copolymers or other nanosized tracers with a core-shell topology in which dyes were loaded through the diffusion [380]. Moreover, the major disadvantage of dye-labeled tracers with labels attached directly to the particle surface would allow

dyes to escape by a simple diffusion, thus the synthesis of particles with core-shell topology according with Van Blaaderen method allowed to minimize such effects [372]. Different types of functional groups like e.g., amine in APTS and thiols in (3-mercaptopropyl)triethoxysilane (MPTS) can be introduced onto the surface of SiNPs and conjugated biomolecules and reactive dyes containing functional groups [375]. In addition, the properties of the silica surface makes SiNPs chemically inert and physically stable [374], so they are excellent labeling reagents for bioanalysis and bioimaging [381-385]. The second strategy of the preparation SiNPs [386] depends on the polycondensation of TEOS in a water-in-oil (W/O) microemulsion with the addition of surfactants (e.g., Triton X-100). In this process water nanodroplets in solvents (e.g., cyclohexane) work as nanoreactors to form reversed micelles which are converted into nanoparticles [385]. Thus, the ammonium hydroxide solution (NH_4OH) initiates the hydrolysis of $Si(OR)_4$ and the polycondensation process of the silane species carries out in "water pools" of reverse micelles. The TEOS molecules which are not amphiphilic are compartmentalized in the bulk oil phase but after hydrolysis they are translocated to the micellar phase. So, the $Si(OR)_3(OH)$ species would be located in the palisade surfactant layer (e.g., Triton X-100) but $Si(OH)_4$ in the water pool. Depending on the lipophilicity of dyes they can be entrapped in an unaggregated form inside the silica pores like e.g., hydrophobic tertamethylrodamine (TMRA) linked to a hydrophilic dextran molecule (TMRA-dextran) [383]. Likewise, luminophore tris(2,2'-bipyridyl)dichlororuthenium (II) hexahydrate (Rubpy, λEx=458 nm λEm=594 nm) with methylene blue which formed a FRET pair of the model donor-aceptor [368,382] doped SiNPs. This model was used as a probe of leukemia cells [387]. Furthermore, analogues of cyanine dye-APTS were usefully employed to produce fluorescent SiNPs [379,387]. Derivatives of cyanine NHS-ester dyes containing sulfonic groups on the indoleninic rings introduce a hydrophilicity to fluorophores that labeled APTS. In this case SiNPs doped with cyanine dyes e.g., Cy5, NIR-664-*N*-succinimidyl ester (λEx=672 nm λEm=694 nm), AlexaFluor 670 and squaraines which have a fluorescence maximum excitation greater than λ=650 nm can be widely used in life science because in the NIR region an autofluorescence of bio-markers is much reduced. The versatility of this approach enables incorporation of various classes of fluorophores that cover the entire UV-vis absorption and emission spectrum [388]. The SiNPs with incorporated organic dyes: AlexaFluors (350, 488, 555, 568, 680, 750), *N*-(7-(dimethylamino)-4-methylcoumarin-3-yl), FITC, TRITC, Texas Red are illustrated in Figure 36. These highly fluorescent SiNPs with the core/shell architecture consisting of a fluorophore-rich center protected within a siliceous shell fulfilled requirements of a quantum dot brightness level (referred to as CU) [371,389]. They exhibit more than two orders of magnitude improvement in fluorescence intensity compared with a single dye molecule [390].

The potential of these silica dots as markers for biological imaging was demonstrated to label of FcεRI receptor of rat basophilic leukemia (RBL) mast cells [388]. The positively charged biomolecules (e.g., IgG, polylysine) conjugated Cy5 were used as a core material which was coated with a silica shell [391]. These Cy5-IgG-doped-core/shell-SiNPs as a NIR fluorescent marker (λEx=653 nm, λEm=667 nm) selectively recognized the breast cancer cells. The biological modification of SiNPs depends on the activation of their surface by using the cyanogen bromide (CNBr) method then coupled the C-erb-B2 antibody [392]. The simlar method [393] was developed with the Au colloid core which exhibited strong chemisorption of the thiol functional groups of oligonucleotides labeled with cyanine dyes Cy5 (λEx=630 nm) and Cy3 (λEx=543 nm) molecules. The probes were formed by coupling of the fluorophore with e.g., alkanethiol oligonucleotides (5'-thiolated (dT)20-Cy5 and 5'-thiolated (dT)20-Cy3) to Au seeds. The use of oligonucleotides (dT)20 as a spacer arm allowed to avoid the proximity of fluorophores to the Au surface thus effectively prevented fluorescence quenching. Moreover, the class of cyanine dye doped-gold/core covered with silica/shell NPs provided a well-built doping mechanism which allowed to keep the problems of dye leaking off and limited a different amount of dye molecules in individual SiNPs. So, the host colloidal gold stability is preserved by the deposition of a thin silica shell which was produced from the hydrolysis of organosilane MPTS/TEOS. These SiNPs were directly coupled with the signaling probes of DNA by using the heterobifunctional cross-linker sulfo-KMUS endowed with NHS ester at one end (reacted with primary amine formed amide bond)

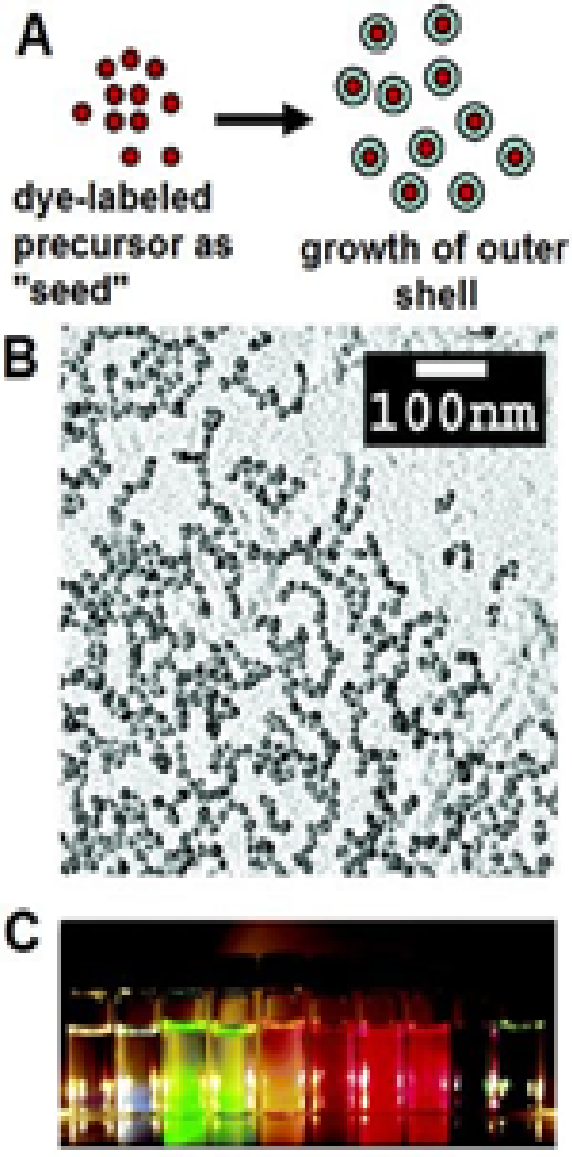

Figure 36: (A) Schematic representation of the synthesis of coreshell fluorescent silica nanoparticles. (B) The image of 30 nm particles prepared by transmission electron microscopy (TEM) C) Fluorescent core-shell SiNPs doped organic dyes described respectively from left to right: Alexa 350, *N*-(7-(dimethylamino)4-methylcoumarin-3-yl), Alexa 488, FITC, TMRITC, Alexa 555, Alexa 568, Texas Red, Alexa 680, Alexa 750.

and a maleimide group at the other end (reacted with a thiol to form a stable thioether bond). However, this method is complicated and expensive because of the thiolated oligonucleotide. Other silica probes doped with far-red fluorescent cyanine dyes (Cy5 and FR670) were also reported [394]. At last, the MnO nanoparticles offer an excellent matrix to accommodate optical imaging modalities by coniugation NIR dyes [395]. The carboxyl silane *N*-(trimethoxysilylpropyl)ethylene diamine triacetic acid trisodium salt) (TETT) can modify of the manganese oxide-oleate complex (MnO-AO) to MnO-TETT. Obtained nanoparticles were coniugated to the water-dispersible PEG-Cy5.5 (achieved as a result of the reaction H_2N-PEG500-NH_2 with Cy5.5-NHS) in the presence of ethyl(dimethylaminopropyl) carbodiimide (EDC) and *N*-hydroxy succinimide (NHS). These MnO-PEG-Cy5.5 nanoparticles were used in magnetic resonance (MR) and NIR fluorescence as dual-modal imaging of brain gliomas, due to their preferential accumulation in the tumor region [395]. However, the sensitivity of MR imaging is relatively low in comparison to other biomedical imaging techniques, so NIR is the most relevant imaging modality in line with MR imaging. The biocompatibility of red fluorescent MnO-PEG-Cy5.5 (λEx=675 nm, λEm=710 nm) nanoparticles proved that in the bio-imaging applications the cell proliferation was dose-dependent. However, the cell viability higher than 90% suggested no significant cytotoxicity. Such MR/NIR dual-modal nanoprobes enabled to obtain both anatomical and physiological information from deep inside the body and simultaneously acquire more sensitive information at the cellular level.

Conclusions

There have been many recent advances in the field of molecular imaging, particularly in the utilization of different strategies for the discovery and development of new 'smart' polymeric carriers of therapeutics agents (e.g., by using LbL or self-assembly methods) [396]. Introducing new photoswichable on-off fluorescent probes with optimized properties to the polymer capsules can help boosting individual molecules or group of moieties strong fluorescence and it allows for high emission enhancement. Polymer capsules with the photo-responsive fluorescent wall provide a fascinating mechanism for an efficient molecular detection which can be applied to improve imaging in live cells by using optical fluorescence. The significant progress in the ability to prepare polymeric capsules with precisely designed various aspects of macromolecular structures including material properties and architectures using facile coupling techniques allowed to develop the field of therapeutics in medicine. Moreover, the tailored polymer capsules as carriers constituted the important tool for advance diagnostics thus improved results in the treatment. Therefore, the development of polymer capsules endowed with an excellent targeting ability to deliver drugs for a better therapeutic efficiency is still desired in the clinical usage. The versatile nature of a broad range of polymer building blocks-labeled with fluorescent dyes sensitive to biological stimuli allowed to understand the interactions between cells and polymeric markers. Although great achievements have been attained on the self-assembly of different amphiphilic polymers, there still exists plenty of room to expand sophisticated self-assemblies library with multifunctional properties and new recognition motifs which search different biomedical applications. The new 'theranostic' platform which combines diagnostic and therapeutic functions requires multifunctional hybrid self-assembly materials as nanocarriers with fluorescence specific recognition ability, multiple stimuli-responsiveness photodynamic/photothermal properties to endow this field of vigorous vitality. Both 'activatable' and 'biomarker' imaging strategies have been found useful for tracking of a mechanism of action along the drug development. This kind of research will greatly expand because the number of available imaging probes and carrier constructs can design new concepts of multimodal devices.

Acknowledgements

The author thanks the National Centre for Science in Poland, Grant no. NN 209 762 440 for the financial support. I am grateful to Deborah and Mike Reppert and Patrycja Miksa (University of Warsaw, Institute of Applied Linguistcs) for valuable guides.

References

1. Garnett MC (2001) Targeted drug conjugates: principles and progress. Adv Drug Deliv Rev 53: 171-216.
2. Yun SW, Kang NY, Park SJ, Ha HH, Kim YK, et al. (2014) Diversity oriented fluorescence library approach (DOFLA) for live cell imaging probe development. Acc Chem Res 47: 1277-1286.
3. Deng T, Li JS, Jiang JH, Shen GL, Yu RQ (2006) Preparation of Near-Ir fluorescent nanoparticles for fluorescence-anisotropy-based immunoagglutination assay in whole blood. Advanced Functional Materials 16: 2147-2155.
4. Stender AS, Marchuk K, Liu C, Sander S, Meyer MW, et al. (2013) Single cell optical imaging and spectroscopy. Chem Rev 113: 2469-2527.
5. Fihey A, Perrier A, Browne WR, Jacquemin D (2015) Multiphotochromic molecular systems. Chem Soc Rev 44: 3719-3759.
6. Nagy A, Schally AV, Halmos G, Armatis P, Cai RZ, et al. (1998) Synthesis and biological evaluation of cytotoxic analogs of somatostatin containing doxorubicin or its intensely potent derivative, 2-pyrrolinodoxorubicin. Proc Natl Acad Sci U S A 95: 1794-1799.
7. Sun H, Wong EH, Yan Y, Cui J, Dai Q, et al. (2015) The role of capsule stiffness on cellular processing. Chemical Science 6: 3505-3514.
8. Torchilin VP (2000) Drug targeting. European Journal of Pharmaceutical Sciences 11: S81-91.
9. Elbayoumi TA, Torchilin VP (2007) Enhanced cytotoxicity of monoclonal anticancer antibody 2C5-modified doxorubicin-loaded PEGylated liposomes against various tumor cell lines. Eur J Pharm Sci 32: 159-168.
10. Miksa B. Recent progress in designing shell cross-linked polymer capsules for drug delivery. RSC Advances 5: 87781-87805.
11. Song J, Huang P, Duan H, Chen X (2015) Plasmonic Vesicles of Amphiphilic Nanocrystals: Optically Active Multifunctional Platform for Cancer Diagnosis and Therapy. Acc Chem Res 48: 2506-2515.
12. Wang S, Kim YK, Chang YT (2008) Diversity-oriented fluorescence library approach (DOFLA) to the discovery of chymotrypsin sensor. Journal of combinatorial chemistry 10: 460-465.
13. Fei X, Gu Y (2009) Progress in modifications and applications of fluorescent dye probe. Progress in Natural Science 19: 1-7.
14. Murade CU, Subramaniam V, Otto C, Bennink ML (2009) Interaction of oxazole yellow dyes with DNA studied with hybrid optical tweezers and fluorescence microscopy. Biophys J 97: 835-843.
15. Nishimura Y, Bereczky B, Ono M (2007) The EGFR inhibitor gefitinib suppresses ligand-stimulated endocytosis of EGFR via the early/late endocytic pathway in non-small cell lung cancer cell lines. Histochem Cell Biol 127: 541-553.
16. Nishimura Y, Itoh K, Yoshioka K, Tokuda K, Himeno M (2003) Overexpression of ROCK in human breast cancer cells: evidence that ROCK activity mediates intracellular membrane traffic of lysosomes. Pathol Oncol Res 9: 83-95.
17. Nishimura Y, Yoshioka K, Bernard O, Bereczky B, Itoh K (2006) A role of LIM kinase 1/cofilin pathway in regulating endocytic trafficking of EGF receptor in human breast cancer cells. Histochem Cell Biol 126: 627-638.
18. Isaksen K, Jonsson R, Omdal R (2008) Anti-CD20 treatment in primary Sjögren's syndrome. Scand J Immunol 68: 554-564.
19. Gisselbrecht C (2008) Use of rituximab in diffuse large B-cell lymphoma in the salvage setting. Br J Haematol 143: 607-621.
20. Jean GW, Shah SR (2008) Epidermal growth factor receptor monoclonal antibodies for the treatment of metastatic colorectal cancer. Pharmacotherapy 28: 742-754.

21. Balhorn R, Hok S, Burke PA, Lightstone FC, Cosman M, et al. (2007) Selective high-affinity ligand antibody mimics for cancer diagnosis and therapy: initial application to lymphoma/leukemia. Clin Cancer Res 13: 5621s-5628s.

22. Hall PS, Cameron DA (2009) Current perspective - trastuzumab. Eur J Cancer 45: 12-18.

23. Chari RV (1998) Targeted delivery of chemotherapeutics: tumor-activated prodrug therapy. Adv Drug Deliv Rev 31: 89-104.

24. Ojima I, Geng X, Wu X, Qu C, Borella CP, et al. (2002) Tumor-specific novel taxoid-monoclonal antibody conjugates. J Med Chem 45: 5620-5623.

25. Wu X, Ojima I (2004) Tumor specific novel taxoid-monoclonal antibody conjugates. Curr Med Chem 11: 429-438.

26. Peters C, Brown S. Antibody–drug conjugates as novel anti-cancer chemotherapeutics. Bioscience reports 35: e00225.

27. Pollyea DA, Gutman JA, Gore L, Smith CA, Jordan CT (2014) Haematologica 99: 1277-1284.

28. Giles F, Estey E, O'Brien S (2003) Gemtuzumab ozogamicin in the treatment of acute myeloid leukemia. Cancer 98: 2095-2104.

29. Chen X, Conti PS, Moats RA (2004) In vivo near-infrared fluorescence imaging of integrin alphavbeta3 in brain tumor xenografts. Cancer Res 64: 8009-8014.

30. Zwanziger D, Beck-Sickinger AG (2008) Radiometal targeted tumor diagnosis and therapy with peptide hormones. Curr Pharm Des 14: 2385-2400.

31. Khan IU, Beck-Sickinger AG (2008) Targeted tumor diagnosis and therapy with peptide hormones as radiopharmaceuticals. Anticancer Agents Med Chem 8: 186-199.

32. Schally AV (2008) New approaches to the therapy of various tumors based on peptide analogues. Horm Metab Res 40: 315-322.

33. Bagwe RP, Hilliard LR, Tan W (2006) Surface modification of silica nanoparticles to reduce aggregation and nonspecific binding. Langmuir 22: 4357-4362.

34. Mallikaratchy P, Tang Z, Tan W (2008) Cell specific aptamer-photosensitizer conjugates as a molecular tool in photodynamic therapy. ChemMedChem 3: 425-428.

35. Chu TC, Marks JW, Lavery LA, Faulkner S, Rosenblum MG, et al. (2006) Aptamer: toxin conjugates that specifically target prostate tumor cells. Cancer research 66: 5989-5992.

36. Wang W, Zhou F, Ge L, Liu X, Kong F (2012) Transferrin-PEG-PE modified dexamethasone conjugated cationic lipid carrier mediated gene delivery system for tumor-targeted transfection. Int J Nanomedicine 7: 2513-2522.

37. Wagner E, Curiel D, Cotten M (1994) Delivery of drugs, proteins and genes into cells using transferrin as a ligand for receptor-mediated endocytosis. Advanced Drug Delivery Reviews 14: 113-135.

38. Yan H, Tram K (2007) Glycotargeting to improve cellular delivery efficiency of nucleic acids. Glycoconj J 24: 107-123.

39. Koeller KM, Wong CH (2000) Synthesis of complex carbohydrates and glycoconjugates: enzyme-based and programmable one-pot strategies. Chem Rev 100: 4465-4494.

40. Bradley MO, Webb NL, Anthony FH, Devanesan P, Witman PA, et al. (2001) Tumor targeting by covalent conjugation of a natural fatty acid to paclitaxel. Clin Cancer Res 7: 3229-3238.

41. Kassab K (2002) Photophysical and photosensitizing properties of selected cyanines. J Photochem Photobiol B 68: 15-22.

42. Field LD, Delehanty JB, Chen Y, et al. (2015) Peptides for specifically targeting nanoparticles to cellular organelles: quo vadis? Acc Chem Res 48: 1380-1390.

43. Shell TA, Lawrence DS (2015) Vitamin B12: a tunable, long wavelength, light-responsive platform for launching therapeutic agents. Acc Chem Res 48: 2866-2874.

44. Corti A, Curnis F, Arap W, Pasqualini R (2008) The neovasculature homing motif NGR: more than meets the eye. Blood 112: 2628-2635.

45. Low PS, Kularatne SA (2009) Folate-targeted therapeutic and imaging agents for cancer. Curr Opin Chem Biol 13: 256-262.

46. Leamon CP, Reddy JA (2004) Folate-targeted chemotherapy. Adv Drug Deliv Rev 56: 1127-1141.

47. Leamon CP, Low PS (2001) Folate-mediated targeting: from diagnostics to drug and gene delivery. Drug discovery today 6: 44-51.

48. Gupta Y, Kohli DV, Jain SK (2008) Vitamin B12-mediated transport: a potential tool for tumor targeting of antineoplastic drugs and imaging agents. Crit Rev Ther Drug Carrier Syst 25: 347-379.

49. Brannon-Peppas L, Blanchette JO (2004) Nanoparticle and targeted systems for cancer therapy. Advanced drug delivery reviews 56: 1649-1659.

50. Lu Y, Low PS (2002) Folate-mediated delivery of macromolecular anticancer therapeutic agents. Adv Drug Deliv Rev 54: 675-693.

51. Low PS, Henne WA, Doorneweerd DD (2008) Discovery and development of folic-acid-based receptor targeting for imaging and therapy of cancer and inflammatory diseases. Acc Chem Res 41: 120-129.

52. Choi SK, Thomas T, Li MH, Kotlyar A, Desai A, (2010) Light-controlled release of caged doxorubicin from folate receptor-targeting PAMAM dendrimer nanoconjugate. Chemical Communications 46: 2632-2634.

53. Fei XN, Liu Y, Li C (2012) Folate conjugated chitosan grafted thiazole orange derivative with high targeting for early breast cancer cells diagnosis. J Fluoresc 22: 1555-1561.

54. Lee JW, Lu JY, Low PS, Fuchs PL (2002) Synthesis and evaluation of taxol-folic acid conjugates as targeted antineoplastics. Bioorg Med Chem 10: 2397-2414.

55. Lokeshwar VB, Mirza S, Jordan A (2014) Targeting hyaluronic acid family for cancer chemoprevention and therapy. Advances in cancer research 123: 35-65.

56. Liang J, Jiang D, Noble PW (2016) Hyaluronan as a therapeutic target in human diseases. Adv Drug Deliv Rev 97: 186-203.

57. Saxena V, Sadoqi M, Shao J (2003) Degradation kinetics of indocyanine green in aqueous solution. J Pharm Sci 92: 2090-2097.

58. Hilderbrand SA, Kelly KA, Weissleder R, Tung CH (2005) Monofunctional near-infrared fluorochromes for imaging applications. Bioconjug Chem 16: 1275-1281.

59. Lu YJ, Deng Q, Hou JQ, Hu DP, Wang ZY, et al. (2016) Molecular Engineering of Thiazole Orange Dye: Change of Fluorescent Signaling from Universal to Specific upon Binding with Nucleic Acids in Bioassay. ACS Chem Biol 11: 1019-1029.

60. Kennedy MD, Jallad KN, Thompson DH, Ben-Amotz D, Low PS (2003) Optical imaging of metastatic tumors using a folate-targeted fluorescent probe. J Biomed Opt 8: 636-641.

61. Milstein AB, Kennedy MD, Low PS, Bouman CA, Webb KJ (2005) Statistical approach for detection and localization of a fluorescing mouse tumor in Intralipid. Appl Opt 44: 2300-2310.

62. Tung CH, Lin Y, Moon WK, Weissleder R (2002) A receptor-targeted near-infrared fluorescence probe for in vivo tumor imaging. Chembiochem 3: 784-786.

63. Moon WK, Lin Y, O'Loughlin T, Tang Y, Kim DE, et al. (2003) Enhanced tumor detection using a folate receptor-targeted near-infrared fluorochrome conjugate. Bioconjug Chem 14: 539-545.

64. He W, Wang H, Hartmann LC, Cheng JX, Low PS (2007) In vivo quantitation of rare circulating tumor cells by multiphoton intravital flow cytometry. Proc Natl Acad Sci U S A 104: 11760-11765.

65. Becker A, Hessenius C, Licha K, Ebert B, Sukowski U, et al. (2001) Receptor-targeted optical imaging of tumors with near-infrared fluorescent ligands. Nat Biotechnol 19: 327-331.

66. Cai W, Shin DW, Chen K, Gheysens O, Cao Q, et al. (2006) Peptide-labeled near-infrared quantum dots for imaging tumor vasculature in living subjects. Nano Lett 6: 669-676.

67. Gibson AP, Hebden JC, Arridge SR (2005) Recent advances in diffuse optical imaging. Physics in medicine and biology 50: R1.

68. Michalet X, Pinaud FF, Bentolila LA, Tsay JM, Doose S, et al. (2005) Quantum dots for live cells, in vivo imaging, and diagnostics. Science 307: 538-544.

69. Schnall M, Rosen M (2006) Primer on imaging technologies for cancer. J Clin Oncol 24: 3225-3233.

70. Kratz F, Müller IA, Ryppa C, Warnecke A (2008) Prodrug strategies in anticancer chemotherapy. ChemMedChem 3: 20-53.

71. Sega EI, Low PS (2008) Tumor detection using folate receptor-targeted imaging agents. Cancer Metastasis Rev 27: 655-664.

72. Kularatne SA, Venkatesh C, Santhapuram HK, Wang K, Vaitilingam B, et al. (2010) Synthesis and biological analysis of prostate-specific membrane antigen-targeted anticancer prodrugs. J Med Chem 53: 7767-7777.

73. Ojima I (2008) Guided molecular missiles for tumor-targeting chemotherapy--case studies using the second-generation taxoids as warheads. Acc Chem Res 41: 108-119.

74. Gómez-Hens A, Aguilar-Caballos MP (2004) Long-wavelength fluorophores: new trends in their analytical use. TrAC Trends in Analytical Chemistry 23: 127-136.

75. Luo S, Zhang E, Su Y, Cheng T, Shi C (2011) A review of NIR dyes in cancer targeting and imaging. Biomaterials 32: 7127-7138.

76. Gayathri Devi D, Cibin TR, Ramaiah D, Abraham A (2008) Bis(3,5-diiodo-2,4,6-trihydroxyphenyl)squaraine: a novel candidate in photodynamic therapy for skin cancer models in vivo. J Photochem Photobiol B 92: 153-159.

77. Allison RR, Moghissi K (2013) Photodynamic Therapy (PDT): PDT Mechanisms. Clin Endosc 46: 24-29.

78. Celli JP, Spring BQ, Rizvi I, Evans CL, Samkoe KS, et al. (2010) Imaging and photodynamic therapy: mechanisms, monitoring, and optimization. Chem Rev 110: 2795-2838.

79. Kuimova MK, Collins HA, Balaz M, Dahlstedt E, Levitt JA, et al. (2009) Photophysical properties and intracellular imaging of water-soluble porphyrin dimers for two-photon excited photodynamic therapy. Org Biomol Chem 7: 889-896.

80. Luu QT, Levy RP, Miller DW, Shahnazi K, Yonemoto LT, et al. (2005) A clinical interactive technique for MR-CT image registration for target delineation of intracranial tumors. Technol Cancer Res Treat 4: 275-281.

81. Detty MR, Gibson SL, Wagner SJ (2004) Current clinical and preclinical photosensitizers for use in photodynamic therapy. J Med Chem 47: 3897-3915.

82. Hill TK, Abdulahad A, Kelkar SS, Marini FC, Long TE, et al. (2015) Indocyanine green-loaded nanoparticles for image-guided tumor surgery. Bioconjug Chem 26: 294-303.

83. Mishra A, Behera RK, Behera PK, Mishra BK, Behera GB (2000) Cyanines during the 1990s: a review. Chemical Reviews 100: 1973-2012.

84. Kovalska VB, Volkova KD, Losytskyy MY, Tolmachev OI, Balanda AO, et al. (2006) 6,6'-Disubstituted benzothiazole trimethine cyanines--new fluorescent dyes for DNA detection. Spectrochim Acta A Mol Biomol Spectrosc 65: 271-277.

85. Yarmoluk SM, Kovalska VB, Lukashov SS, Slominskii YL (1999) Interaction of cyanine dyes with nucleic acids. XII. Beta-substituted carbocyanines as possible fluorescent probes for nucleic acids detection. Bioorg Med Chem Lett 9: 1677-1678.

86. Mohammed HS, Delos Santos JO, Armitage BA (2011) Noncovalent binding and fluorogenic response of cyanine dyes to DNA homoquadruplex and PNA-DNA heteroquadruplex structures. Artif DNA PNA XNA 2: 43-49.

87. Lee H, Mason JC, Achilefu S (2006) Heptamethine cyanine dyes with a robust C-C bond at the central position of the chromophore. J Org Chem 71: 7862-7865.

88. Kim JS, Kodagahally R, Strekowski L, Patonay G (2005) A study of intramolecular H-complexes of novel bis(heptamethine cyanine) dyes. Talanta 67: 947-954.

89. Gragg JL (2010) Synthesis of Near-Infrared Heptamethine Cyanine Dyes Chemistry Theses 28: 1-132.

90. Ye Y, Bloch S, Kao J, Achilefu S (2005) Multivalent carbocyanine molecular probes: synthesis and applications. Bioconjug Chem 16: 51-61.

91. Oswald B, Lehmann F, Simon L, Terpetschnig E, Wolfbeis OS (2000) Red laser-induced fluorescence energy transfer in an immunosystem. Anal Biochem 280: 272-277.

92. Volkova KD, Kovalska VB, Tatarets AL, Patsenker LD, Kryvorotenko DV, (2007) Spectroscopic study of squaraines as protein-sensitive fluorescent dyes. Dyes and Pigments 72: 285-292.

93. Nakazumi H, Ohta T, Etoh H, Uno T, Colyer CL, (2005) Near-infrared luminescent bis-squaraine dyes linked by a thiophene or pyrene spacer for noncovalent protein labeling. Synthetic metals 153: 33-36.

94. Umezawa K, Citterio D, Suzuki K (2008) Water-soluble NIR fluorescent probes based on squaraine and their application for protein labeling. Anal Sci 24: 213-217.

95. Umezawa K, Citterio D, Suzuki K (2014) New trends in near-infrared fluorophores for bioimaging. Anal Sci 30: 327-349.

96. Gassensmith JJ, Baumes JM, Smith BD (2009) Discovery and early development of squaraine rotaxanes. Chem Commun (Camb) 6329-6338.

97. Bashkatov AN, Genina EA, Kochubey VI, Tuchin VV (2005) Optical properties of human skin, subcutaneous and mucous tissues in the wavelength range from 400 to 2000 nm. Journal of Physics D: Applied Physics 38: 2543.

98. Brown SB, Brown EA, Walker I (2004) The present and future role of photodynamic therapy in cancer treatment. Lancet Oncol 5: 497-508.

99. Allison RR, Downie GH, Cuenca R, Hu XH, Childs CJ, et al. (2004) Photosensitizers in clinical PDT. Photodiagnosis Photodyn Ther 1: 27-42.

100. Li J, Kim IH, Roche ED, Beeman D, Lynch AS, et al. (2006) Design, synthesis, and biological evaluation of BODIPY-erythromycin probes for bacterial ribosomes. Bioorg Med Chem Lett 16: 794-797.

101. Loudet A, Burgess K (2007) BODIPY dyes and their derivatives: syntheses and spectroscopic properties. Chem Rev 107: 4891-4932.

102. Li F, Wang Y, Wang Z, Cheng Y, Zhu C (2015) Red colored CPL emission of chiral 1, 2-DACH-based polymers via chiral transfer of the conjugated chain backbone structure. Polymer Chemistry 6: 6802-6805.

103. Donuru VR, Zhu S, Green S, Liu H (2010) Near-infrared emissive BODIPY polymeric and copolymeric dyes. Polymer 51: 5359-2368.

104. Killoran J, McDonnell SO, Gallagher JF, O'Shea DF (2008) A substituted BF 2-chelated tetraarylazadipyrromethene as an intrinsic dual chemosensor in the 650–850 nm spectral range. New Journal of Chemistry 32: 483-489.

105. Yamashina M, Sartin MM, Sei Y, Akita M, Takeuchi S, et al. (2015) Preparation of Highly Fluorescent Host-Guest Complexes with Tunable Color upon Encapsulation. J Am Chem Soc 137: 9266-9269.

106. Liour SS, Kraemer SA, Dinkins MB, Su CY, Yanagisawa M, et al. (2006) Further characterization of embryonic stem cell-derived radial glial cells. Glia 53: 43-56.

107. Leong C, Zhai D, Kim B, Yun SW, Chang YT (2013) Neural stem cell isolation from the whole mouse brain using the novel FABP7-binding fluorescent dye, CDr3. Stem Cell Res 11: 1314-1322.

108. Lee JS, Kang NY, Kim YK, Samanta A, Feng S, et al. (2009) Synthesis of a BODIPY library and its application to the development of live cell glucagon imaging probe. J Am Chem Soc 131: 10077-10082.

109. Kang NY, Lee SC, Park SJ, Ha HH, Yun SW, et al. (2013) Visualization and isolation of Langerhans islets by a fluorescent probe PiY. Angew Chem Int Ed Engl 52: 8557-8560.

110. Leong C, Lee SC, Ock J, Li X, See P, et al. (2014) Microglia specific fluorescent probes for live cell imaging. Chem Commun (Camb) 50: 1089-1091.

111. Yamashina M, Sartin MM, Sei Y, Akita M, Takeuchi S, et al. (2015) Preparation of Highly Fluorescent Host-Guest Complexes with Tunable Color upon Encapsulation. J Am Chem Soc 137: 9266-9269.

112. Lee MH, Yang Z, Lim CW, Lee YH, Dongbang S, et al. (2013) Disulfide-cleavage-triggered chemosensors and their biological applications. Chem Rev 113: 5071-5109.

113. Traverso N, Ricciarelli R, Nitti M, Marengo B, Furfaro AL, et al. (2013) Role of glutathione in cancer progression and chemoresistance. Oxid Med Cell Longev 2013: 972913.

114. Chen X, Zhou Y, Peng X, Yoon J (2010) Fluorescent and colorimetric probes for detection of thiols. Chem Soc Rev 39: 2120-2135.

115. Shahrokhian S (2001) Lead phthalocyanine as a selective carrier for preparation of a cysteine-selective electrode. Anal Chem 73: 5972-5978.

116. Townsend DM, Tew KD, Tapiero H (2003) The importance of glutathione in human disease. Biomed Pharmacother 57: 145-155.

117. Griffith OW (1999) Biologic and pharmacologic regulation of mammalian glutathione synthesis. Free Radic Biol Med 27: 922-935.

118. Lu SC (2013) Glutathione synthesis. Biochim Biophys Acta 1830: 3143-3153.

119. Zheng ZB, Zhu G, Tak H, Joseph E, Eiseman JL, et al. (2005) N-(2-hydroxypropyl)methacrylamide copolymers of a glutathione (GSH)-activated glyoxalase i inhibitor and DNA alkylating agent: synthesis, reaction kinetics with GSH, and in vitro antitumor activities. Bioconjug Chem 16: 598-607.

120. Rahman I, MacNee W (2000) Regulation of redox glutathione levels and gene transcription in lung inflammation: therapeutic approaches. Free Radic Biol Med 28: 1405-1420.

121. Zhai D, Lee SC, Yun SW, Chang YT (2013) A ratiometric fluorescent dye for the detection of glutathione in live cells and liver cancer tissue. Chem Commun (Camb) 49: 7207-7209.

122. Lee MH, Han JH, Kwon PS, Bhuniya S, Kim JY, et al. (2012) Hepatocyte-targeting single galactose-appended naphthalimide: a tool for intracellular thiol imaging in vivo. J Am Chem Soc 134: 1316-1322.

123. Lee MH, Han JH, Lee JH, Choi HG, Kang C, et al. (2012) Mitochondrial thioredoxin-responding off-on fluorescent probe. J Am Chem Soc 134: 17314-17319.

124. Lee MH, Kim JY, Han JH, Bhuniya S, Sessler JL, et al. (2012) Direct fluorescence monitoring of the delivery and cellular uptake of a cancer-targeted RGD peptide-appended naphthalimide theragnostic prodrug. J Am Chem Soc 134: 12668-12674.

125. Lin W, Yuan L, Cao Z, Feng Y, Long L (2009) A sensitive and selective fluorescent thiol probe in water based on the conjugate 1,4-addition of thiols to alpha,beta-unsaturated ketones. Chemistry 15: 5096-5103.

126. Jung HS, Ko KC, Kim GH, Lee AR, Na YC, et al. (2011) Coumarin-based thiol chemosensor: synthesis, turn-on mechanism, and its biological application. Org Lett 13: 1498-1501.

127. Chen H, Tang Y, Ren M, Lin W (2016) Single near-infrared fluorescent probe with high-and low-sensitivity sites for sensing different concentration ranges of biological thiols with distinct modes of fluorescence signals. Chemical Science 7: 1896-1903.

128. Li H, Fan J, Wang J, Tian M, Du J, et al. (2009) A fluorescent chemodosimeter specific for cysteine: effective discrimination of cysteine from homocysteine. Chem Commun (Camb) 5904-5906.

129. Jones LR, Goun EA, Shinde R, Rothbard JB, Contag CH, et al. (2006) Releasable luciferin-transporter conjugates: tools for the real-time analysis of cellular uptake and release. J Am Chem Soc 128: 6526-6527.

130. Chen L, Wright LR, Chen CH, Oliver SF, Wender PA, et al. (2001) Molecular transporters for peptides: delivery of a cardioprotective epsilonPKC agonist peptide into cells and intact ischemic heart using a transport system, R(7). Chem Biol 8: 1123-1129.

131. Jenkins DE, Oei Y, Hornig YS, Yu SF, Dusich J, et al. (2003) Bioluminescent imaging (BLI) to improve and refine traditional murine models of tumor growth and metastasis. Clin Exp Metastasis 20: 733-744.

132. Jenkins DE, Hornig YS, Oei Y, Dusich J, Purchio T (2005) Bioluminescent human breast cancer cell lines that permit rapid and sensitive in vivo detection of mammary tumors and multiple metastases in immune deficient mice. Breast Cancer Res 7: R444-454.

133. Cao X, Lin W, Yu Q (2011) A ratiometric fluorescent probe for thiols based on a tetrakis(4-hydroxyphenyl)porphyrin-coumarin scaffold. J Org Chem 76: 7423-7430.

134. Ottl J, Gabriel D, Marriott G (1998) Preparation and photoactivation of caged fluorophores and caged proteins using a new class of heterobifunctional, photocleavable cross-linking reagents. Bioconjug Chem 9: 143-151.

135. Tian Z, Li AD (2013) Photoswitching-enabled novel optical imaging: innovative solutions for real-world challenges in fluorescence detections. Acc Chem Res 46: 269-279.

136. Kiskin NI, Chillingworth R, McCray JA, Piston D, Ogden D (2002) The efficiency of two-photon photolysis of a" caged" fluorophore, o-1-(2-nitrophenyl) ethylpyranine, in relation to photodamage of synaptic terminals. European Biophysics Journal 30: 588-604.

137. Ottl J, Gabriel D, Marriott G (1998) Preparation and photoactivation of caged fluorophores and caged proteins using a new class of heterobifunctional, photocleavable cross-linking reagents. Bioconjug Chem 9: 143-151.

138. Gee KR, Weinberg ES, Kozlowski DJ (2001) Caged Q-rhodamine dextran: a new photoactivated fluorescent tracer. Bioorg Med Chem Lett 11: 2181-2183.

139. Tian Z, Li AD (2013) Photoswitching-enabled novel optical imaging: innovative solutions for real-world challenges in fluorescence detections. Acc Chem Res 46: 269-279.

140. Zhao Y, Zheng Q, Dakin K, Xu K, Martinez ML, et al. (2004) New caged coumarin fluorophores with extraordinary uncaging cross sections suitable for biological imaging applications. J Am Chem Soc 126: 4653-4663.

141. Zheng G, Guo YM, Li WH (2007) Photoactivatable and water soluble FRET dyes with high uncaging cross section. J Am Chem Soc 129: 10616-10617.

142. Petchprayoon C, Yan Y, Mao S, Marriott G (2011) Rational design, synthesis, and characterization of highly fluorescent optical switches for high-contrast optical lock-in detection (OLID) imaging microscopy in living cells. Bioorg Med Chem 19: 1030-1040.

143. Mao S, Benninger RK, Yan Y, Petchprayoon C, Jackson D, et al. (2008) Optical lock-in detection of FRET using synthetic and genetically encoded optical switches. Biophys J 94: 4515-4524.

144. Mizukami S, Watanabe S, Akimoto Y, Kikuchi K (2012) No-wash protein labeling with designed fluorogenic probes and application to real-time pulse-chase analysis. J Am Chem Soc 134: 1623-1629.

145. Mizukami S, Watanabe S, Hori Y, Kikuchi K (2009) Covalent protein labeling based on noncatalytic beta-lactamase and a designed FRET substrate. J Am Chem Soc 131: 5016-5017.

146. Watanabe S, Mizukami S, Hori Y, Kikuchi K (2010) Multicolor protein labeling in living cells using mutant β-lactamase-tag technology. Bioconjug Chem 21: 2320-2326.

147. Jones RN, Wilson HW, Novick WJ Jr (1982) In vitro evaluation of pyridine-2-azo-p-dimethylaniline cephalosporin, a new diagnostic chromogenic reagent, and comparison with nitrocefin, cephacetrile, and other beta-lactam compounds. J Clin Microbiol 15: 677-683.

148. Faraci WS, Pratt RF (1986) Mechanism of inhibition of RTEM-2 beta-lactamase by cephamycins: relative importance of the 7 alpha-methoxy group and the 3' leaving group. Biochemistry 25: 2934-2941.

149. Watanabe S, Mizukami S, Akimoto Y, Hori Y, Kikuchi K (2011) Intracellular protein labeling with prodrug-like probes using a mutant β-lactamase tag. Chemistry 17: 8342-8349.

150. Chen S, Zhao X, Chen J, Chen J, Kuznetsova L, et al. (2010) Mechanism-based tumor-targeting drug delivery system. Validation of efficient vitamin receptor-mediated endocytosis and drug release. Bioconjug Chem 21: 979-987.

151. Russell-Jones G, McTavish K, McEwan J, Rice J, Nowotnik D (2004) Vitamin-mediated targeting as a potential mechanism to increase drug uptake by tumours. J Inorg Biochem 98: 1625-1633.

152. Henne WA, Doorneweerd DD, Hilgenbrink AR, Kularatne SA, Low PS (2006) Synthesis and activity of a folate peptide camptothecin prodrug. Bioorg Med Chem Lett 16: 5350-5355.

153. Redy O, Shabat D (2012) Modular theranostic prodrug based on a FRET-activated self-immolative linker. J Control Release 164: 276-282.

154. Barman S, Mukhopadhyay SK, Gangopadhyay M, Biswas S, Dey S, et al. (2015) Coumarin–benzothiazole–chlorambucil (Cou–Benz–Cbl) conjugate: an ESIPT based pH sensitive photoresponsive drug delivery system. Journal of Materials Chemistry B 3: 3490-3497.

155. Barman S, Mukhopadhyay SK, Gangopadhyay M, Biswas S, Dey S, et al. (2015) J Mater Chem B 3: 3490-3497.

156. Zhu S, Lin W, Yuan L (2013) Development of a ratiometric fluorescent pH probe for cell imaging based on a coumarin–quinoline platform. Dyes and Pigments 99: 465-471.

157. Furuta T, Watanabe T, Tanabe S, Sakyo J, Matsuba C (2007) Phototriggers for nucleobases with improved photochemical properties. Org Lett 9: 4717-4720.

158. Lusic H, Uprety R, Deiters A (2010) Improved synthesis of the two-photon caging group 3-nitro-2-ethyldibenzofuran and its application to a caged thymidine phosphoramidite. Org Lett 12: 916-919.

159. Furuta T, Wang SS, Dantzker JL, Dore TM, Bybee WJ, et al. (1999) Brominated 7-hydroxycoumarin-4-ylmethyls: photolabile protecting groups with biologically useful cross-sections for two photon photolysis. Proc Natl Acad Sci U S A 96: 1193-1200.

160. Sherif MH, Yossef AM (2015) Synthesis and anticancer evaluation of some fused coumarino-[4, 3-d]-pyrimidine derivatives. Research on Chemical Intermediates 41: 383-390.

161. El Alaoui A, Schmidt F, Amessou M, Sarr M, Decaudin D, et al. (2007) Shiga toxin-mediated retrograde delivery of a topoisomerase I inhibitor prodrug. Angew Chem Int Ed Engl 46: 6469-6472.

162. Santra S, Kaittanis C, Santiesteban OJ, Perez JM (2011) Cell-specific, activatable, and theranostic prodrug for dual-targeted cancer imaging and therapy. J Am Chem Soc 133: 16680-16688.

163. Karton-Lifshin N, Albertazzi L, Bendikov M, Baran PS, Shabat D (2012) "Donor-two-acceptor" dye design: a distinct gateway to NIR fluorescence. J Am Chem Soc 134: 20412-20420.

164. Johnsson N, Johnsson K (2007) Chemical tools for biomolecular imaging. ACS Chem Biol 2: 31-38.

165. Yuan L, Lin W, Yang Y, Chen H (2012) A unique class of near-infrared functional fluorescent dyes with carboxylic-acid-modulated fluorescence ON/OFF switching: rational design, synthesis, optical properties, theoretical calculations, and applications for fluorescence imaging in living animals. J Am Chem Soc 134: 1200-1211.

166. Kisin-Finfer E, Shabat D (2013) New repertoire of 'donor-two-acceptor' NIR fluorogenic dyes. Bioorg Med Chem 21: 3602-3608.

167. Gnaim S, Shabat D (2014) Quinone-methide species, a gateway to functional molecular systems: from self-immolative dendrimers to long-wavelength fluorescent dyes. Acc Chem Res 47: 2970-2984.

168. Redy-Keisar O, Kisin-Finfer E, Ferber S, Satchi-Fainaro R, Shabat D (2014) Synthesis and use of QCy7-derived modular probes for the detection and imaging of biologically relevant analytes. Nat Protoc 9: 27-36.

169. Karton-Lifshin N, Segal E, Omer L, Portnoy M, Satchi-Fainaro R, et al. (2011) A unique paradigm for a Turn-ON near-infrared cyanine-based probe: noninvasive intravital optical imaging of hydrogen peroxide. J Am Chem Soc 133: 10960-10965.

170. Han J, Lee TH, Tung CH, Lee DY (2014) Design and synthesis of a mitochondria-targeting carrier for small molecule drugs. Org Biomol Chem 12: 9793-9796.

171. Weinstain R, Segal E, Satchi-Fainaro R, Shabat D (2010) Real-time monitoring of drug release. Chem Commun (Camb) 46: 553-555.

172. Yuan L, Lin W, Zhao S, Gao W, Chen B, et al. (2012) A unique approach to development of near-infrared fluorescent sensors for in vivo imaging. J Am Chem Soc 134: 13510-13523.

173. Vlassiouk I, Park CD, Vail SA, Gust D, Smirnov S (2006) Control of nanopore wetting by a photochromic spiropyran: a light-controlled valve and electrical switch. Nano Lett 6: 1013-1017.

174. Montenegro J, Ghadiri MR, Granja JR (2013) Ion channel models based on self-assembling cyclic peptide nanotubes. Acc Chem Res 46: 2955-2965.

175. Reiß P, Koert U (2013) Ion-channels: goals for function-oriented synthesis. Acc Chem Res 46: 2773-2780.

176. De Riccardis F, Izzo I, Montesarchio D, Tecilla P (2013) Ion transport through lipid bilayers by synthetic ionophores: modulation of activity and selectivity. Acc Chem Res 46: 2781-2790.

177. Mosgaard LD, Heimburg T (2013) Lipid ion channels and the role of proteins. Acc Chem Res 46: 2966-2976.

178. Otis F, Auger M, Voyer N (2013) Exploiting peptide nanostructures to construct functional artificial ion channels. Acc Chem Res 46: 2934-2943.

179. Gong B, Shao Z (2013) Self-assembling organic nanotubes with precisely defined, sub-nanometer pores: formation and mass transport characteristics. Acc Chem Res 46: 2856-2866.

180. Sumaru K, Ohi K, Takagi T, Kanamori T, Shinbo T (2006) Photoresponsive properties of poly(N-isopropylacrylamide) hydrogel partly modified with spirobenzopyran. Langmuir 22: 4353-4356.

181. Nicoletta FP, Cupelli D, Formoso P, De Filpo G, Colella V, et al. (2012) Light responsive polymer membranes: a review. Membranes (Basel) 2: 134-197.

182. Schumers JM, Fustin CA, Gohy JF (2010) Light-responsive block copolymers. Macromol Rapid Commun 31: 1588-1607.

183. Okahata Y, Seki T (1984) pH-sensitive capsule membranes. Reversible permeability control from the dissociative bilayer-coated capsule membrane by an ambient pH change. Journal of the American Chemical Society 106: 8065-8070.

184. Sebai SC, Cribier S, Karimi A, Massotte D, Tribet C (2010) Permeabilization of lipid membranes and cells by a light-responsive copolymer. Langmuir 26: 14135-14141.

185. Sebai SC, Milioni D, Walrant A, Alves ID, Sagan S, et al. (2012) Photocontrol of the translocation of molecules, peptides, and quantum dots through cell and lipid membranes doped with azobenzene copolymers. Angew Chem Int Ed Engl 51: 2132-2136.

186. Ishii K, Hamada T, Hatakeyama M, Sugimoto R, Nagasaki T, et al. (2009) Reversible control of exo- and endo-budding transitions in a photosensitive lipid membrane. Chembiochem 10: 251-256.

187. Sierant M, Paluch P, Florczak M, Rozanski A, Miksa B (2013) Photosensitive nanocapsules for use in imaging from poly(styrene-co-divinylbenzene) cross-linked with coumarin derivatives. Colloids Surf B Biointerfaces 111: 571-578.

188. Darszon A, Montal M, Zarco J (1977) Light increases the ion and non-electrolyte permeability of rhodopsin-phospholipid vesicles. Biochem Biophys Res Commun 76: 820-827.

189. Morgan CG, Sandhu SS, Yianni YP, Dodd NJ (1987) The phase behaviour of dispersions of Bis-Azo PC: photoregulation of bilayer dynamics via lipid photochromism. Biochim Biophys Acta 903: 495-503.

190. Bisby RH, Mead C, Morgan CG (2000) Active uptake of drugs into photosensitive liposomes and rapid release on UV photolysis. Photochem Photobiol 72: 57-61.

191. Morgan CG, Yianni YP, Sandhu SS, Mitchell AC (1995) Liposome fusion and lipid exchange on ultraviolet irradiation of liposomes containing a photochromic phospholipid. Photochem Photobiol 62: 24-29.

192. Bisby RH, Mead C, Mitchell AC, Morgan CG (1999) Fast laser-induced solute release from liposomes sensitized with photochromic lipid: effects of temperature, lipid host, and sensitizer concentration. Biochem Biophys Res Commun 262: 406-410.

193. Bisby RH, Mead C, Morgan CG (2000) Wavelength-programmed solute release from photosensitive liposomes. Biochem Biophys Res Commun 276: 169-173.

194. Shimomura M, Kunitake T (1987) Fluorescence and photoisomerization of azobenzene-containing bilayer membranes. Journal of the American Chemical Society 109: 5175-5183.

195. Liu XM, Yang B, Wang YL, Wang JY (2005) Photoisomerisable cholesterol derivatives as photo-trigger of liposomes: effect of lipid polarity, temperature, incorporation ratio, and cholesterol. Biochim Biophys Acta 1720: 28-34.

196. Uda RM, Hiraishi E, Ohnishi R, Nakahara Y, Kimura K (2010) Morphological changes in vesicles and release of an encapsulated compound triggered by a photoresponsive Malachite Green leuconitrile derivative. Langmuir 26: 5444-5450.

197. Liang X, Yue X, Dai Z, Kikuchi J (2011) Photoresponsive liposomal nanohybrid cerasomes. Chem Commun (Camb) 47: 4751-4753.

198. Sierant M, Kazmierski S, Paluch P, Bienias U, Miksa BJ (2015) Nanocapsules for 5-fluorouracil delivery decorated with a poly(2-ethylhexyl methacrylate-co-7-(4-trifluoromethyl)coumarin acrylamide) cross-linked wall. New J Chem 39: 1506-1516.

199. Bléger D, Liebig T, Thiermann R, Maskos M, Rabe JP, et al. (2011) Light-orchestrated macromolecular "accordions": reversible photoinduced shrinking of rigid-rod polymers. Angew Chem Int Ed Engl 50: 12559-12563.

200. Gokel GW, Negin S (2013) Synthetic ion channels: from pores to biological applications. Acc Chem Res 46: 2824-2833.

201. Koçer A, Walko M, Meijberg W, Feringa BL (2005) A light-actuated nanovalve derived from a channel protein. Science 309: 755-758.

202. Koçer A, Walko M, Bulten E, Halza E, Feringa BL, et al. (2006) Rationally designed chemical modulators convert a bacterial channel protein into a pH-sensory valve. Angew Chem Int Ed Engl 45: 3126-3130.

203. Banghart MR, Volgraf M, Trauner D (2006) Engineering light-gated ion channels. Biochemistry 45: 15129-15141.

204. Lester HA, Krouse ME, Nass MM, Wassermann NH, Erlanger BF (1980)

A covalently bound photoisomerizable agonist: comparison with reversibly bound agonists at Electrophorus electroplaques. J Gen Physiol 75: 207-232.

205. Dante S, Advincula R, Frank CW, Stroeve P (2009) Langmuir, Photoisomerization of azobenzene moiety in crosslinking polymer. Materials 15: 193-201.

206. Bléger D, Liebig T, Thiermann R, Maskos M, Rabe JP, et al. (2011) Light-orchestrated macromolecular "accordions": reversible photoinduced shrinking of rigid-rod polymers. Angew Chem Int Ed Engl 50: 12559-12563.

207. Banghart M, Borges K, Isacoff E, Trauner D, Kramer RH (2004) Light-activated ion channels for remote control of neuronal firing. Nat Neurosci 7: 1381-1386.

208. Bedard M, Skirtach AG, Sukhorukov GB (2007) Rapid Communoptically Driven Encapsulation Using Novel Polymeric Hollow Shells Containing an Azobenzene Polymer. Macromol 28: 1517-1521.

209. Lin Y, Cheng X, Qiao C, Yu Y, Li Z, et al. (2010) Creation of photo-modulated multi-state and multi-scale molecular assemblies via binary-state molecular switch. Soft Matter 6: 902-908.

210. Wang G, Tong X, Zhao Y (2004) Preparation of Azobenzene-Containing Amphiphilic Diblock Copolymers for Light-Responsive Micellar Aggregates. Macromolecules 37: 8911-8917.

211. Jochum FD, Theato P (2010) Thermo- and light responsive micellation of azobenzene containing block copolymers. Chem Commun (Camb) 46: 6717-6719.

212. Lopez-Vilanova L, Martinez I, Corrales T, Catalina F (2014) Photoreversible crosslinking of poly-(ethylene-butyl-acrylate) copolymers functionalized with coumarin chromophores using microwave methodology. React Funct Polym 85: 28-35.

213. Skirtach AG, Karageorgiev P, Bédard MF, Sukhorukov GB, Möhwald H (2008) Reversibly permeable nanomembranes of polymeric microcapsules. J Am Chem Soc 130: 11572-11573.

214. Skirtach AG, Antipov AA, Shchukin DG, Sukhorukov GB (2004) Remote activation of capsules containing Ag nanoparticles and IR dye by laser light. Langmuir 20: 6988-6992.

215. Goodwin AP, Mynar JL, Ma Y, Fleming GR, Fréchet JM (2005) Synthetic micelle sensitive to IR light via a two-photon process. J Am Chem Soc 127: 9952-9953.

216. Chen CJ, Liu GY, Shi YT, Zhu CS, Pang SP, et al. (2011) Biocompatible micelles based on comb-like PEG derivates: formation, characterization, and photo-responsiveness. Macromol Rapid Commun 32: 1077-1081.

217. Fisher WG, Partridge WP Jr, Dees C, Wachter EA (1997) Simultaneous two-photon activation of type-I photodynamic therapy agents. Photochem Photobiol 66: 141-155.

218. Frederiksen PK, Jørgensen M, Ogilby PR (2001) Two-photon photosensitized production of singlet oxygen. J Am Chem Soc 123: 1215-1221.

219. Dichtel WR, Serin JM, Edder C, Fréchet JM, Matuszewski M, et al. (2004) Singlet oxygen generation via two-photon excited FRET. J Am Chem Soc 126: 5380-5381.

220. Ogawa K, Kobuke Y (2013) Two-photon photodynamic therapy by water-soluble self-assembled conjugated porphyrins. Biomed Res Int 2013: 125658.

221. Gerasimov OV, Boomer JA, Qualls MM, Thompson DH (1999) Cytosolic drug delivery using pH- and light-sensitive liposomes. Adv Drug Deliv Rev 38: 317-338.

222. Kean ZS, Gossweiler GR, Kouznetsova TB, Hewage GB, Craig SL (2015) A coumarin dimer probe of mechanochemical scission efficiency in the sonochemical activation of chain-centered mechanophore polymers. Chem Commun (Camb) 51: 9157-9160.

223. Palazzo G, Magliulo M, Mallardi A, Angione MD, Gobeljic D, et al. (2014) Electronic transduction of proton translocations in nanoassembled lamellae of bacteriorhodopsin. ACS Nano 8: 7834-7845.

224. Erokhina S, Benassi L, Bianchini P, Diaspro A, Erokhin V, et al. (2009) Light-driven release from polymeric microcapsules functionalized with bacteriorhodopsin. J Am Chem Soc 131: 9800-9804.

225. Zaitsev SY, Solovyeva DO, Nabiev I (2012) Thin films and assemblies of photosensitive membrane proteins and colloidal nanocrystals for engineering of hybrid materials with advanced properties. Adv Colloid Interface Sci 183-184: 14-29.

226. Corbitt TS, Sommer JR, Chemburu S, Ogawa K, Ista LK, et al. (2009) Conjugated polyelectrolyte capsules: light-activated antimicrobial micro "Roach Motels". ACS Appl Mater Interfaces 1: 48-52.

227. Wen L, Hou X, Tian Y, Zhai J, Jiang L (2010) Bio-inspired Photoelectric Conversion Based on Smart-Gating Nanochannels. Adv Funct Mater 20: 2636-2642.

228. Lanyi JK (1993) Proton translocation mechanism and energetics in the light-driven pump bacteriorhodopsin. Biochim Biophys Acta 1183: 241-261.

229. Petrosyan R, Bippes CA, Walheim S, Harder D, Fotiadis D, et al. (2015) Single-molecule force spectroscopy of membrane proteins from membranes freely spanning across nanoscopic pores. Nano Lett 15: 3624-3633.

230. Hildebrand P, Stochburger M (1984) Role of water in bacteriorhodopsin's chromophore: resonance Raman study. Biochemistry 23: 5539-5548.

231. Oesterhelt D, Stoeckenius W (1971) Rhodopsin-like protein from the purple membrane of Halobacterium halobium. Nat New Biol 233: 149-152.

232. He JA, Samuelson L, Li L, Kumar J, Tripathy SK (1998) Photoelectric Properties of Oriented Bacteriorhodopsin/Polycation Multilayers by Electrostatic Layer-by-Layer Assembly. J Phys Chem B 102: 7067-7072.

233. Hwang SB, Korenbrot JI, Stoeckenius W (1977) Structural and spectroscopic characteristics of bacteriorhodopsin in air-water interface films. J Membr Biol 36: 115-135.

234. Gutman M, Nachliel E (1997) Time-resolved dynamics of proton transfer in proteinous systems. Annu Rev Phys Chem 48: 329-356.

235. Birge RR (1990) Photophysics and molecular electronic applications of the rhodopsins. Annu Rev Phys Chem 41: 683-733.

236. Oesterhelt D, Bräuchle C, Hampp N (1991) Bacteriorhodopsin: a biological material for information processing. Q Rev Biophys 24: 425-478.

237. Kononenko AA, Maximychev AV, Lukashev EP, Chamorovsky SK, Rubin AB, et al. (1986) Oriented purple-membrane films as a probe for studies of the mechanism of bacteriorhodopsin functioning. I. The vectorial character of the external electric-field effect on the dark state and the photocycle of bacteriorhodopsin. Biochim Biophys Acta, 850: 162-169.

238. Chu J, Li X, Zhang J, Tang J (2003) Fabrication and photoelectric response of poly(allylamine hydrochloride)/PM thin films by layer-by-layer deposition technique. Biochem Biophys Res Commun 305: 116-121.

239. SzymaNski W, Yilmaz D, KoÃ§er A, Feringa BL (2013) Bright ion channels and lipid bilayers. Acc Chem Res 46: 2910-2923.

240. Balamurugan S, Nithyanandan S, Selvarasu C, Yeap GY, Kannan P (2012) Photophysical and photochemical investigations on triazole ring linked chalcone containing polymethacrylates Polymer 53: 4101-4111.

241. Yu Z, Ho LY, Lin Q (2011) Rapid, photoactivatable turn-on fluorescent probes based on an intramolecular photoclick reaction. J Am Chem Soc 133: 11912-11915.

242. Fang X, Yang B, Cheng Z, Yang M, Su N, et al. (2013) Synthesis and antitumor activity of novel nitrogen mustard-linked chalcones. Arch Pharm (Weinheim) 346: 292-299.

243. Wagner BD (2009) The use of coumarins as environmentally-sensitive fluorescent probes of heterogeneous inclusion systems. Molecules 14: 210-237.

244. Fleischhaker F, Haehnel AP, Misske AM, Blanchot M, Haremza S (2014) Glass-Transition-, Melting-, and Decomposition Temperatures of Tailored Polyacrylates and Polymethacrylates: General Trends and Structure–Property Relationships. Chem Phys 215: 1192-1200.

245. Chen Y, Geh JL (1996) Copolymers derived from 7-acryloyloxy-4-methylcoumarin and acrylates: 2. Reversible photocrosslinking and photocleavage. Polymer 37: 4481-4486.

246. Mukumoto K, Averick AE, Park S, Nese A, Mpoukouvalas A, et al. (2014) Phototunable Supersoft Elastomers using Coumarin Functionalized Molecular Bottlebrushes for Cell-Surface Interactions Study. Macromolecules 47: 7852-7857.

247. Tietz K, Finkhäuser S, Samwer K, Vana P (2014) Stabilizing the Microphase Separation of Block Copolymers by Controlled Photo-crosslinking. Macromol Chem Phys 215: 1563-1572.

248. Sato E, Nagai S, Matsumoto A (2013) Reversible thickness control of polymer thin films containing photoreactive coumarin derivative units. Progress in Organic Coatings 76: 1747-1751.

249. Hribar KC, Lee MH, Lee D, Burdick JA (2011) Enhanced release of small molecules from near-infrared light responsive polymer-nanorod composites. ACS Nano 5: 2948-2956.

250. Jiang J, Qi B, Lepage M, Zhao Y (2007) Polymer Micelles Stabilization on Demand through Reversible Photo-Cross-Linking. Macromolecules 40: 790-792.

251. Liu Y, Pauloehrl T, Presolski SI, Albertazzi L, Palmans AR, et al. (2015) Modular Synthetic Platform for the Construction of Functional Single-Chain Polymeric Nanoparticles: From Aqueous Catalysis to Photosensitization. J Am Chem Soc 137: 13096-13105.

252. Kim JC (2015) Hydroxyethyl acrylate-based copolymer-immobilized liposomes as UV and thermo dual-triggerable carriers. Eur J Lipid Sci Technol 117: 45-54.

253. Jin Q, Mitschang F, Agarwal S (2011) Biocompatible drug delivery system for photo-triggered controlled release of 5-Fluorouracil. Biomacromolecules 12: 3684-3691.

254. Bischof AA, Mangiarotti A, Wilke N (2015) Searching for line active molecules on biphasic lipid monolayers. Soft Matter 11: 2147-2156.

255. Hassan-Zadeh E, Baykal-Caglar E, Alwarawrah M, Huang J (2014) Complex roles of hybrid lipids in the composition, order, and size of lipid membrane domains. Langmuir 30: 1361-1369.

256. Shimokawa N, Nagata M, Takagi M (2015) Physical properties of the hybrid lipid POPC on micrometer-sized domains in mixed lipid membranes. Phys Chem Chem Phys 17: 20882-20888.

257. Kumar S, Allard JF, Morris D, Dory YL, Lepage M (2012) Near-infrared light sensitive polypeptide block copolymer micelles for drug delivery J Mater Chem 22: 7252-7257.

258. Jiang J, Tong X, Morris D, Zhao Y (2006) Toward Photocontrolled Release Using Light-Dissociable Block Copolymer Micelles. Macromolecules 39: 4633-4640.

259. Babin J, Pelletier M, Lepage M, Allard JF, Morris D, et al. (2009) A new two-photon-sensitive block copolymer nanocarrier. Angew Chem Int Ed Engl 48: 3329-3332.

260. Babin J, Lepage M, Zhao Y (2008) "Decoration" of Shell Cross-Linked Reverse Polymer Micelles Using ATRP: A New Route to Stimuli-Responsive Nanoparticles. Macromolecules 41: 1246-1253.

261. Bretler S, Margel S (2015) Synthesis and characterization of new spiropyran micrometer-sized photochromic fluorescent polymeric particles of narrow size distribution by a swelling process. Polymer 61: 68-74.

262. Chen S, Jiang F, Cao Z, Wang G, Dang ZM (2015) Photo, pH, and thermo triple-responsive spiropyran-based copolymer nanoparticles for controlled release. Chem Commun (Camb) 51: 12633-12636.

263. Berkovic G, Krongauz V, Weiss V (2000) Spiropyrans and Spirooxazines for Memories and Switches. Chem Rev 100: 1741-1754.

264. Hu D, Tian Z, Wu W, Wan W, Li AD (2008) Photoswitchable nanoparticles enable high-resolution cell imaging: PULSAR microscopy. J Am Chem Soc 130: 15279-15281.

265. Zhu MQ, Zhu L, Han JJ, Wu W, Hurst JK, et al. (2006) Spiropyran-based photochromic polymer nanoparticles with optically switchable luminescence. J Am Chem Soc 128: 4303-4309.

266. Tian Z, Wu W, Wan W, Li AD (2009) Single-chromophore-based photoswitchable nanoparticles enable dual-alternating-color fluorescence for unambiguous live cell imaging. J Am Chem Soc 131: 4245-4252.

267. Menju A, Hayashi K, Irie M (1981) Photoresponsive polymers. 3. Reversible solution viscosity change of poly(methacrylic acid) having spirobenzopyran pendant groups in methanol. Macromolecules 14: 755-758.

268. Achilleos DS, Vamvakaki M (2010) Multiresponsive Spiropyran-Based Copolymers Synthesized by Atom Transfer Radical PolymerizationMacromolecules 43: 7073-7081.

269. Xue Y, Tian J, Tian W, Gong P, Dai J, (2015) Significant Fluorescence Enhancement of Spiropyran in Colloidal Dispersion and Its Light-Induced Size Tunability for Release Control. J Phys Chem C 119: 20762-20772.

270. Lee HI, Wu W, Oh JK, Mueller L, Sherwood G, et al. (2007) Light-induced reversible formation of polymeric micelles. Angew Chem Int Ed Engl 46: 2453-2457.

271. Jin Q, Liu G, Ji J (2010) Micelles and reverse micelles with a photo and thermo double-responsive block copolymer. J Polym Sci Part A: Polym Chem 48: 2855-2861.

272. Arisaka Y, Tamura A, Uchida K, Yajima H (2010) Photoinduced Particle Size Change of Core-Shell Polymeric Micelle Containing Spirobenzopyran in Its Inner Core. Chemistry Letters 39: 58-59.

273. Zhang J, Zhang Y, Chen F, Zhang W, Zhao H (2015) Self-assembly of photoswitchable diblock copolymers: salt-induced micellization and the influence of UV irradiation. Phys Chem Chem Phys 17: 12215-12221.

274. Shen H, Zhou M, Zhang Q, Keller A, Shen Y (2015) Zwitterionic light-responsive polymeric micelles for controlled drug delivery Colloid. Polym. Sci 293: 1685-1694.

275. Chen J, Zhong W, Tang Y, Wu Z, Li Y, et al. (2015) Amphiphilic BODIPY-Based Photoswitchable Fluorescent Polymeric Nanoparticles for Rewritable Patterning and Dual-Color Cell Imaging. Macromolecules 48: 3500-3508.

276. Kotharangannagari VK, Sánchez-Ferrer A, Ruokolainen J, Mezzenga R (2011) Photoresponsive Reversible Aggregation and Dissolution of Rod–Coil Polypeptide Diblock Copolymers. Macromolecues 44: 4569-4573.

277. Angelini N, Corrias B, Fissi A, Pieroni O, Lenci F (1998) Photochromic polypeptides as synthetic models of biological photoreceptors: a spectroscopic study. Biophys J 74: 2601-2610.

278. Pieroni O, Fissi A, Angelini N, Lenci F (2001) Photoresponsive polypeptides. Acc Chem Res 34: 9-17.

279. Ciardelli F, Fabbri D, Pieroni O, Fissi A (1989) Photomodulation of polypeptide conformation by sunlight in spiropyran-containing poly(L-glutamic acid). J Am Chem Soc 111: 3470-3472.

280. Ming L, Si ZK, Zhang Q, Sheng QR, Xue MZ, et al. (2015) Photochemical characterization of bi-functional compounds containing indolinospiropyran and chalcone groups. Res Chem Intermed 41: 3017-3029.

281. Moebius D, Miller R (2001) Novel methods to study interfacial layers. Elsevier 384-415.

282. Sukhorukov GB, Brumen M, Donath E, Mohwald H (1999) Hollow Polyelectrolyte Shells: Exclusion of Polymers and Donnan Equilibrium. J Phys Chem B 103: 6434-6440.

283. Shi M, Lu J, Shoichet MS (2009) Organic nanoscale drug carriers coupled with ligands for targeted drug delivery in cancer. J Mater Chem 10: 5485-5498.

284. Cortez C, Tomaskovic-Crook E, Johnston APP, Radt B, Cody SH, et al. (2006) Targeting and Uptake of Multilayered Particles to Colorectal Cancer Cells. Adv Mater, 18, 1998-2003.

285. Ochs CJ, Such GK, Städler B, Caruso F (2008) Low-fouling, biofunctionalized, and biodegradable click capsules. Biomacromolecules 9: 3389-3396.

286. Kamphuis MM, Johnston AP, Such GK, Dam HH, Evans RA, et al. (2010) Targeting of cancer cells using click-functionalized polymer capsules. J Am Chem Soc 132: 15881-15883.

287. Becker AL, Johnston AP, Caruso F (2010) Layer-by-layer-assembled capsules and films for therapeutic delivery. Small 6: 1836-1852.

288. Becker AL, Orlotti NI, Folini M, Cavalieri F, Zelikin AN, et al. (2011) Redox-active polymer microcapsules for the delivery of a survivin-specific siRNA in prostate cancer cells. ACS Nano 5: 1335-1344.

289. Such GK, Yan Y, Johnston AP, Gunawan ST, Caruso F (2015) Interfacing materials science and biology for drug carrier design. Adv Mater 27: 2278-2297.

290. Cui J, van Koeverden MP, Müllner M, Kempe K, Caruso F (2014) Emerging methods for the fabrication of polymer capsules. Adv Colloid Interface Sci 207: 14-31.

291. Kim D, Kim E, Lee J, Hong S, Sung W, et al. (2010) Direct synthesis of polymer nanocapsules: self-assembly of polymer hollow spheres through irreversible covalent bond formation. J Am Chem Soc 132: 9908-9919.

292. Picart C, Schneider A, Etienne O, Mutterer J, Schaaf P, et al. (2005) Controlled Degradability of Polysaccharide Multilayer Films In Vitro and In Vivo. Adv Funct Mater 15: 1771-1780.

293. Vázquez E, Dewitt DM, Hammond PT, Lynn DM (2002) Construction of hydrolytically-degradable thin films via layer-by-layer deposition of degradable polyelectrolytes. J Am Chem Soc 124: 13992-13993.

294. Jewell CM, Zhang J, Fredin NJ, Lynn DM (2005) Multilayered polyelectrolyte films promote the direct and localized delivery of DNA to cells. J Control Release 106: 214-223.

295. Fredin NJ, Zhang J, Lynn DM (2005) Surface analysis of erodible multilayered polyelectrolyte films: nanometer-scale structure and erosion profiles. Langmuir 21: 5803-5811.

296. Wood KC, Boedicker JQ, Lynn DM, Hammond PT (2005) Tunable drug release from hydrolytically degradable layer-by-layer thin films. Langmuir 21: 1603-1609.

297. Zhang J, Chua LS, Lynn DM (2004) Multilayered thin films that sustain the release of functional DNA under physiological conditions. Langmuir 20: 8015-8021.

298. Lynn DM (2007) Peeling back the layers: controlled erosion and triggered disassembly of multilayered polyelectrolyte thin films. Advanced Materials 19: 4118-4130.

299. Lynn DM (2006) Layers of opportunity: nanostructured polymer assemblies for the delivery of macromolecular therapeutics. Soft Matter 2: 269-273.

300. Liu X, Zhang J, Lynn DM (2008) Polyelectrolyte Multilayers Fabricated from 'Charge-Shifting' Anionic Polymers: A New Approach to Controlled Film Disruption and the Release of Cationic Agents from Surfaces. Soft Matter 4: 1688-1695.

301. Jewell CM, Zhang J, Fredin NJ, Wolff MR, Hacker TA, et al. (2006) Release of plasmid DNA from intravascular stents coated with ultrathin multilayered polyelectrolyte films. Biomacromolecules 7: 2483-2491.

302. Hatakeyama H, Akita H, Harashima H (2011) A multifunctional envelope type nano device (MEND) for gene delivery to tumours based on the EPR effect: a strategy for overcoming the PEG dilemma. Adv Drug Deliv Rev 63: 152-160.

303. Luo D, Saltzman WM (2000) Synthetic DNA delivery systems. Nat Biotechnol 18: 33-37.

304. Castanotto D, Rossi JJ (2009) The promises and pitfalls of RNA-interference-based therapeutics. Nature 457: 426-433.

305. Schluep T, Hwang J, Hildebrandt IJ, Czernin J, Choi CH, et al. (2009) Pharmacokinetics and tumor dynamics of the nanoparticle IT-101 from PET imaging and tumor histological measurements. Proc Natl Acad Sci U S A 106: 11394-11399.

306. Hu-Lieskovan S, Heidel JD, Bartlett DW, Davis ME, Triche TJ (2005) Sequence-specific knockdown of EWS-FLI1 by targeted, nonviral delivery of small interfering RNA inhibits tumor growth in a murine model of metastatic Ewing's sarcoma. Cancer Res 65: 8984-8992.

307. Davis ME, Zuckerman JE, Choi CH, Seligson D, Tolcher A, et al. (2010) Evidence of RNAi in humans from systemically administered siRNA via targeted nanoparticles. Nature 464: 1067-1070.

308. Zhou Q, Guo X, Chen T, Zhang Z, Shao S, et al. (2011) Target-specific cellular uptake of folate-decorated biodegradable polymer micelles. J Phys Chem B 115: 12662-12670.

309. Zhang J, Ma PX (2009) Polymeric core-shell assemblies mediated by host-guest interactions: versatile nanocarriers for drug delivery. Angew Chem Int Ed Engl 48: 964-968.

310. Hu QD, Tang GP, Chu PK (2014) Cyclodextrin-based host-guest supramolecular nanoparticles for delivery: from design to applications. Acc Chem Res 47: 2017-2025.

311. Harada A, Takashima Y, Nakahata M (2014) Supramolecular polymeric materials via cyclodextrin-guest interactions. Acc Chem Res 47: 2128-2140.

312. Raymo FM, Stoddart JF (1999) Interlocked Macromolecules. Chem Rev 99: 1643-1664.

313. Wenz G, Han BH, Müller A (2006) Cyclodextrin rotaxanes and polyrotaxanes. Chem Rev 106: 782-817.

314. Harada A, Hashidzume A, Yamaguchi H, Takashima Y (2009) Polymeric rotaxanes. Chem Rev 109: 5974-6023.

315. Quan CY, Chen JX, Wang HY, Li C, Chang C, et al. (2010) Core-shell nanosized assemblies mediated by the alpha-beta cyclodextrin dimer with a tumor-triggered targeting property. ACS Nano 4: 4211-4219.

316. De Temmerman ML, De Vos F, Demeester J, De Smedt SC (2010) Protein encapsulation in polyelectrolyte microcapsules for antigen delivery. Journal of Controlled Release 148: e54-56.

317. Franssen O, Hennink WE (1998) A novel preparation method for polymeric microparticles without the use of organic solvents. International Journal of Pharmaceutics 168: 1-7.

318. Van Tomme SR, van Steenbergen MJ, De Smedt SC, van Nostrum CF, Hennink WE (2005) Self-gelling hydrogels based on oppositely charged dextran microspheres. Biomaterials 26: 2129-2135.

319. De Geest BG, Van Camp W, Du Prez FE, De Smedt SC, Demeester J, et al. (2008) Biodegradable microcapsules designed via 'click' chemistry. Chem Commun (Camb) : 190-192.

320. De Geest BG, McShane MJ, Demeester J, De Smedt SC, Hennink WE (2008) Microcapsules ejecting nanosized species into the environment. J Am Chem Soc 130: 14480-14482.

321. De Geest BG, Déjugnat C, Prevot M, Sukhorukov GB, Demeester J, et al. (2007) Self-Rupturing and Hollow Microcapsules Prepared from Bio-polyelectrolyte-Coated Microgels. Advanced Functional Materials 17: 531-537.

322. Zhu H, McShane MJ (2005) Macromolecule encapsulation in diazoresin-based hollow polyelectrolyte microcapsules. Langmuir 21: 424-430.

323. de Jesus MB, Ferreira CV, de Paula E, Hoekstra D, Zuhorn IS (2010) Design of solid lipid nanoparticles for gene delivery into prostate cancer. Journal of Controlled Release 148: e89-90.

324. Naeye B, Raemdonck K, Remaut K, Sproat B, Demeester J, et al. (2010) PEGylation of biodegradable dextran nanogels for siRNA delivery. Eur J Pharm Sci 40: 342-351.

325. Naeye B, Deschout H, Röding M, Rudemo M, Delanghe J, et al. (2011) Hemocompatibility of siRNA loaded dextran nanogels. Biomaterials 32: 9120-9127.

326. Remaut K, Symens N, Lucas B, Demeester J, De Smedt SC (2014) Cell division responsive peptides for optimized plasmid DNA delivery: the mitotic window of opportunity? J Control Release 179: 1-9.

327. Kong SD, Zhang W, Lee JH, Brammer K, Lal R, et al. (2010) Magnetically vectored nanocapsules for tumor penetration and remotely switchable on-demand drug release. Nano Lett 10: 5088-5092.

328. Ariga K, Lvov Y, Kunitake T (1997) Assembling alternate dye-polyion molecular films by electrostatic layer-by-layer adsorption. Journal of the American Chemical Society 119: 2224-2231.

329. Linford MR, Auch M, Möhwald H (1998) Nonmonotonic effect of ionic strength on surface dye extraction during dye-polyelectrolyte multilayer formation. Journal of the American Chemical Society 120: 178-182.

330. Cooper TM, Campbell AL, Crane RL (1995) Formation of polypeptide-dye multilayers by electrostatic self-assembly technique. Langmuir 11: 2713-2718.

331. Shchukin DG, Patel AA, Sukhorukov GB, Lvov YM (2004) Nanoassembly of biodegradable microcapsules for DNA encasing. J Am Chem Soc 126: 3374-3375.

332. Sukhorukov GB, Donath E, Davis S, Lichtenfeld H, Caruso F, et al. (1998) Stepwise polyelectrolyte assembly on particle surfaces: a novel approach to colloid design. Polymers for Advanced Technologies 9: 759-767.

333. Ibarz G, Dähne L, Donath E, Moehwald H (2001) Smart micro-and nanocontainers for storage, transport, and release. Advanced Materials 13: 1324-1327.

334. Schüler C, Caruso F (2001) Decomposable hollow biopolymer-based capsules. Biomacromolecules 2: 921-926.

335. Evenson D, Darzynkiewicz Z, Jost L, Janca F, Ballachey B (1986) Changes in accessibility of DNA to various fluorochromes during spermatogenesis. Cytometry 7: 45-53.

336. Pelta J Jr, Durand D, Doucet J, Livolant F (1996) DNA mesophases induced by spermidine: structural properties and biological implications. Biophys J 71: 48-63.

337. Bloomfield VA (1991) Condensation of DNA by multivalent cations: considerations on mechanism. Biopolymers 31: 1471-1481.

338. Kabanov AV, Felgner PL, Seymour LW (1998) Self-assembling complexes for gene delivery. From laboratory to clinical trial 197-218.

339. Caruso F, Lichtenfeld H, Donath E, Möhwald H (1999) Investigation of electrostatic interactions in polyelectrolyte multilayer films: binding of anionic fluorescent probes to layers assembled onto colloids. Macromolecules 32: 2317-2328.

340. Caruso F, Donath E, Möhwald H, Georgieva R (1998) Fluorescence studies of the binding of anionic derivatives of pyrene and fluorescein to cationic polyelectrolytes in aqueous solution. Macromolecules 31: 7365-7377.

341. Tedeschi C, Caruso F, Möhwald H, Kirstein S (2000) Adsorption and desorption behavior of an anionic pyrene chromophore in sequentially deposited polyelectrolyte-dye thin films. Journal of the American Chemical Society 122: 5841-5848.

342. Klitzing RV, Möhwald H (1996) A realistic diffusion model for ultrathin polyelectrolyte films. Macromolecules 29: 6901-6906.

343. Makarova OV, Ostafin AE, Miyoshi H, Norris JR, Meisel D (1999) Adsorption and encapsulation of fluorescent probes in nanoparticles. The Journal of Physical Chemistry B 103: 9080-9084.

344. Liz-Marzán LM, Giersig M, Mulvaney P (1996) Synthesis of nanosized gold-silica core-shell particles. Langmuir 12: 4329-4335.

345. Lynge ME, van der Westen R, Postma A, Städler B (2011) Polydopamine--a nature-inspired polymer coating for biomedical science. Nanoscale 3: 4916-4928.

346. Lee H, Dellatore SM, Miller WM, Messersmith PB (2007) Mussel-inspired surface chemistry for multifunctional coatings. Science 318: 426-430.

347. Park JH, Kim K, Lee J, Choi JY, Hong D, et al. (2014) A cytoprotective and degradable metal-polyphenol nanoshell for single-cell encapsulation. Angew Chem Int Ed Engl 53: 12420-12425.

348. Ping Y, Guo J, Ejima H, Chen X, Richardson JJ, et al. (2015) pH-Responsive Capsules Engineered from Metal-Phenolic Networks for Anticancer Drug Delivery. Small 11: 2032-2036.

349. Ejima H, Richardson JJ, Liang K, Best JP, van Koeverden MP, et al. (2013) One-step assembly of coordination complexes for versatile film and particle engineering. Science 341: 154-157.

350. Ku SH, Ryu J, Hong SK, Lee H, Park CB (2010) General functionalization route for cell adhesion on non-wetting surfaces. Biomaterials 31: 2535-2541.

351. Chen X, Yan Y, Müllner M, van Koeverden MP, Noi KF, et al. (2014) Engineering fluorescent poly(dopamine) capsules. Langmuir 30: 2921-2925.

352. Wu J, Zhang L, Wang Y, Long Y, Gao H, et al. (2011) Mussel-inspired chemistry for robust and surface-modifiable multilayer films. Langmuir 27: 13684-13691.

353. Cui J, Yan Y, Such GK, Liang K, Ochs CJ, et al. (2012) Immobilization and intracellular delivery of an anticancer drug using mussel-inspired polydopamine capsules. Biomacromolecules 13: 2225-2228.

354. Postma A, Yan Y, Wang Y, Zelikin AN, Tjipto E, et al. (2009) Self-polymerization of dopamine as a versatile and robust technique to prepare polymer capsules. Chemistry of Materials 21: 3042-3044.

355. Cui J, Wang Y, Postma A, Hao J, Hosta-Rigau L, et al. (2010) Monodisperse polymer capsules: tailoring size, shell thickness, and hydrophobic cargo loading via emulsion templating. Advanced Functional Materials 20: 1625-1631.

356. Ochs CJ, Hong T, Such GK, Cui J, Postma A, et al. (2011) Dopamine-mediated continuous assembly of biodegradable capsules. Chemistry of Materials 23: 3141-3143.

357. Lee Y, Chung HJ, Yeo S, Ahn CH, Lee H, et al. (2010) Thermo-sensitive, injectable, and tissue adhesive sol–gel transition hyaluronic acid/pluronic composite hydrogels prepared from bio-inspired catechol-thiol reaction. Soft Matter 6: 977-983.

358. Guo J, Ping Y, Ejima H, Alt K, Meissner M, et al. (2014) Engineering multifunctional capsules through the assembly of metal-phenolic networks. Angew Chem Int Ed Engl 53: 5546-5551.

359. Ju Y, Cui J, Müllner M, Suma T, Hu M, et al. (2015) Engineering low-fouling and pH-degradable capsules through the assembly of metal-phenolic networks. Biomacromolecules 16: 807-814.

360. Yu B, Wang DA, Ye Q, Zhou F, Liu W (2009) Robust polydopamine nano/microcapsules and their loading and release behavior. Chem Commun (Camb) : 6789-6791.

361. Liu Q, Yu B, Ye W, Zhou F (2011) Highly selective uptake and release of charged molecules by pH-responsive polydopamine microcapsules. Macromol Biosci 11: 1227-1234.

362. Gregory A, Stenzel MH (2012) Complex polymer architectures via RAFT polymerization: From fundamental process to extending the scope using click chemistry and nature's building blocks. Progress in Polymer Science 37: 38-105.

363. Springsteen G, Wang B (2002) A detailed examination of boronic acid–diol complexation. Tetrahedron 58: 5291-5300.

364. Scarano W, Lu H, Stenzel MH (2014) Boronic acid ester with dopamine as a tool for bioconjugation and for visualization of cell apoptosis. Chem Commun (Camb) 50: 6390-6393.

365. Gao Y, Chen Y, Ji X, He X, Yin Q, et al. (2011) Controlled intracellular release of doxorubicin in multidrug-resistant cancer cells by tuning the shell-pore sizes of mesoporous silica nanoparticles. ACS Nano 5: 9788-9798.

366. Qhobosheane M, Santra S, Zhang P, Tan W (2001) Biochemically functionalized silica nanoparticles. Analyst 126: 1274-1278.

367. Santra S, Zhang P, Wang K, Tapec R, Tan W (2001) Conjugation of biomolecules with luminophore-doped silica nanoparticles for photostable biomarkers. Anal Chem 73: 4988-4993.

368. Wang K, He X, Yang X, Shi H (2013) Functionalized silica nanoparticles: a platform for fluorescence imaging at the cell and small animal levels. Acc Chem Res 46: 1367-1376.

369. Liu JN, Bu WB, Shi JL (2015) Silica coated upconversion nanoparticles: a versatile platform for the development of efficient theranostics. Acc Chem Res 48: 1797-1805.

370. Stöber W, Fink A, Bohn E (1968) Controlled growth of monodisperse silica spheres in the micron size range. Journal of colloid and interface science 26: 62-69.

371. Ow H, Larson DR, Srivastava M, Baird BA, Webb WW, et al. (2005) Bright and stable core-shell fluorescent silica nanoparticles. Nano Lett 5: 113-117.

372. Van Blaaderen A, Vrij A (1992) Synthesis and characterization of colloidal dispersions of fluorescent, monodisperse silica spheres. Langmuir 8: 2921-2931.

373. Tapec R, Zhao XJ, Tan W (2002) Development of organic dye-doped silica nanoparticles for bioanalysis and biosensors. J Nanosci Nanotechnol 2: 405-409.

374. Imhof A, Megens M, Engelberts JJ, De Lang DT, Sprik R, et al. (1999) Spectroscopy of fluorescein (FITC) dyed colloidal silica spheres. The Journal of Physical Chemistry B 103: 1408-1415.

375. Dewar PJ, MacGillivray TF, Crispo SM, Smith-Palmer T (2000) Interactions of Pyrene-Labeled Silica Particles. J Colloid Interface Sci 228: 253-258.

376. Larson DR, Ow H, Vishwasrao HD, Heikal AA, Wiesner U, et al. (2008) Silica nanoparticle architecture determines radiative properties of encapsulated fluorophores. Chemistry of materials 20: 2677-2684.

377. Kim HK, Kang SJ, Choi SK, Min YH, Yoon CS (1999) Highly efficient organic/inorganic hybrid nonlinear optic materials via sol-gel process: synthesis, optical properties, and photobleaching for channel waveguides. Chemistry of materials 11: 779-788.

378. Graf C, Schärtl W, Fischer K, Hugenberg N, Schmidt M (1999) Dye-labeled poly (organosiloxane) microgels with core-shell architecture. Langmuir 15: 6170-6180.

379. Alberto G, Caputo G, Viscardi G, Coluccia S, Martra G (2012) Molecular engineering of hybrid dye–silica fluorescent nanoparticles: influence of the dye structure on the distribution of fluorophores and consequent photoemission brightness. Chemistry of Materials 24: 2792-2801.

380. Jungmann N, Schmidt M, Ebenhoch J, Weis J, Maskos M (2003) Dye loading of amphiphilic poly(organosiloxane) nanoparticles. Angew Chem Int Ed Engl 42: 1714-1717.

381. Bagwe RP, Yang C, Hilliard LR, Tan W (2004) Optimization of dye-doped silica nanoparticles prepared using a reverse microemulsion method. Langmuir 20: 8336-8342.

382. Yao G, Wang L, Wu Y, Smith J, Xu J, et al. (2006) FloDots: luminescent nanoparticles. Anal Bioanal Chem 385: 518-524.

383. Zhao X, Bagwe RP, Tan W (2004) Development of Organic-Dye-Doped Silica Nanoparticles in a Reverse Microemulsion. Advanced Materials 16: 173-176.

384. Smith JE, Wang L, Tan W (2006) Bioconjugated silica-coated nanoparticles for bioseparation and bioanalysis. Trac Trends in Analytical Chemistry 25: 848-855.

385. Bagwe RP, Khilar KC (2000) Effects of intermicellar exchange rate on the formation of silver nanoparticles in reverse microemulsions of AOT. Langmuir 16: 905-910.

386. Bagwe RP, Mishra BK, Khilar KC (1999) Effect of chain length of oxyethylene group on particle size and absorption spectra of silver nanoparticles prepared in non-ionic water-in-oil micro emulsions. Journal of Dispersion Science and Technology 20: 1569-1579.

387. He X, Wang Y, Wang K, Chen M, Chen S (2012) Fluorescence resonance energy transfer mediated large Stokes shifting near-infrared fluorescent silica nanoparticles for in vivo small-animal imaging. Anal Chem 84: 9056-9064.

388. Verhaegh NA, Blaaderen AV (1994) Dispersions of rhodamine-labeled silica spheres: synthesis, characterization, and fluorescence confocal scanning laser microscopy. Langmuir 10: 1427-1438.

389. Herz E, Ow H, Bonner D, Burns A, Wiesner U (2009) Dye structure–optical property correlations in near-infrared fluorescent core-shell silica nanoparticles. Journal of Materials Chemistry 19: 6341-6347.

390. Nooney RI, McCahey CM, Stranik O, Le Guevel X, McDonagh C, et al. (2009) Experimental and theoretical studies of the optimisation of fluorescence from near-infrared dye-doped silica nanoparticles. Anal Bioanal Chem 393: 1143-1149.

391. He X, Chen J, Wang K, Qin D, Tan W (2007) Preparation of luminescent Cy5 doped core-shell SFNPs and its application as a near-infrared fluorescent marker. Talanta 72: 1519-1526.

392. He X, Wang K, Tan W, Li J, Yang X, et al. (2002) Photostable luminescent nanoparticles as biological label for cell recognition of system lupus erythematosus patients. J Nanosci Nanotechnol 2: 317-320.

393. Zhou X, Zhou J (2004) Improving the signal sensitivity and photostability of DNA hybridizations on microarrays by using dye-doped core-shell silica nanoparticles. Anal Chem 76: 5302-5312.

394. Nooney R, O'Connell C, Roy S, Boland K, Keegan G, et al. (2015) Synthesis and characterisation of far-red fluorescent cyanine dye doped silica nanoparticles using a modified microemulsion method for application in bioassays. Sensors and Actuators B: Chemical 221: 470-479.

395. Chen N, Shao C, Li S, Wang Z, Qu Y, et al. (2015) Cy5. 5 conjugated MnO nanoparticles for magnetic resonance/near-infrared fluorescence dual-modal imaging of brain gliomas. Journal of colloid and interface science 457: 27-34.

396. Gross S, Piwnica-Worms D (2006) Molecular imaging strategies for drug discovery and development. Curr Opin Chem Biol 10: 334-342.